Current Awareness Bulletin

of

SCHOLARLY ARTICLES PUBLISHED BY

Faculty, Students and Alumni

~ December 2012 ~

DELHI TECHNOLOGICAL UNIVERSITY CENTRAL LIBRARY
(formerly Delhi College of Engineering, Bawana Road, DELHI)

PREFACE

This is a Current Awareness Bulletin Service started by Delhi Technological University Library. The aim of the bulletin is to compile, preserve and disseminate information published by the Faculty, Students and Alumni for mutual benefits. The bulletin also aims to propagate the intellectual contribution of DTU as a whole to the academia. It contains information resources available in the internet in the form of articles, reports, presentation published in international journals, websites, etc. by the faculty and students of Delhi Technological University in the field of science and technology. The publication of Faculty and Students, which are not covered in this bulletin, may be because of the reason that the full text either was not accessible or could not be searched by the search engine used by the library for this purpose. To make the bulletin more comprehensive, the learned faculty and Students may provide their uncovered publication to the library either through email or in CD, etc.

This issue contains the information published during December 2012. The arrangement of the contents is alphabetical wise starting from A-Z. The Full text of the article, which is either subscribed by the University or available in the web, is provided in this Bulletin.

CONTENTS

13. Study of Maximum Acceptable Weight of Lift for Indian Male Industrial Workers by *Jaswinder Singh, Dr. P Kalra* and ****Dr. R S Walia***.

14. Taxonomy of Nature Inspired Computational Intelligence: A Remote Sensing Perspective by ***@Lavika Goel, @Daya Gupta***, *V.K. Panchal and Ajith Abraham.*

***** **Faculty**
@ **Students/Research Scholars**
**Alumni**

2012 Fourth International Conference on Computational Intelligence and Communication Networks

A Fuzzy Nearest Neighbor classifier for Speaker Identification

Seba Susan and Srishti Sharma
Department of Information Technology,
Delhi Technological University,
New Delhi, India

Abstract— **Mel-frequency Cepstral coefficients (MFCC) are popular features extracted from speech data for speaker identification. The speech signal is fragmented into frames and the MFCC features extracted from each frame show some temporal redundancy which forms the basis of the fuzzy classifier proposed in this paper. We propose a fuzzy nearest neighbor classifier that defines a frame prototype for each training audio sample using a weighted mean technique with the weights being probability values, and the class label for each test sample is decided from fuzzy membership functions involving the frame prototypes. The classification results of the proposed classifier on audio samples from the VidTIMIT database show a superior performance to the Nearest Neighbor classifier, GMM, HMM and MLP neural networks. It is observed that the execution time of the fuzzy classifier is a very small fraction of the time taken by the HMM and neural network classifiers and the training database is significantly reduced due to the use of frame prototypes instead of actual frames.**

Keywords- *Mel-frequency cepstral coeffecients, Gaussian fuzzy membership functions, fuzzy classifer***.**

I. INTRODUCTION

Biometrics is a science that establishes the identity of an individual based on one or more intrinsic physiological or behavioral traits and uses modalities like voice, face, fingerprint, retina and iris [1] to uniquely identify or characterize an individual. Voice is one of the most reliable biometric trait used to identify a speaker from audio-visual clips and the Mel-frequency cepstral coefficients (MFCC) [2-4],[10] are the most preferred audio features in terms of the low computational cost involved and temporal consistency of features with higher inter-class variability [11-14]. Some of the other popular audio features are LPC [4]-[7],[10], PLP[3],[8],[10] and RASTA[6],[9]-[10] though the MFCC features are more popular among researchers due to its simple use and high reliability. Many classifiers have been proposed for audio classification over the years with the prominent ones being based on neural networks [3],[16-18], Gaussian Mixture models (GMM) [15] and Hidden Markov model (HMM) [18]. The multilayer perceptron neural network (MLP) [18] and radial basis function [3] neural networks are widely used for speaker classification due to their non-linearity property which is further enhanced by increasing the number of neurons in the hidden layer. The disadvantage of all the conventional non-linear classifiers based on neural networks, GMM or HMM is the total time involved for training and the large and varied training database required. Alternatively fuzzy [19] and neuro-fuzzy techniques [20] have been proposed for speaker identification with an aim to remove the training overhead and save memory space. In this paper a novel fuzzy classification of audio features is proposed that translates the Euclidean distance between training and test feature vectors into fuzzy domain using Gaussian membership functions. The proposed technique outperforms the non-linear neural network in terms of execution time and the size of the training database. The paper is organized as follows. Section 2 reviews the steps for the extraction of MFCC features from a audio file. In Section 3 the proposed fuzzy classification scheme is presented. Section 4 reports the experimental results and Section 5 outlines the conclusions from the results.

II. EXTRACTION OF MFCC FEATURES- A BASIC REVIEW

The Mel-frequency cepstral coefficients (MFCC) approximate the human audio perception since its frequency bands are positioned logarithmically quite similar to the human auditory response. The Mel-scale was developed in accordance with the pitch or frequency observed by the human ear with the basic unit being in mel. The speech signal is divided into frames to facilitate spectral analysis which is defined by short time segments in milliseconds called frames in which the signal is assumed to be stationary. A pre-emphasis is carried out initially to reduce the high frequency falloff and a hamming window is applied to each segment to minimize spectral leakage. The magnitude of the Discrete Fourier Transform of the speech signal sampled as per Nyquist criterion is warped into mel frequency using a filter bank. This is equivalent to a logarithmic mapping of the normal frequency scale into mel frequency in which the log total energy of the critical band around the center frequency is included. The Discrete Cosine Transform (DCT) of the mel frequency gives the DC coefficient and first 12 AC coefficients which when taken in order form the 13 MFCC features derived from a audio

978-0-7695-4850-0/12 $26.00 © 2012 IEEE
DOI 10.1109/CICN.2012.16

frame. The MFCC Features along with their corresponding delta and accelerations (to capture changes between frames) form a 39 dimensional audio feature vector for each frame in the given sample.

III. PROPOSED FUZZY NEAREST NEIGHBOR CLASSSIFER

Any classification procedure is divided into two phases namely, the training and test phases. The term 'Fuzzy classifier' refers to the use of fuzzy membership functions to compute 'soft' class labels that are eventually defuzzified to classify the test sample to a known class. The training and test samples are initially segregated and 39 MFCC coefficients are extracted from a single frame of each speech sample in the manner explained in Section II. The first phase of fuzzy classification is the preparation of a compact training database by computing the expected values of the 39 MFCC features over all the temporal frames in the audio sample. The computational steps are detailed below:

Preparation of a compact training database using frame prototypes

The preparation of the compact training database exploits the temporal consistency of the MFCC coefficients derived from the different fragments or frames of the training audio sample. This is achieved by averaging the related MFCC coefficients over time. Let the histogram of h^{th} MFCC coefficient z_{ih} over all frames i=1,2,..,N, in an audio sample be denoted by the probability value $p(z_{ih})$ where h=1,2,...,39. Then the expected value of the h^{th} MFCC coefficient when averaged over all temporal frames is given by,

$$m_h = \sum_{i=1}^{N} z_{ih} p(z_{ih}) \tag{1}$$

Therefore the weighted mean m_h for each column h in the *Nx39* feature matrix is calculated by (1) and a mean feature vector of dimension 1x39 is computed for each training audio sample. This mean feature vector constitutes the frame prototype used to represent the class or category of the training sample. Therefore similar to the conventional nearest neighbor classifier the computations are made between each test and training sample. However in this case while the test input is a 1x39 frame feature vector, the training sample is now a category or class representing a particular frame configuration to which the membership of the test frame is computed. The Categorical memberships are computed for all the training samples or categories. The speaker label is finally assigned to the test sample by assembling and comparing all the computed category memberships of its constituent frames in the manner as explained in the *testing phase* below.

Testing Phase:

A fuzzy membership function is computed for each frame of the test audio sample based on the Euclidean distance of its MFCC features from each frame prototype in the training database. The Gaussian function is used to compute the fuzzy membership due to its inherent advantages of being non-linear and a monotonically decreasing function. The fuzzy membership of the j^{th} test feature vector $\{x_{jh}\}$, h=1,2,…,39, to the k^{th} training class prototype vector $\{m_{kh}\}$, h=1,2,…,39, is given by,

$$\mu_{jk} = e^{-\|x_{jh} - m_{kh}\|^2} \tag{2}$$

where, ||.|| is the Euclidean distance norm. Assume there are M audio samples per speaker in the training database. This implies that the compact database would comprise of MxS feature vectors, where S is the number of speakers in the experiment. Therefore there are MxS classes and MxS fuzzy memberships. Then the speaker label p assigned to the j^{th} test feature vector is decided by averaging the fuzzy memberships of the M samples that belong to the same speaker and finding the maximum of the results for all speakers p=1,2,…,S.

$$\mu_{jp} = \frac{\left| \sum_{k=(p-1)M+1}^{(p-1)M+M} \mu_{jk} \right|}{M} \tag{3}$$

$$class_j = \arg\max_{p}(\mu_{jp}) \tag{4}$$

Each test frame j from the test audio sample, j=1,2,…,N, is thus labeled with a speaker label as in (4). Finally the entire test audio sample is classified as belonging to the speaker whose label is most frequent among the constituent frames of the test sample.

IV. EXPERIMENTAL RESULTS AND DISCUSSION

The experiments are conducted on audio samples from the robust VidTIMIT database [22] that contains audio-visual recordings of 43 people reciting sentences from TIMIT corpus [23]. It has been recorded in 3 sessions with a gap of 7 days between sessions 1 and 2 and 6 days between sessions 2 and 3.The gap between sessions accounts for the possibility of mood and appearance changes that may occur in real life. There are a total of 10 sentences per person, 6 of them recorded in session 1 and two each in sessions 2 and 3. Two sentences are common to all speakers while the other eight sentences are different for each speaker.

We conducted the speaker identification experiments for a hierarchical subset of 5, 10, 15, 20, 25, 30, 35, 43 speakers and study the variability in results as the number of users is increased. Out of the ten audio samples per speaker, nine have been used for training and one has been used for testing taking into account the robust nature of the database.

This implies that S=5,10,15, 20, 25, 30, 35, 40, 43 and M=9, for the equations in Section III. Each audio sample in the ".wav" format is divided into 50 frames (N=50) using a 25 ms window with 50% overlap, and the 39-dimensional feature vector (comprising the MFCC coefficients and their delta and accelerations) is derived from each frame as explained in Section II. The training and test datasets are then segregated and the fuzzy classification procedure is applied for assigning a class to the test audio sample. The label of the speaker associated with nearest frame prototype is assigned to the test frame. The MATLAB 7.9 version software is used for implementing the code on a 2.16 GHz processor. For evaluating the efficiency of our classifier we use the Multi-layer Perceptron (MLP) neural network, Hidden Markov model (HMM), Nearest Neighbor, Gaussian Mixture Model (GMM) classifiers for comparison and the results are indicated in Table 1 and 2. It is observed from Table 1 that the fuzzy nearest neighbor classifier is highly successful in distinguishing between speakers as seen from the high classification rate of 80% for all three subsets S=5,10,15 while the MLP neural network (with 100 neurons in the hidden layer), GMM and HMM (for 3 states and 2 mixtures) are unable to perform in the absence of sufficient training. It is observed from Table 2 that the computational time is still much lower as compared to MLP neural network, GMM and HMM and comparable to that of the nearest neighbor classifier due to the simple computations involved. Another reason for its speedy execution is the reduced size of the training database since only a single prototype of the frame is stored per training sample as seen from the feature dimension D column in Table 2. The Nearest Neighbor classifier starts to become slower as the number of users is increased from 5 to 43 whereas its fuzzy counterpart is not much affected as seen from Table 2. The primary advantage of the proposed fuzzy nearest neighbor classifier for audio features is its high accuracy and a reduced or compact storage of training vectors and execution time of a few seconds.

V. CONCLUSION

A new fuzzy classification scheme for MFCC audio features is proposed in this paper that gives high classification accuracy for a compact database and execution time in a couple of seconds. The Gaussian membership function is used for fuzzifying the distance between training and test feature vectors. The performance is evaluated with respect to MLP neural network, Nearest Neighbor Classifier, HMM and GMM and is found to outperform all of them with a high accuracy at a reduced training database and extremely low computation time.

REFERENCES

[1] Ross, A. and Jain, A. K., "Multimodal biometrics:an overview," *Procc. EUSIPCO*, pp. 1221-1224, Sept.2004.

[2] Zhiping Dan,Sheng Zheng, Shuifa Sun, Ren Dong," Speaker Recognition based on LS-SVM**",** *3rd International Conference on Innovative Computing Information and Control* (ICICIC'08).

[3] Nima Yousefian, Azarakhsh Jalalvand, Pooyan Ahmadi, Morteza Analoui," Speech Recognition with a Competitive Probabilistic Radial Basis Neural Network", *IEEE Conference Intelligent Systems*, 2008

[4] Hemant A. Patil, Prakhar Kant Jain, Robin Jain," A Novel Approach To Identification Of Speakers From Their Hum"**,** *Seventh International Conference on Advances in Pattern Recognition*, 2009.

[5] Z. Uzdy, "Human Speaker Recognition Performance of LPC Voice Processors**",** *IEEE Transactions on Acoustics, Speech, and Signal processing*, vol. assp-33, no. 3**,** June 1985

[6] Rajparthiban Kumar, Aravind CV, Kanendra Naidu, Anis Fariza," Development of a Novel Voice Verification System using Wavelets", *Proceedings of the International Conference on Computer and Communication Engineering* 2008 May 13-15, 2008 Kuala Lumpur.

[7] Dr. Gwyn P. Edwards," A Speech/Speaker Recognition and Response System*, , IEEE Procc. ICASSP* 1980

[8] Wu Guo, Yanhua Long, Yijie Li, Lei Pan, Eryu Wang, Lirong Dai*,"* iFLY System For The NIST 2008 Speaker Recognition Evaluation"*, IEEE Procc. ICASSP 2009*.

[9] Ramon F. Astudillo, Dorothea Kolossa, Reinhold Orglmeister," Uncertainty Propagation for Speech Recognition using RASTA Features in Highly Nonstationary Noisy Environments", *ITG-Fachtagung Sprachkommunikation* 8- 10 October 2008 in Aachen

[10] Tilo Schiirer," An Experimental Comparison Of Different Feature Extraction And Classification Methods For Telephone Speech*", 2nd IEEE Workshop on Interactive Voice Technology for Telecommunications Applications* **(**IvTTA94),1994.

[11] Aleksic, P. S. and Katsaggelos, A. K., "Audio-visual biometrics," *Procc. IEEE*, vol. 94, no. 11, pp. 2025-2044, Nov. 2006.

[12] Sanderson, C., "Automatic person verification using speech and face information," *Ph.D. Thesis*.

[13] Chetty, G. and Wagner, M., "Speaking faces for facevoice speaker identity verification," *Proc. Interspeech*, pp. 513-516, Sept. 2006.

[14] Erzin, E., Yemez, Y., and Tekalp, A. M., "Multimodal speaker identification using an adaptive classifier cascade based on modality reliability*," IEEE Trans. Multimedia*, vol. 7, no. 5, pp. 840-852, Oct. 2005.

[15] D.Reynolds, T.Quatieri, and R.Dunn, ""Speaker Verification Using Adaptive Mixture Models", *Digital Signal processing*, 2000, 10,pp.181-202.

[16] Zhiping Dan.,Sheng Zheng.,Shuifa Sun.,Ren Dong., "Speaker Recognition Based on LS-SVM" , *3rd International Conference On Innovative Computing And Information And Control,*2008.

[17]H.Hattori, "Text Independent speaker recognition using neural networks", *IEEE conf. proceeding ICASSP* 1992, pp. 153-156

[18] Y. Arriola, R A Carrasco," Integration Of Multilayer Perceptron And Markov Models For Automatic Speech Recognition", *UK IT* 1990 Conference

[19] Tongtao Zheng, Dat Tran and Michael Wagner "Fuzzy Nearest Prototype Classifier Applied to Speaker Identification", in *Proceedings of the European Symposium on Intelligent Techniques (ESIT'99),*1999

[20] Jyh-Shing Roger Jang and Jiuann Jye-Chen, " Neuro-Fuzzy and Soft Computing for Speaker Recognition**",** *IEEE conf. proceeding* 1997

[21] M. Hanmandlu, J. Grover, V. K. Madasu, S. Vasikarla, "Input Fuzzy Modeling for the Recognition of Handwritten Hindi Numerals", *International Conference on Information Technology (ITNG'07).*

[22] Sanderson, C., Biometric person recognition : face, speech, and fusion. *VDM Verlag*, June 2008.

[23] Garofolo, J. S., Lamel, L.F., Fisher, W. M., Fiscus, J. G., Pallett, D. S., and Dahlgren, N. L., "The DARPA TIMIT acoustic-phonetic continuous speech corpus CDROM," NIST order number PB91-100354, 1992.

Table 1: Percentage of correct classification for MLP-NN, Nearest Neighbor, HMM, GMM and Proposed Fuzzy Classifier (with highest values shown in bold)

No. of speakers	MLP Neural Network	Nearest Neighbor Classifier	HMM	GMM	Proposed Fuzzy Classifier
5	**80%**	**80%**	**80%**	60%	**80%**
10	70%	50%	50%	40%	**80%**
15	40%	46.67%	26.67%	40%	**80%**
20	45%	50%	40%	45%	**65%**
25	36%	40%	28%	40%	**56%**
30	30%	33.33%	30%	43.33%	**46.67%**
35	28.57%	31.43%	28.57%	40%	**51.43%**
40	30%	37.5%	25%	40%	**50%**
43	23.26%	48.17%	23.26%	41.86%	**48.84%**

Table 2: Time Complexity (T) in seconds and Feature Dimension of the Training data (D) for the MLP-Neural Network, Nearest Neighbor, HMM, GMM classifiers and the Proposed Fuzzy Classifier
(with most optimum values shown in bold)

No. of speakers	MLP Neural Network		Nearest Neighbor Classifier		HMM Classifier		GMM Classifier		Proposed Fuzzy Classifier	
	T(secs)	D	T(secs)	D	T(secs)	D	T(secs)	D	T(secs)	D
5	93.78	2250x39	**0.34**	2250x39	58.18	2250x39	1.08	2250x39	1.93	**45x39**
10	337.85	4500x39	**1.35**	4500x39	137.26	4500x39	8.68	4500x39	1.96	**90x39**
15	683.30	6750x39	3.08	6750x39	365.09	6750x39	30.83	6750x39	**2.02**	**135x39**
20	536.95	9000x39	5.62	9000x39	402.14	9000x39	30.13	9000x39	**2.45**	**180x39**
25	1122. 2	11250x39	7.96	11250x39	541.75	11250x39	33.41	11250x39	**3.06**	**225x39**
30	1021.68	13500x39	11.00	13500x39	995.43	13500x39	127.85	13500x39	**3.86**	**270X39**
35	1172.92	15750x39	15.11	15750x39	1215.76	15750x39	170.67	15750x39	**5.14**	**315x39**
40	2048.08	18000x39	19.55	18000x39	1386.35	18000x39	219.198	18000x39	**6.41**	**360x39**
43	1686.48	19350x39	23.12	19350x39	1420.71	19350x39	254.57	19350x39	**7.7**	**387x39**

A Novel Approach for Providing Fault Tolerance to FPGA-Based Reconfigurable Systems

Upasana Sharma, *Member, IACSIT* and Shampa Chakraverty

***Abstract*—The dynamically reconfigurable Field Programmable Gate Arrays (FPGAs) are most frequently employed for developing adaptive embedded systems. They are also being increasingly used as co-processors in high performance computing applications. For these systems to be fielded in harsh environments such as those encountered in space, extra- terrestrial locations and regions of extreme conditions on the earth, one must adopt fault tolerant design techniques to ensure uninterrupted and reliable operation despite the occurrence of faults. Commercial Off-the-Shelf (COTS) FPGA components offer a cost effective design trajectory where the designer can choose among a rich variety of FT approaches and techniques. This paper compares the various FT techniques and proposes a novel method in which these techniques can work together to provide a synergetic approach for fault tolerant FPGA design.**

***Index Terms*—FPGA, fault tolerance techniques, dynamic partial reconfiguration.**

I. Introduction

Reconfigurable Computing (RC) is an upcoming field that bridges the gap between hardware and software. The principal benefits of RC are the ability to execute larger hardware designs with fewer gates and to realize the flexibility of a software-based solution while retaining the execution speed of a more traditional, hardware-based approach.

Field Programmable Gate Arrays (FPGAs) are a general class of RC hardware which contain an array of programmable logic blocks (PLBs), with programmable interconnect between PLBs, as well as programmable I/O cells. The configuration bits used to program the FPGA determine the function of the device.

Advances in digital technology provide the means to make each generation of FPGAs significantly more attractive and useful than their predecessors. Each generation introduces additional benefits and utilities besides the expected larger size and faster processing. One of the advancements of significant importance is the ability to reconfigure a portion of an FPGA, leaving the others unchanged. This feature is called Partial Reconfiguration (PR). It is much faster than the reconfiguration of the entire FPGA board, especially when only a small part of the FPGA logic needs to be changed. Dynamic PR is a step ahead as it allows PR to be executed at runtime. It therefore can potentially reduce the number of devices or the device size, thereby reducing both size and power consumption. As an example, a system that requires either transmit or receive capabilities at any given time, but not both, can switch between the two modes in a fraction of a second using "partial reconfiguration".

FPGAs are excellent candidates for applications that require hardware software co-design. They can also serve as hardware acceleration coprocessors for building high performance computing applications. Practical experience with FPGA-based coprocessors shows at least a ten-fold improvement in the execution speed of algorithms as compared to processors alone [1]. FPGAs especially find applications in any area or algorithm that can make use of the massive parallelism offered by their architecture. Some examples of the applications areas of FPGAs are code breaking (in particular brute-force attack, of cryptographic algorithms), digital signal processing, ASIC prototyping, image processing, encryption/decryption engines, space missions, speech recognition, defense, avionics, industrial control, automotive, medicine and a growing range of many other areas.

In all these applications, and, specifically applications deployed in mission critical environments, there is a strong need for availability and reliability. This is achieved through the provision of Fault Tolerance (FT) to such systems. As a result a lot of academic research has been done in the recent past in this area and various methods/techniques of providing FT to reconfigurable platforms have been developed. This paper emphasizes on the need of a flexible FT approach by comparing the important proposals/techniques that have been devised for the provision of FT on RC platforms. It proposes a new technique that incorporates hierarchical levels of online FT for applications running on reconfigurable platforms.

The paper is organized as follows – Section II talks about the need of FT for FPGAs. Section III discusses some key FPGA features and tools that are used in providing FT. Section IV discusses the related work. Section V provides a comparative analysis of the FT techniques. Section VII describes the proposed FT technique. Finally, we conclude in Section VIII.

II. Need for FT for FPGAS

Fault tolerance is defined as the ability of a system to operate normally given the presence of malfunctioning resources, or faults [2]. A fault tolerant system, therefore,

Manuscript received June 22, 2012; revised July 28, 2012. This work was funded by the Department of Science and Technology, Government of India under the Women Scientist Scheme.

Upasana Sharma was with the Division of Computer Engineering, Netaji Subhas Institute of Technology, New Delhi, India -110078. She is now with Safenet Inc., Noida, (U.P.), India - 201301 (e-mail: upasanash@yahoo.com).

Shampa Chakraverty is with the Division of Computer Engineering, Netaji Subhas Institute of Technology, New Delhi, India - 110078 (e-mail: apmahs@gmail.com).

consists of two parts: fault detection and fault repair (if possible) or fault bypass.

The provision of FT gains significant importance for mission critical applications like space, automotive, avionics and medicine. Since FPGAs are being used in such mission critical systems, there is a strong need for the provision of fault tolerance (FT) to the reconfigurable platforms as well. The provision of FT for an FPGA-based system is typical because it involves reconfiguration of the FPGA. This might hamper the performance of the FPGA-based system. Hence FT does not just entail overcoming the faults, but also overcoming the faults with minimum impact to performance and delays.

There can be various kinds of faults that can occur in an FPGA-based system:

- Aging faults: These types of faults are caused due to the degradation of the components, which can be attributed to a number of mechanisms [3].
- Manufacturing defects: These can be exhibited as circuit nodes which are stuck-at 0 or 1 or switch too slowly to meet the timing specification. Defects also affect the interconnect network and can cause short or open circuits and stuck open or closed pass transistors [4].
- Single Event Upsets (SEUs) and Single Event Transients (SETs): These faults occur when an energetic particle (typically a proton, neutron or a heavy ion) collides with atoms in the silicon lattice and leaves electric charge in its wake. SEUs can cause state bits to change and logic outputs to evaluate incorrectly.
- Software Faults: FPGAs are being used in applications that require hardware software co-design. In such applications, software faults are always a possibility that must be catered.

III. FPGA Features Used for FT

The recent technological development in FPGAs has led to the availability of some very useful FPGA features and tools. These features/tools are often coupled along with the traditional FT techniques discussed in section IV, to develop a robust fault-tolerant FPGA-based system. The features/tools are:

- Placement and Routing Tools: These tools physically place and map the application design to the physical resources of the FPGA [5], [6].
- Readback: Configuration is the process of loading a design bit stream into the FPGA internal configuration. Readback is the process of reading that data [7].
- Scrubbing: It involves periodical reloading of the contents of the configuration memory [8].
- Dynamic Partial Reconfiguration: It is the ability to reconfigure only a specific portion of an FPGA at runtime [9].

IV. Related Work

Most of the earlier works focused on tolerating the manufacturing defects and aging faults and manufacturing defects at either device level or configuration level using offline FT methods [2], [10]-[15]. However, provision of online FT is required to cater SEUs and software faults. With the advent of the dynamic partial reconfiguration capabilities of the new generation of FPGAs, the recent focus is on the provision of online FT, which is certainly the need of the hour.

Ambramovici et al [16]-[18] have demonstrated how self testing of small portions of a circuit can be carried out simultaneously with normal functioning of other parts. In [17], [18], a Self Testing Area, so called STAR, is first offloaded by reconfiguring its functionality on another area so that normal functioning is not affected at all, thus enabling online self testing using BIST (Built In Self Testing).

The TMR technique has been exploited for systems requiring high reliability, safety-critical applications, such as space missions [19]-[22]. The Xilinx Triple Modular Architecture [23], [24] replicates three identical copies of the same circuit and generates their voted outputs.

A volume of work has been done for providing FT to space applications built using SRAM-based FPGAs [19]- [22], [25]. The case of space applications is typical because here the FPGAs are exposed to high radiation environments. Radiation can cause both short term and permanent device failures. In short term they can cause transient upsets in circuits (SEUs and SETs). Additionally, radiation can cause permanent damage to silicon devices over time, rendering all or part of the device unusable. Authors of [21] have concluded that the TMR technique is not able to mask all the faults induced by SEUs. TMR is often coupled with scrubbing [8] to avoid fault accumulation. The authors of [6] have proposed coupling of reliability oriented place and route algorithms in order to make complete SEU immune circuits.

The concept of partial TMR has been introduced in [19]. Using device level TMR and a separate radiation hardened voter ASIC with integrated configuration management logic is another FT technique [20]. D. Fay et al [22] talk about device level TMR accompanied with adaptive FT for the distributed memory system. The authors of [25] have proposed and demonstrated a framework for Reconfigurable Fault Tolerance (RFT) that enables FPGA-based systems to change at run-time the amount of fault tolerance being used.

V. COMPARISION of FT Techniques Used for FPGAS

The design exploration process of an application must be able to weigh the pros and cons of different FT methodologies on factors such as system performance, cost, power etc. Table I provides a comprehensive summary of the comparative analysis between the various FT techniques that can be devised for an FPGA based system.

VI. The Proposal

The comparison amongst the various FT techniques for RC platforms in Section 5 clearly indicates that choosing a single FT technique for a given application shall require a tradeoff between the robustness of FT and factors like cost, system performance and power. The TMR technique is one of the most robust online FT techniques; however, it incurs

significant penalties in terms of area utilization, so much so, that, for certain designs it's not even feasible to use this technique.

The partial dynamic reconfiguration feature of the latest generation of FPGAs has opened gates for a very effective and an entirely new methodology for the provision of FT for FPGA-based systems. This methodology allows the choice of any of the available FT techniques as per the application and environment requirements. Two very recent works have been based on this approach [25], [27]. In the case of [25], an application is run in different modes, with each mode having a different FT level. In the case of [27], the demonstrator application autonomously improves its FT features based on the current workload.

TABLE I: COMPARISON OF VARIOUS FAULT-TOLERANT TECHNIQUES FOR FPGA BASED SYSTEM DESIGN.

FT Parameter	**Built-in Self Test(BIST) [16][17][18]**	**Duplicate & Compare(D&C) [25][27]**	**Triple Modular Redundancy (TMR) [19][25][27]**	**Concurrent Error Correcting Codes(CEC) [25][26]**
Mode of checking: Offline or Online	Generally, testing is carried out in offline mode. [17][18] overlaps testing of portions of FPGA with online functioning of remaining portions	Online provision for error security.	Online error correction by majority voting.	Online error detection / correction with information redundancy.
Ability to handle transient faults	No. In [17][18], time to detect fault is upper bounded by time to reconfigure and test full FPGA area.	Yes: Can detect transient faults	Yes: Can correct transient faults.	Yes: Can detect /correct transient faults.
Space overhead due to A) Added FT functions	BIST circuitry.	Duplication circuitry and Comparator	Triplication, And Voter circuitry	Circuitry for error code generation, checker and code converters.
Space overhead due to B) Communications requirement	Routing test clock, test data input and output through scan chain path.	Routing input signals to both modules and error signal to other parts of system	Routing input signals to triplicate modules and their outputs to voter.	Routing error signal to dependant circuits and diagnosis/ recovery system
Memory space requirement	Stores signatures of the circuit as in [17] [18]	None*.	None*.	*For data storage integrity, CRC codes are stored with data.
		*To diagnose permanent fault an *n*-bit history needs to be recorded		
Time overhead	Time for offline testing. In [17] [18], time incurred for reconfiguring and roving the STARS	*Time for comparison and propagating error signal	*Time for voting on multiple results.	*Time to generate coded values, detect non-code values and rectify errors.
		*In all cases, pipelining techniques increase throughput at the cost of initial latency and extra space required by latches.		
Diagnostic capability	Can diagnose all stuck-at logic faults at test clock speed. Provides very high fault coverage.	Can detect faulty pair.	Identifies minority unit as faulty.	Can identify faulty module at run time and additionally locate faults.
Recovery mechanism	Bypass faulty blocks by reconfiguring their functionality.	*Avoid unsafe operation by blocking output of erroneous modules.	*Use majority output as correct. Can switch to *error secure* mode when a faulty module is removed.	*Avoid unsafe operation by blocking output of erroneous modules. For error-correcting circuits, rectify erroneous data.
		*By monitoring past results, permanently faulty module can be identified and isolated. Its functionality can then be reconfigured on spare logic cells and switched in.		
Comments	Gives best diagnosis. But continuous self testing incurs time overhead and extra power dissipation	Eliminates unsafe operation. However, it is not possible to identify which of the pair is the faulty.	Highest hardware redundancy incurs high cost but gives the best reliability	Hardware redundancy is usually less than duplicated. Using extra redundancy in coding data, errors can also be located and corrected.

Our proposal is also based on this novel methodology and intends to provide hierarchical levels of FT. Unlike [25] and [27], we intend to attach an FT level with each task comprising of the application that is being run on the FPGA. Thus, our approach combines scheduling along with the provision of FT. FPGA Scheduling is itself a very typical and wide topic that attracts the interest of a lot of researchers and various techniques are being devised and proposed for the same [28]-[32].

The three major functional components of our proposed design along with their roles are presented below:

- Task Analyzer

This module analyzes the task graph of the given application that is to be run on the FPGA. Depending on the criticality of a task, it assigns a level of FT to it. As an example, the most critical tasks are provided the highest level of FT using the TMR technique; the tasks with a defined second level of criticality are duplicated and the tasks that are not critical at all are not provided any FT.

- Scheduler

This is an enhanced version of the scheduler discussed in [32]. When a task is being scheduled, the FT level assigned to that task also plays an important role along with the other factors. For example, if a task has been assigned the highest level of FT, the scheduler will have to schedule three copies of that task.

- FT Manager

This module is responsible for the provision of FT using the framework created by the other two modules. It has a list of the executing tasks along with their assigned FT level. Depending on the FT technique assigned to a task, it checks for the proper functioning of that task. In case of a fault, this module is responsible for taking corrective actions.

VII. Conclusions

We have presented the work being done by the various research groups for the provision of FT for reconfigurable platforms. A comparative analysis of the various FT techniques has also been done. We have proposed a novel FT technique that shall integrate scheduling to provide an optimum, flexible and hierarchical FT to an application. The implementation part of the proposed approach is in progress and our future work shall focus on deriving significant experimental results out of the same.

Acknowledgement

The authors would like to thank the Department of Science and Technology, Govt. of India, for funding this work under the *Women Scientist Scheme*.

References

[1] Accelerating high-performance computing with FPGAs. [Online]. Available: http://www.altera.com/literature/wp/wp-01029.pdf.

[2] J. A. Chetham, J. M. Emmert, and S. Baumgart, "A survey of fault tolerant methodologies for FPGAs," *ACM Transactions on Design Automation of Electronic Systems*, vol. 11, no. 2, April 2006.

[3] S. Srinivasan *et al*., "FLAW: FPGA lifetime awareness," *Design Automation Conference*, pp. 630-635, 2006.

[4] I. G. Harris *et al*., "Testing and diagnosis of interconnect faults in cluster-based FPGA architectures," *IEEE Transactions on CAD of Integrated Circuits and Systems*, vol. 21, no. 11, pp. 1337-43 Nov. 2002.

[5] L. Sterpone and M. Violante, "A new reliability-oriented place and route algorithm for SRAM-based FPGAs," *IEEE Transactions on Computers*, vol. 55, Issue 6, pp. 732 – 744, June 2006.

[6] L. Sterphone and N. Battezzati, "A novel design flow for the performance optimization of fault tolerant circuits on SRAM-based FPGAs," *NASA/ESA conference on Adaptive Hardware Systems, IEEE* 2008.

[7] Xilinx Application Notes XAPP015, "Using the XC4000 readback capability".

[8] J. Heiner, B. Sellers, M. Wirthlin, and J. Kalb, "FPGA partial reconfiguration via configuration scrubbing," *International Conference on FPL*, 2009.

[9] Correcting single event upset through Virtex partial reconfiguration, *Xilinx Application Notes XAPP216*, 2000.

[10] H. Ito Doumar, "Detecting, diagnosing, and tolerating faults in SRAM-based Field Programmable Gate Arrays; a survey," *IEEE Transactions on VLSI Systems*, vol. 11, no. 3, June 2003.

[11] N. Goel and K. Paul, "Hardware controlled and software independent fault tolerant FPGA architecture," *15th International Conference on Advanced Computing and Communications, IEEE* 2007.

[12] N. Campregher, P. Y. K. Cheung, G. A. Constantinides, and M. Vasilko, "Yield modeling and yield enhancement for FPGAs using fault tolerant schemes," *International Conference on Field Programmable Logic and Applications*, 2005.

[13] J. Lach, W. H. Mangione-Smith, and M. Potkonjak, "Efficiently supporting fault-tolerance in FPGAs," *International Symposium on Field Programmable Gate Arrays*, pp. 105-15, 1998.

[14] F. Hanchek and S. Dutt, "Methodologies for tolerating cell and interconnect faults in FPGAs," *IEEE Transactions on Computers*, vol. 47, no. 1, pp. 15 – 33, 1998.

[15] J. Lach, W. H. Mangione-Smith, and M. Potkonjak, "Low overhead fault-tolerant FPGA systems," *IEEE Transactions on Very Large Scale Integration (VLSI) Systems*, vol. 6, no. 2, pp. 212 – 221, 1998.

[16] J. Emmert, C. Stroud, B. Skaggs, and M. Abramovici, "Dynamic fault tolerance in FPGAs via partial reconfiguration," *Field-Programmable Custom Computing Machines, 2000 IEEE Symposium* on 17-19 April 2000, pp.165 – 174.

[17] M. Ambramovici, C. Stroud, C. Hamilton, S. Wijesuriya, and V. Verma, "Using roving STARs for on-line testing and diagnosis of FPGAs in fault-tolerant applications," in *Proc. International Test Conference*, 1999.

[18] J. Emmert, C. Stroud, and M. Ambramovici, "Online fault-tolerance for FPGA logic blocks," *IEEE Transactions on VLSI*, 2007.

[19] Pratt, M. Caffery, P. Graham, K. Morgan, and M. Wirthlin, "Improving FPGA design robustness with partial TMR," *MAPLD* 2005.

[20] G. L. Smith and L. de la Torre, "Techniques to enable FPGA based reconfigurable fault tolerant space computing," *IEEEAC*, vol. 5, pp. 1592, 2006.

[21] P. Bernardi, M. S. Reorda, L. Sterpone, and M. Violante, "On the evaluation of SEU sensitiveness in SRAM-based FPGAs," in *Proceedings of the 10th International On-Line Testing Symposium* 2004.

[22] D. Fay, A. Shye, S. Bhattacharya, D. A. Connors, and S. Wichmann, "An adaptive fault-tolerant memory system for FPGA-based Architectures in the space environment," *Second NASA/ESA Conference on Adaptive Hardware Systems* 2007.

[23] *Xilinx Inc., XTMR Tool User Guide*, UG156, August 2006.

[24] Carmichael, "Triple module redundancy design techniques for Virtex FPGAs," Xilinx Corporation, November 2001, pp. 197.

[25] A. Jacobs, A. D. George, and G. Cieslewski, "Reconfigurable fault Tolerance: A framework for environmentally adaptive fault Mitigation in space," *IEEE* 2009.

[26] W.-J. Huang, S. Mitra, and E. J. McCluskey, "Fast run-time fault location in dependable FPGA-based applications," in *Proceedings of the 2001 IEEE International Symposium on Defect and Fault Tolerance in VLSI Systems (DFT'01).*

[27] J. Soto Vargas, J. M. Moreno, J. Madrenas, and J. Cabestany, "Implementation of a dynamic fault-tolerance scaling technique on a self-adaptive hardware architecture," *International Conference on Reconfigurable Computing and FPGAs*, 2009.

[28] A. Ahmadinia, C. Bobda, S. P. Fekete, J. Teich, and J. C. van der Veen, "Optimal free-space management and routing-conscious dynamic

placement for reconfigurable devices," *IEEE Transactions on Computers*, vol. 56, no. 5, May 2007.

[29] R. Cordone, F. Redaelli, M. A. Redaelli, M. D. Santambrogio, and D. Sciuto, "Partitioning and scheduling of task graphs on partially dynamically reconfigurable FPGAs," *IEEE Transactions on Computer-Aided Design of Integrated Circuits and Systems*, vol. 28, no. 5, May 2009.

[30] C. Steiger, H. Walder, and M. Platzner, "Operating systems for reconfigurable embedded platforms: online scheduling of real-time tasks," *IEEE Transactions on Computers*, vol. 53, no. 11, November 2004.

[31] Y. Lu, T. Marconi, K. Bertels, and G. Gaydadjiev, "A communication aware online task scheduling algorithm for FPGA-based partially reconfigurable systems," *18th IEEE Annual International Symposium on Field-Programmable Custom Computing Machines*, 2010.

[32] J. A. Clemente, C. González, J. Resano, and D. Mozos, "A hardware task-graph scheduler for reconfigurable multi-tasking systems," *International Conference on Reconfigurable Computing and FPGAs*, 2008.

Upasana Sharma received the M.Sc degree in Computer Science from the G.B. Pant University of Agriculture and Technology, Uttarakhand, India in 2000. She has worked on a research project on the devising of fault-tolerance techniques for reconfigurable platforms at Netaji Subhas Institute of Technlogy, New Delhi, India. She also carries a rich experience in software development and is currently a senior developer at Safenet (http://www.safenet-inc.com/) at its Noida (India) office.

Shampa Chakraverty is professor in the Computer Engineering Division at Netaji Subhas Institute of Technology, New Delhi, India. She completed her Bachelor's degree in Electronics and Communication ('83) from Delhi College of Engineering, MTech in Integrated Electronics and Circuits from IIT-Delhi ('92) and PhD in Computer Engineering from Delhi University, India. Her research interests include reconfigurable computing, design exploration for multiprocessor embedded systems, fault tolerant design, Information retrieval and complex adaptive systems.

Automated NFC Enabled Rural Healthcare for Reliable Patient Record Maintainance.

http://www.ncbi.nlm.nih.gov/pubmed/23138085

Sethia D, Jain S, Kakkar H.
Source
Department of Computer Engineering, Delhi Technological University, India.

Abstract

Body sensor networks can be used for health monitoring of patients by expert medical doctors, in remote locations like rural areas in developing countries, and can also be used to provide medical aid to areas affected by natural disasters in any part of the world. An important issue to be addressed, when the number of patients is large, is to reliably maintain the patient records and have simple automated mobile applications for healthcare helpers to use. We propose an automated healthcare architecture using NFC-enabled mobile phones and patients having their patient ID on RFID tags. It utilizes NFC-enabled mobile phones to read the patient ID, followed by automated gathering of healthcare vital parameters from body sensors using Bluetooth, analyses the information and transmits it to a medical server for expert feedback. With limited hospital resources and less training requirement for healthcare helpers through simpler applications, this automation of healthcare processing can provide time effective and reliable mass health consultation from medical experts in remote locations.

PMID: 23138085 [PubMed - in process]

In Vitro Micropropagation of Different species of Citrus

Kumar Gaurav[1*] and Srivastava Richa [2]
1. Department of Biotechnology, Delhi Technological University, Delhi-110042, INDIA
2. Department of Applied Chemistry and Polymer Technology,
Delhi Technological University, Delhi-110042, INDIA
* gauravbiotech@rediffmail.com

Abstract

In vitro approaches became necessary for overcoming the hurdles of cultivation of Citrus, a commercially important fruit. The present study deals with establishment of protocol for micropropagation of six different species of Citrus viz.Citrus sinensis, Citrus jambhiri, Citrus limonia, Carrizo citrange, Citrus limon and Citrus pectinifera via callus induction and regeneration. Leaf segments, epicotyl, shoot apex and axillary bud segments excised from in vitro raised seedlings were used as explants. The Explants were cultured on Murashige and Skoog medium (MS) containing 30 g/L sucrose and 8 g/L agar supplemented with different concentrations and combinations of different phyto-hormones; 6-benzylaminopurine (BAP), naphthalene acetic acid (NAA), 2,4-dichloro phenoxy acetic acid (2,4 D).

The maximum callus induction was observed from axillary bud of Citrus limonia observed on MS medium supplemented with 2,4 D (3 mg/L) followed by MS medium supplemented with BAP (3 mg/L). Maximum shoot regeneration response (75%) was observed on MS medium supplemented with BAP (3 mg/L) in Carrizo citrange. The in vitro regeneration system developed in this study can be used for effective propagation of selected genotypes and can be an ideal source of homogenous material for regeneration of genetically modified plants.

Keywords: Citrus, callus induction, shoot regeneration, tissue culture.

Introduction

Citrus, member of family Rutaceae refers to all edible and rootstock species and a few closely related genera such as lemons, oranges, grape fruits, kinnows and mandarins. They are grown throughout the world and are known for their fine flavor and quality. They have high nutritional value as good source of vitamin C[1]. The peel of some species also exhibits antimutagenic[2], anti-inflammatory[3,4], antioxidant[5,6], antitumor[7,8] and antiatherosclerosis[9,10] functions. They also contain volatile oils, limonene, α-terpinene, α-pinene, β-pinene, citral, coumarins, bioflavonoids, vitamins and mucilage. Moreover, the citrus industry is considered to be a major fruit industry[11].

Conventional propagation methods like budding and grafting are not only cumbersome and time consuming but also lead to virus transmission from mother plant to the propagated plants. They are also dependent on particular season and availability of plant material. For assuring the availability of Citrus plants throughout the year, plant tissue culture and micropropagation[12] can be considered as powerful tools and can be successfully used for the commercial production of microbe free[13,14]. Tissue culture technique involves various steps such as callus induction from explants, morphogenesis, shoot and finally root development to regenerate into a complete somaclone[15-21]. This is useful for the genetic improvement of fruit crops. Micropropagation offers rapid propagation of such crops in limited space and time under controlled conditions throughout the year.

The present study was conducted to identify the best type of explant from *in vitro* grown seedling for callus induction from different explants such as leaf, epicotyl, shoot apex, and axillary bud and then shoot regeneration from callus of different species of Citrus.

Material and Methods

Plant material and preparation of explants: The different species of Citrus (*Citrus sinensis, Citrus jambhiri, Citrus limonia, Carrizo citrange, Citrus limon* and *Citrus pectinifera*) were obtained from different regions of India. Explants (Leaf segments, epicotyl, shoot apex and axillary bud) were cut into appropriate size and washed in tap water thoroughly followed by rinse with dilute savlon solution for five minutes and finally with distilled water three times. These explants were surface sterilized with 0.1% (w/v) mercuric chloride ($HgCl_2$) solution for 5 minutes and rinsed with autoclaved distilled water 3-4 times in laminar flow hood.

The explants were cultured on MS medium[22] containing 30 g/L sucrose and 8 g/L agar supplemented with different phyto-hormones; 6-benzylaminopurine (BAP), naphthalene acetic acid (NAA), 2,4-dichloro phenoxy acetic acid (2,4D) (individually or in combination) with concentration of 0.5 to 5 mg/L. The pH of medium was adjusted to 5.7 using 1 N NaOH. Ten ml of medium was dispensed into glass culture tubes and finally autoclaved at 121^0C for 20 minutes. The inoculation was carried out in horizontal laminar flow hood that was thoroughly swabbed with alcohol and surface sterilized with UV light for 30 minutes prior to inoculation. The sterilized explants were inoculated on MS medium with different growth regulators. All the cultures were maintained at a temperature of 25± 2^0C under 16 h light/8 h dark.

Callus induction: Different explants like leaf, epicotyl, shoot apex and auxiliary bud were cultured on MS medium supplemented with different concentration of phyto-hormones viz. 2,4 D, BAP, NAA. Explants were aseptically inoculated on culture medium supplemented with different phyto-hormones. All the cultures were maintained at a 25± 2^0C under 16 h light/8 h dark. The effect of different treatments was observed visually and the observations were quantified on the basis of percentage of explants showing response for callus induction.

Shoot regeneration: Shoot regeneration from callus was performed in glass culture tubes containing 10 mL of MS medium containing 3% sucrose and solidified with 0.8% agar, having different concentrations of shoot-regenerating hormones individually or in combination. The healthy green portion of callus was taken and cut into pieces and these pieces were then placed on a shoot regeneration medium. The effect of different treatments was observed visually and the observations were quantified on the basis of percentage of calli showing response for shoot regeneration.

Results and Discussion

Callus induction: Plant system composed of highly organized tissue can be differentiated into mass of callus cells by manipulation of media. This has been accomplished in various cultivars of Citrus. In the present studies, the callus was successfully induced in *Citrus sinensis, Citrus jambhiri* and *Citrus limonia* using different seedling explants such as leaf, epicotyl and shoot apex. The callus induction was tried on MS medium with various combinations of growth regulators. The frequency of callusing varied with the explant and the composition of growth regulators in the medium .The details regarding the media used, extent of callus, color and type of callus after 4 weeks and 8 weeks of callus induction are given in table 1.

The lowest callus induction of leaf explant of *Citrus sinensis* was observed on MS medium supplemented with 2,4 D (3 mg/L) (Fig.1 A) followed by basal medium. It was interesting to note that in the leaf explant, the callus was initiated from leaf lamina and petiole. This is also supported by a report that in sweet orange (*Citrus sinensis*) the callus developed on MS medium supplemented with 2,4 D (1 mg/L) or NAA (1 mg/L)[23] and MS medium supplemented with BA (1 mg/L) +NAA (0.5 mg/L) was the most effective medium for callus induction in sweet orange (*Citrus sinensis*)[24].

Optimal callus induction of epicotyl of *Citrus jambhiri* was observed on MS medium supplemented with BAP (0.5 mg/L) and NAA (1 mg/L) followed by MS medium supplemented with 2, 4 D (3 mg/L) (Fig.1 B). The callus induction in *Citrus aurantifolia*[25] and *Citrus reticulate*[26] was maximum from epicotyl using MS media supplemented with BA (1.0 mg/L) and NAA (10.0 mg/L). The MS medium supplemented with 2,4 D (1.5 mg/L) was the best medium for callus induction for all type of explants (leaves, stem segments, cotyledons and roots) of rough lemon (*Citrus jambhiri* Lush), followed by MS medium supplemented with 2,4 D (1 mg/L)[27]. On the other hand it was found that MS medium supplemented with BA (1.0 mg/L) + 2,4 D (1.0 mg/L) + NAA (5.0 mg/L) was the best callus induction medium for full leaves in rough lemon (*Citrus jambhiri*)[28].

The best callus induction of axillary bud of *Citrus limonia* was observed on MS medium supplemented with 2,4 D (3 mg/L) (Fig. 1 C) followed by MS medium supplemented with BAP (3 mg/L). So, the MS medium supplemented with 2,4 D (3 mg/L) proved to the best medium for callus induction followed by MS medium supplemented with BAP (3 mg/L).The callus induction increases with increasing the concentration of 2,4 D and NAA in the media[29,30].

Shoot regeneration from callus: For shoot regeneration, indirect method was performed. It is known that different concentration of growth hormones significantly affects the shoot regeneration in Citrus plant[31]. BAP is effective in inducing *in vitro* morphogenesis in shoot regeneration and proliferation of several horticultural crops[32]. In the present study, healthy calli, cut into small pieces, were cultured on MS medium supplemented with BAP (3 mg/L) and (5 mg/L) as well as MS medium supplemented with BAP (0.5 mg/L + NAA 1 mg/L). The results of regeneration in different Citrus species (*Carrizo citrange, Citrus limon* and *Citrus pectinifera*) are given in table 2 and figure 2.

Maximum shoot regeneration response (75%) was observed on MS medium supplemented with BAP (3 mg/L) in *Carrizo citrange* (Fig. 2 A) followed by 55% on MS medium supplemented with BAP (0.5 mg/L) + NAA (1mg/L) in *Citrus pectinifera* (Fig.2 C). The minimum shoot response was 25% in *Citrus limon* on MS medium supplemented with BAP (5 mg/L) (Fig.2 B). Regeneration of different species of Citrus has been already investigated using MS medium supplemented with BAP (3 mg/L) or with BAP (1 mg/L)[33,34]. The shoot regeneration at BAP from 0.5 – 4 mg/L was the best at 2 mg/L for *Citrus paradise* (Macf) epicotyl explants[35].

The direct (stem explant) and indirect (callus) methods were employed for shoot regeneration in MS medium supplemented with BAP 3 mg/L on rough lemon (*Citrus jambhiri* Lush)[27]. The BAP induced shoots in undifferentiated callus in *Citrus grandis*[36]. MS medium supplemented with BAP (2.22 µM) was effective in multiple shoot induction from nucellar embryo in *Citrus limonia* Obseck[37]. It is also known that MS medium supplemented with BA (3 mg/L) + NAA (2 mg/L) produces the maximum number of shoot in *Citrus sinensis*[24] where shoot tip explants cultured in MS media supplemented with BAP (1 mg/L) and Kinetin (1.5 mg/L) showed highest shoot percentage[38]. The average length of regenerated shoot

was highest in calli culture on MS medium supplemented with NAA (0.5 mg/L), Kinetin (0.5 mg/L), and BA (1.0 mg/L) in *Citrus jambhiri*[28]. BAP (1mg/L) and GA_3 (2 mg/L) in MS medium showed maximum shoot regeneration in *Citrus depressa*[39].

Conclusion

The present study describes the protocol for micropropagation of six different species of Citrus and it is concluded that these methods hold a great potential for its clonal propogation via callus induction and regeneration. Leaf segments, epicotyl, shoot apex and auxiliary bud segments excised from in vitro raised seedlings were used as explants. The responses of all the Citrus varieties on the three callus induction media were variable. This protocol may be used in Citrus genetic improvement programs and may find application in the development of new hybrids reducing the propagation time in respect to conventional methods.

References

1. Nwaoguikpe R.N. and Braide W., Some Fruit Juices as Environmental Sickling Agents, *World J Med Sci*., **5**, 98-104 **(2010)**

2. Kootstra A., Protection from UV-B-induced DNA damage by flavonoids, *Plant Mol Biol*., **26**, 771-774 **(1994)**

3. Lin N., Sato T., Takayama Y., Mimaki Y., Sashida Y., Yano M. and Ito A., Novel anti-inflammatory actions of nobiletin, a citrus polymethoxy flavonoid, on human synovial fibroblasts and mouse macrophages, *Biochem Pharmacol*., **65**, 2065-2071 **(2003)**

4. Emim J.A., Oliveira A.B. and Lapa A.J., Pharmacological evaluation of the anti-inflammatory activity of a citrus bioflavonoid, hesperidin and the isoflavonoids, duartin and claussequinone, in rats and mice, *J. Pharm Pharmacol.*, **46**, 118-122 **(1994)**

5. Benavente-García O., Castillo J., Marin F.R., Ortuño A. and Del Río J.A., Uses and properties of *Citrus* flavonoids, *J. Agric. Food Chem.*, **45**, 4505-4515 **(1997)**

6. Majo D.D., Giammanco M., Guardia M.L., Tripoli E., Giammanco S. and Finotti E., Flavanones in Citrus fruit: Structure–antioxidant activity relationships. *Food Res. Int.*, **38**, 1161-1166 **(2005)**

7. Bracke M.E., Vyncke B.M., Van Larebeke N.A., Bruyneel E.A., De Bruyne G.K., De Pestel G.H., De Coster W.J., Espeel M.F. and Mareel M.M., The flavonoid tangeretin inhibits invasion of MO4 mouse cells into embryonic chick heart in vitro, *Clin Exp Metas*., **7**, 283-300 **(1989)**

8. Bracke M., Vyncke B., Opdenakker G., Foidart J.M., Pestel G.D. and Mareel M., Effect of catechins and citrus flavonoids on invasion in vitro, *Clin. Exp. Metas.*, **9**, 13-25 **(1991)**

Table 1
Callus induction response of A) *Citrus sinensis*; B) *Citrus jambhiri* and C) *Citrus limonia* on different media.

Age of culture (weeks)	Media used	Differentiation of callus	Callus color	Type of callus
A) *Citrus sinensis* (explant used: leaf)				
4	MS+ 2, 4 D (3 mg/L)	No	No	-
8	MS+ 2, 4 D (3 mg/L)	Yes	Light brown	Friable
12	MS+ 2, 4 D (3 mg/L)	Yes	Dark brown	Friable
16	MS	Yes	Dark brown	Friable
20	MS	Yes	Dark brown	Nodular
24	MS	Yes	Dark brown	Compact, nodular
B) *Citrus jambhiri* (explant used: epicotyl)				
4	MS + BAP (0.5 mg/L) + NAA (1 mg/L)	No	No	-
8	MS + BAP (0.5 mg/L) + NAA (1 mg/L)	Yes	Green	-
12	MS + 2, 4 D (3 mg/L)	Yes	Greenish brown	Friable
16	MS	Yes	Greenish brown	Friable
20	MS	Yes	Greenish brown	Nodular
24	MS	Yes	Greenish brown	Compact, nodular
C) *Citrus limonia* (explant used: shoot apex)				
4	MS+ 2, 4 D (3 mg/L);	No	No	-
8	MS+ 2, 4 D (3 mg/L);	Yes	Green	-
12	MS+ BAP (3 mg/L)	Yes	Creamish brown	Semi friable
16	MS+ BAP (3 mg/L)	Yes	Light brown	Compact, nodular
20	MS+ BAP (3 mg/L)	Yes	Light brown	Compact, nodular
24	MS+ BAP (3 mg/L)	Yes	Light brown	Compact, nodular

Table 2
Shoot regeneration response of A) *Carrizo citrange*; B) *Citrus limon* and C) *Citrus pectinifera*

Age of culture (week)	Media used	Shooting	Average number of shoots /explant	Leaf morphology	Color of leaves and shoots	Vitrific-ation response
A) *Carrizo citrange* (explant used: axillary bud)						
4	MS+BAP (3 mg/L)	Yes	11	The leaves were hairy with normal lamina	Green	No
8	MS+ BAP (3 mg/L)	Yes	13	The leaves were expanded lamina and curved	Dark green	No
12	MS	Yes	16	The leaves were in normal sized	Dark green	No
16	MS	Yes	20	The leaves were in normal sized	Dark green	No
20	MS	Yes	23	The leaves were in normal sized	Dark green	No
24	MS	Yes	24	The leaves were in normal sized	Dark green	No
B) *Citrus limon* (explant used: axillary bud)						
4	MS+ BAP (5 mg/L)	Yes	7	The leaves were cyli-ndrical and elongated	Dark green	No
8	MS+ BAP (5 mg/L)	Yes	9	The leaves were cylindrical,elongated, slightly large in size and hairy	Dark green	No
12	MS	Yes	10	Yellowing of leaves after 10 weeks	Dark green	No
16	MS	Yes	12	Leaves became pale green	Dark green	No
20	MS	Yes	12	Leaves became pale green	Dark green	No
24	MS	Yes	12	Leaves became pale green	Dark green	No
C) *Citrus pectinifera* (explant used: shoot apex)						
4	MS+ BAP (0.5 mg/L) + NAA (1 mg/L)	Yes	8	The leaves were cylindrical and elongated	Dark green	No
8	MS+ BAP (0.5 mg/L) + NAA (1 mg/L)	Yes	10	The leaves were cylindrical,elongated, slightly large in size and hairy	Dark green	No
12	MS	Yes	12	The leaves were cylindrical,elongated, slightly large in size and hairy leaves became pale green	Dark green	No
16	MS	Yes	15	Leaves became pale green	Dark green	No
20	MS	Yes	18	Leaves became pale green	Dark green	No
24	MS	Yes	18	Leaves became pale green	Dark green	No

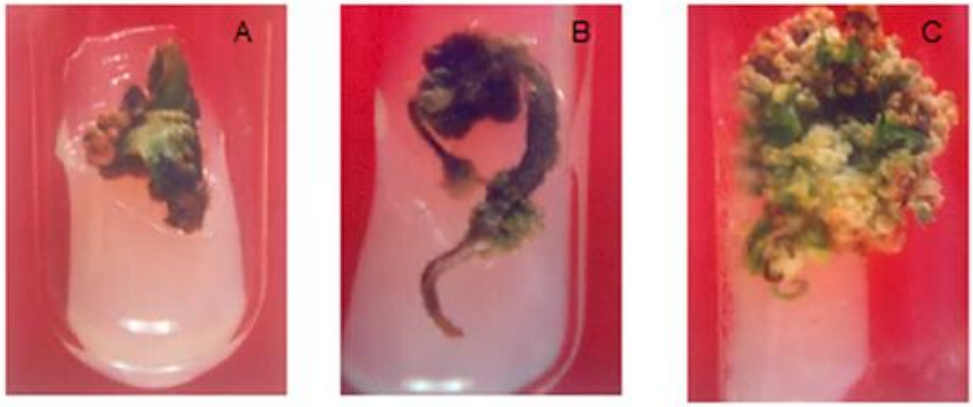

Figure 1 : A) Callus response of leaf explant (*Citrus sinensis*) on MS medium supplemented with 2,4 D (3 mg/L); B) Callus response of epicotyls explant (*Citrus jambhiri*) on MS medium supplemented with BAP (0.5 mg/L) + NAA (1 mg/L) followed by MS medium supplemented with 2,4 D (3 mg/L); C) Callus response of shoot apex plant (*Citrus limonia*) on MS medium supplemented with 2,4 D (3 mg/L) followed by MS medium supplemented with BAP(3 mg/L).

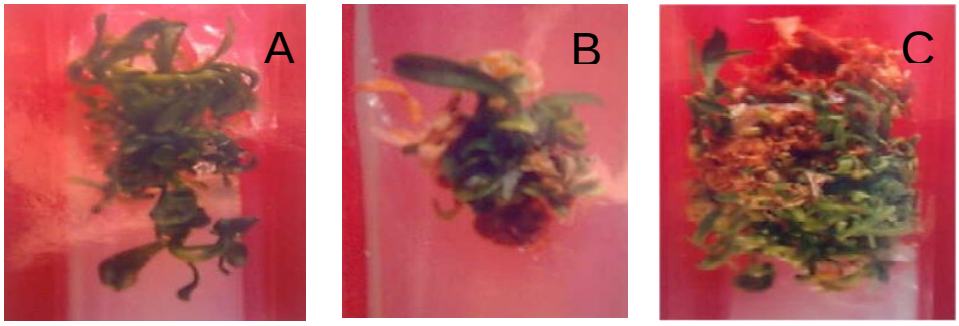

Figure 2: Shoot regeneration response in A) *Carrizo citrange* from calluson MS medium supplemented with BAP (3 mg/L); B) *Citrus limon* from callus on MS medium supplemented with BAP (5 mg/L); C) *Citrus pectinifera* from callus on MS medium supplemented with BAP (5 mg/L) + NAA (1 mg/L).

9. Hertog M.G., Feskens E.J., Hollman P.C., Katan M.B. and Kromhout D., Dietary antioxidant flavonoids and risk of coronary heart disease, the Zutphen Elderly Study, *Lancet*, **342**, 1007-1011 **(1993)**

10. Manach C., Regerat F., Texier O., Agullo G., Demigne C. and Remesy C., Bioavailability, metabolism and physiological impact of 4-oxo-flavonoids, *Nutr Res*., **16**, 517-544 (**1996**)

11. Chaturvedi H. C., Singh S. K., Sharma A. K. and Agnihotri S., Citrus tissue culture employing vegetative explants, *Indian J. Exp. Biol*., **39**, 1080-1095 **(2001)**

12. Honda H., Liu C.Z. and Kobayashi T., Large-scale plant micropropagation, *Adv. Biochem. Eng. Biotech*., **72**,158-182 **(2001)**

13. Parmessur Y.S., Alijanabi S., Saumatally S. and Dookun-Samutually A., Sugarcane yellow virus and sugarcane yellow phytoplasma: elimination by tissue culture, *Plant Pathol*., **51**,561-569 **(2002)**

14. Liao Z., Chen M., Tan F., Sun X. and Tang K., Micropropagation of endangered Chinese Aloe, *Plant Cell, Tissue Organ Cult*., **76**, 83-86 **(2004)**

15. Al-Khayri J.M. and Al–Bahray A.M., In vitro micropropagation of *Citrus aurantifolia* (Lime), *Curr. Sci.*, **81**, 1242- 5 (**2001**)

16. Filho J.C.B., Kobayashi A.K., Peirera L.F.P., Hissano Z. and Vieira L.G.E., In vitro adventitious shoot regeneration from sweet orange using thin epicotyl sections, *Crop Breed. Appl. Biotech*., **1**, 27-34 **(2001)**

17. Usman M., Muhammad S. and Fatima B., In vitro multiple shoot induction from nodal explants of *Citrus* cultivars, *Jour. of Centr. Europ. Agri.*, **6**, 435- 442 **(2005)**

18. Altaf N., Khan A.R., Bhatti I.A. and Ali L., Tissue culture of citrus cultivars, *Electronic Jour. Environ. Agri. Food Chem*., **8**, 43-51 **(2009)**

19. Khan E.H., Fu X.., Wang, J., Fan Q., Huang X., Zhang, G., Shi, J. and Liu, J., Regeneration and characterization of plants derived from leaf *in vitro* culture of two sweet orange (*Citrus sinensis* (L.) Osbeck) cultivars, *Scien. Horticul.*, **120**, 70-76 **(2009)**

20. Laskar M.A., Hynniewta M. and Rao C.S., *In vitro*

propagation of *Citrus indica* Tanaka- An endangered progenitor species, *Indian Jour.Biotech*., **8**, 311-316 **(2009)**

21. Sharma S., Prakash A. and Tele A., *In vitro* propagation of *Citrus* rootstocks. *Notulae Botanicae Horti Agrobotanici Cluj-Napoca*, **37**, 84-88 **(2009)**

22. Murashige T., and Skoog F., A revised medium for rapid growth and bioassays with tobacco tissue culture, *Physiol. Plant*, **15**, 473-497 **(1962)**

23. Das A., Paul A. K. and Chaudhuri S., Micropropagation of sweet orange (*Citrus sinensis* Osbeck) for the development of nucellar seedlings, *Indian J. Exp. Biol*, **38**, 269-272 **(2000)**

24. Khalil S.A., Zamir R., Ahmad N., Sajid M., Fazal H., Khan M.A., Seema N. and Alam R., In vitro regeneration of plantlets from unpollinated ovary culture in sweet orange (*Citrus sinensis* L. Osbeck), *African J. Biotech*., **10**, 15130-15134 **(2011)**

25. Kamble A. B., More T. A. and Patil R. S., In vitro micropropagation and callus induction of acid lime cv. Sai Sharbati, *South Indian Horticulture*, **50**, 329-334 **(2002)**

26. Khan J. A., Jaskani M. J., Haider A. and Khan M. M., Effect of light and dark culture conditions on callus induction and growth in citrus (*Citrus reticulata* Blanco.), *International Journal of Biology and Biotechnology*, **3**, 669-672 **(2006)**

27. Ali S. and Mirza B., Micropropagation of rough lemon (*Citrus jambhiri* Lush.): Effect of explant type and hormone concentration, *Acta Botanica Croatica*, **65**, 137-146 **(2006)**

28. Kumar K., Kaur H., Gill M.I.S., Rattanpal H.S. and Kanika Gosal S.S., An efficient regeneration protocol from callus culture in rough lemon (*Citrus jambhiri*), *Indian J. Agri. Sci*., **81**, 324-329 **(2011)**

29. Gitarani G.S.V. and Vinash N.A., Callus induction and Plantlet regeneration in Sweet orange (*C. sinensis* L.) and Lime (*C. aurantifolia*), *In vitro, Cell and Developmental Biol*., **39**, 468-474 **(2003)**

30. Haoa Y.J., Wen X.P. and Deng X.X., Genetic and epigenetic evaluations of citrus calluses recovered from slow-growth culture, *J. Plant Physiol*., **161**, 479-484 **(2004)**

31. Vestri F., Schiff S. and Bennici A., In vitro shoot regeneration in rough lemon (*C. jambheri* Lush), *In Vitro, Cell and Dev. Biol.*, **39**, 586-594 **(2003)**

32. Chikhale N.J., Karwa A.S. and Rai M.K., In vitro induction of multiple shoots and roots in *Citrus reticulata* Blanco, Proc. Intl. Conf. of SAARC Countries on Biotechnology, Karad, 30-32 **(2002)**

33. Cervera M., Ortega C., Navarro A., Navarro L. and Pena L., Generation of transgenic citrus plants with tolerance-to-salinity gene *HAL2* from yeast, *J. Hort. Sci. Biotechnol*., **75**, 26-30 **(2000)**

34. Dominguez A., Guerri J., Cambra M., Navarro L., Moreno P., and Pena L., Efficient production of transgenic citrus plants expressing the coat protein gene of citrus tristeza virus, *Plant Cell Rep.*, **19**,427-433 **(2000)**

35. Costa M.G.C., Otoni W.C. and Moor G.A., An elevation of factors affecting the efficiency of *Agrobacterium*-mediated transformation of *Citrus paradisi* (macf.) and production of transgenic plants containing carotenoid biosynthetic genes, *Plant Cell Reproduction*, **21**, 365-373 **(2002)**

36. Begum F., Amin M.N., Islam S., Azad M.A.K. and Rehman M.M., In vitro plantlet regeneration from cotyledon derived callus of three varieties of pummelo (*Citrus grandis* (L.) Osb.), *Online J.Bio.Sci*., **3**,751-759 **(2003)**

37. Jajoo A., In vitro Propagation of *Citrus limonia* Osbeck Through Nucellar Embryo Culture, *Curr. Res. J. Bio. Sci*., **2**, 6-8 **(2010)**

38. Mukhtar R., Khan M.M., Rafiq R., Shahid A. and Khan F.A., *In Vitro* Regeneration and Somatic Embryogenesis in (*Citrus aurantifolia* and *Citrus sinensis*), *Int. J. Agric. Biol*., **7**, 518-520 **(2005)**

39. Gill M.I.S. and Gosal S.S., Micropropagation of Pectinifera (*Citrus depressa* Hayata)- A potential citrus rootstock for sweet orange, *Indian J. Citriculture*, **1**, 32-37 **(2002).**

(Received 13th June 2012, accepted 28th September 2012)

Indian Continuing Engineering Education: Challenges and Opportunities

Seema Singh
Department of Humanities
Delhi Technological University
Delhi- 110 042, India

Abstract

Indian Continuing Engineering Education was designed to hone the skills of employed engineers but after initiation of Liberalisation, Privatisation and Globalisation (LPG), nature and structure of employment among engineers have changed. On the basis of responses of CEE students of two surveys, successively done with a gap of a decade, reveals that students enrolled in CEE (academic institution) do not look for linear career progression as it may be the case before opening up of the economy, in fact, they want to get optimal career benefit. Those engineers who pursue CEE for career enhancement prefer to enrol in an engineering institute, but depend on ICT if they are looking to acquire knowledge. There is need to converge both. Faculty and students need to be given opportunity to develop cost-effective CEE module which can be delivered through ICT. The paper also discusses developing engineers for global workforce, to incorporate green technology and to enhance R&D and innovation in the curricula, as main challenges before CEE. Working engineers also need to be sensitised about technological need of deprived group in the society for inclusive growth. These challenges can be transformed into opportunities if engineering institutions work along with corporate sector and professional societies.

Keywords
Continuing Engineering Education, Globalisation, ICT, Growth, Green Technology

1. Introduction

A knowledge economy requires high quality and universal education system from early childhood to highest level of tertiary education and extended into life-long learning opportunities for workers. But Continuing Engineering Education (CEE) has special significance as it is crucial for technical manpower to hone their skills. It was well realised by planners and policy makers and was in place in India. However, changes in macroeconomic variables as liberalisation, globalisation, privatisation (LPG), and advent of information and communication technology (ICT) have drastically changed the scenario. Technology is continuously being upgraded by the firm to enhance quality of products and productivity of resources to sustain in the market. Any such change/ improvement in the existing technology ultimately changes the set of skills required to handle them and hence forth, engineering manpower needs to be re-trained through CEE to remain employable. Added to it, ICT has provided another mode of providing training through CEE. In this background, the paper tries to count challenges which Indian CEE system is facing in the changed environment and how these challenges can be transformed into opportunities. Second section of the papers throws light on emerging pattern of employment among engineers in context of LPG and advent of ICT. Third section of the paper gives brief review of CEE in India. Fourth and fifth section discusses challenges before Indian CEE system in the emerging economic environment and how these challenges can be transformed into opportunities. Last section concludes the discussion.

2. Effect of Liberalisation, Privatisation and Globalisation (LPG) and Advent of ICT on Employment of Engineers

LPG has led to reduction in restrictions on movement of goods, services and capital through reduced transport and production cost all-round. The new technology has made capital mobile and has increased its bargaining strength in relation to labour and the state (Deshpande et.al., 2004). Again, ICT has made it possible to shift a particular segment of the production process to a far-off place if it can be performed in a cost-effective way. This situation has given an opportunity to the Multinational Corporations (MNCs) to shift their labour intensive work to India as India has a large pool of comparatively cheap English speaking engineers. MNCs are bringing new technology and large amount of investment with them which has ultimately made the market very competitive. To survive in the market, firms are continuously upgrading technology. However, any such change makes

corresponding change in the skill set required among engineers. Not only that, LPG has also affected nature and structure of employment among engineers[1] also.

Table1: Comparison between Pattern and Employment Structure among Engineering Manpower before and after implementation of LPG in India

Sl. No	Before Initiation of LPG in the Indian Economy i.e. before1991	After Initiation of LPG in the Indian Economy i.e. after 1991
1.	Government sector/ Public sector was major employer which is considered as formal employment, was major employer	After globalisation, informality has increased. Share of formal sector employment is decreasing in favour of the informal sector. At present, only seven percent of total employment is in formal sector which is secured and formatted.
2	Generally, there was one time employment in the career.	After globalisation and liberalisation, opportunities for engineering manpower have increased. Most of them are practicing job hopping. Every other year they are changing job.
4	Employment of graduate and diploma holders was clearly demarcated.	The demarcation has become fuzzy.
5	Government sector/ public sector were higher paying sector and private sector jobs were lower paying.	Now, the employment structure can be compared as 'small o' surrounded by 'big U'. 'small o' represents government sector/ public sector and the surrounding U represents private sector which may be higher paying than the government sector as well as lower paying (Singh, 2005).

Source: Compiled by Author

Originally, engineers use to be employed (refer Table-1) in two sectors i.e. formal and informal. While formal sector provides protection under various Government provisions, the informal sector provides almost none. If taken two indicators, salary and social security, these two sectors provides just opposite situation. While the formal sector use to provide high salary as well as high social security, the informal sector provides low in terms of both indicators. The newly added MNCs has added a distinctly different work structure. They provide low security, which is more than compensated by very high salary. In the present scenario, MNCs have been able to attract the preference of engineering manpower over the formal sector. Formal sector is generally considered as safety valve of last resort. Initial salary in private sector, public sector/ government sector and MNCs are distinctly different and in the ratio of almost 1:2:4-5 (Singh & Thankachan, 2005). Now, the employment structure of engineers can be compared as 'small o' surrounded by 'big U'. 'Small o' represents government sector/ public sector which may be higher paying than the government sector as well as lower paying (Singh, 2005). Along with it, different form of atypical employment are also coming into practice. Short-term contracts, marginal part-time work, new forms of employment, in- and out sourcing and tele-works are representative of the changing nature of employment in the informal sector (Singh, 2008). Manager, generally, initiate changes in the firms' employment relation practices to improve a firms' performance based on their knowledge and experience. Changes in the post-reform period indicate a 'paradigm shift' in the belief and practices of managers that contrast distinctly from those that exited until the mid-1980s and before. The shift involves wide ranging changes in the areas of skills/multi-skill function), functional integration (from specialized to generalization, employee-control (flexible) and work culture. On the other hand, engineers both degree as well as diploma holders are also ready to explore new avenues in their career. For them, job choice is driven by a desire to achieve higher position in the 'labour market' rather than 'employment' security through robust employable skills and good access to ongoing opportunities (ILO, 2001) However, engineers will be able to explore all the avenues only if they will achieve qualitative continuous training (Singh & Thankachan, 2005).

3. Review of State of Continuing Engineering Education in India

To overcome obsolesce of working engineer, a number of academic institutions, professional bodies and industrial organisations offer continuing engineering education in India. However, CEE through academic institutions has special significance due to its wide acceptability, transferability and universal format.

3.1 CEE offered by Academic Institutions

Jawaharlal Nehru Technological University, Hyderabad was the first university to start continuing engineering education programme at degree level (B E / B. Tech.) in engineering subjects. A School of Continuing and Distance Education was set up in 1983 which started B. Tech. programme in civil, Electrical & Communication and Mechanical engineering. Since then, many institutions have started programme at Degree and Diploma level through 'face-to-face'[2] mode as part-time programme as well as 'distance'[3] mode. At present, there are 44 degree level institution with intake capacity 9247 and 58 diploma level institution with intake capacity of 7222. In the beginning, training was given in the traditional branches as Mechanical, Civil and Electrical engineering but Computer engineering is an addition during post globalised period. However, there are branch wise as well as regional variations. At the degree level, only 1.3% seats are in Eastern State, 22% seats are in Western states, 57% seats are in Southern states and rest of the seats are in Northern states. Not only that, some of the states which are industrially very active have very low intake capacity as in Gujarat or not at all as Punjab and Haryana. Branch wise also, more than one-third of the total intake capacity is in civil engineering (34%) which is followed by mechanical engineering (21%). So, civil and mechanical together have almost sixty percent of the intake capacity and both the branches are being taught in all the states where the facility is available. Rest of the braches in which facility is available are electrical engineering (18%), Electronics engineering (13%), computer engineering (7%) and others (5%). Facility for CEE at diploma level is almost 20% less than degree level. If discusses region wise, almost two-third facility is available at Western region and very low in rest of the three regions which are eastern region (16%), 14% northern region and only 4% in the southern region. If discussed branch wise, mechanical engineering constitute of same percentage as at degree level (i.e. 21%) but contrary to degree level, civil engineering only constitute 12 %. Electronics engineering constitute is highest intake capacity (39%) but electrical and computer are as low as 14% and 3%. Others which include branches like chemical, mining, metallurgy, production, textile etc. It constitutes 11% of the intake capacity (Kumar, 2004).

After initiation of the economic reform programme in 1991, a substantial displacement of organised sector workers was envisaged by the Government of India (GoI). The Industrial Policy in 1991 recognised the possibility and was obliged to protect the interest of labour, enhance their welfare and equip them in all respect to deal with the inevitability of technological change. A National Renewal Fund (NRF) was launched to protect the workers from adverse consequences of technological transformation, provide retraining to them, so that they are in a position to remain active productive partners in the process of modernization (GoI, 1998). However, as the year progressed, CEE has lost some of its significance in favour of Engineering Education (EE) (regular). From, 197-98 onwards, engineering education has experienced exponential growth but CEE has remained almost stagnant. This may be driven by the objective to get the advantage of 'demographic dividend'[4] (Singh, 2012.a). Skill formation is one of the key areas. National Skill Development Fund (NSDF) is in place and in the Union Budget for 2012-13, the allocation under NSDF has almost been doubled. A Credit Guarantee Fund for Skill Development has also been launched. The Finance Minister has also provided tax benefit to the manufacturer for costs incurred in talent development and has exempted vocational training institution from service tax (Mukharjee, 2012).

3.2 Micro Level Survey to study Students' Response of CEE

In marketing parlance, students are buyer and consumer of the services provided by institution and universities. So, their feedback is very important, time-tested and being used all over the world for continuous improvement of the system. This section discusses two such studies which has been made with the gap of 10 years. First evaluation of CEE system is based on responses of 327 part-time B.Tech. students at Delhi College of Engineering (upgraded to Delhi Technological University (DTU) in 2009), Delhi in 2001 which has highlighted that the courses under CEE are long in terms of duration and obsolete in terms of content. As the first year course, mainly consist of those topics, which the students have already done at the diploma level. So, the duration may be made of three years in place of four years at the degree level. Majority of the students opined that latest computer language should be incorporated in their course curricula. Again, majority of the students consider the course coverage as partial. They suggested that to maintain continuity and to enhance the quality of teaching more permanent teachers should be recruited. Guest faculty should be invited only for very specific topic. Though majority of the students were satisfied with the system of examination, but they were concerned about the delay in the examination's result. Academic calendar should be announced well in advance and it

should be maintained. Better library facility and industrial trips should be arranged for the part-time students. They should also get chance to appear for placement through campus placement (Singh and Kumar, 2003). In the second study[5] (Singh, 2012.b), responses from the CEE students of Delhi Technological University (DTU) reveals that though the CEE structure is even now of the same duration but the content has been changed and upgraded. Library and book bank facilities have been improved. But even now, the students have shown their concern about quality of teaching. Again they have emphasized that that their teaching should be made by permanent faculties. However, they do not get opportunity for innovation and R&D. They do not get facilities of campus placement[6] which a student of EE (regular) may be getting. These opportunities are not being given as CEE is based on the hypothesis that the students are already employed and their are acquiring degree for upward movement in the organisational ladder. Some flexibility in terms of duration but with fixed content has been introduced but maximum is eight years in Indira Gandhi National Open University (IGNOU). The enrol student has to complete the degree within eight years. In an answer to the question that why they have opted for 'face to face' method from a famous engineering college rather than a course through ICT, they opined that (answers are chronologically arranged as per its preference given by the student):

0 Acceptance by the employer:

At the time of giving promotion, employers give preference to CEE course done through face to face method rather than any other mode.

0 Cost components:

There are some courses which are already being offered at exorbitant cost. But the respondent have preferred university for its cost-effectiveness.

0 To acquire knowledge:

The respondents have given least preference to the reason for acquiring knowledge to enrol in the course.

3.3 Training through Information and Communication Technology (ICT)

Advent of ICT has given an additional mode for imparting training which overcomes the constraint arising due to distance, language or availability of free time and it is being used in much innovative way by various service providers. To provide adequate infrastructure, even the Government of India has launched EDUSAT, an exclusive satellite for educational purpose. to impart training in a very cost effective quality educational resources in an inclusive manner. Flexibility in terms of duration but with fixed content has been introduced by Indira Gandhi National Open University (IGNOU). There is a special channel of IGNOU, 'Gyan Darpan' to impart training. Various global educational service providers are also in the business, providing services at a very exuberant cost.

In fact, laptop with internet connection has become a symbol of awareness and knowledge. Many engineering institution gives laptop all enrolled students at the time of admission. Many instates have Wi-Fi connection and many more claims that they have. A study of fifty engineer consultants in the area of construction to study how they acquire knowledge about green technology reveals that internet is the mode through which they acquire knowledge about latest development (Singh, 2011). The latest mindset is reflected in the election campaign also. In latest Vidhan Sabha (lower house in the bi-caramel state legislative) election in Uttar Pradesh, the winning party has promised laptop to all youth if they come to power[8] .

4. Challenges before Continuing Engineering Education in the era of LPG

Two broad trends have emerged in CEE system during the era of LPG. They are as i. The students enrolled in CEE (academic institution) do not look for linear career progression rather they want to get optimal career benefit from the opportunity and ii. All those who pursue CEE for career enhancement prefer to take route of engineering institute, but to acquire knowledge, professional engineers follow route through ICT. The challenges which have emerged before CEE may be discussed as follows:

4.1 Preparing Engineers for Global Work Place

With growing number of Multinational and Transnational Corporation, both- Indian and foreign, working in a Multinational and Transnational enterprise has become a normal experience for Indian engineering manpower. So, once working in a gender-neutral team was an issue, Indian engineers is now preparing themselves to work

in cross-cultural team which may be separated by continent which means, they have to learn to overcome time zone also.

4.2 Enhancing R&D and Innovations in the Curriculum

When geographical boundaries have lost its significance and economic boundaries have become fuzzy, technological superiority is going to give the edge to any enterprise. R&D and innovation has become buzz word and any CEE programme must concentrate to incorporate it in the curriculum. Only point of satisfaction is the increasing intake capacity in M. Tech. and Ph.D. is giving to do research activity in CEE.

4.3 Sensitizing towards Green Technology

Unsustainable use of technology and ruthless plundering of natural resources to achieve high economic growth has brought us on the edge. The damage caused to the natural resources has grim consequences and one of them is climate change. The achievement of sustainable development remains the greatest challenges before humanity today. Countries including India, are incorporating sustainable development policies into their development agenda. The essential task of development is to design and implement policies and programmes which encourage the efficient use of resources and adopt technologies that lead to less environmental harm which is intricately linked to labour force skills. There is growing demand for smart buildings and infrastructure. The Indian CEE system should be prepared to impart training in green technology because professional engineers may not have learnt these skills during their engineering degree or diploma curriculum.

4.4 Poverty Eradication and Inclusive Growth

Traditionally, engineering manpower in India was developed to work in industry to enhance productivity. However, it is being realised lately that engineers are not only required to enhance industrial productivity but to improve life of poor and deprived. It is well known fact that poor cannot afford to remain unemployed they work whatever they get. But as their productivity is very low, their earning is low and it is a vicious circle. Poor earn less, have less healthy and nutritious meal to eat and good environment to live which leads to health problem, have lower working capacity and thus, ultimately get employment in low productive work. The LPG has deteriorated condition of the poor. The gap between earning of lowest 10 per cent and highest 10 percent population has grown from six times to twelve times. Planners and policy makers in India are quite concerned about the situation. In eleventh five year plan (2007-12) and again in, the twelfth five year plan (2012-17) has been designed to achieve inclusive growth. The engineers need to be sensitized about problems of poor people and should work for imparting technological help which can improve life of poor and brought them to better life standard than before. This type of sensitition to the professional engineers can be planned through CEE programme.

4.5 Providing Cost-Effective CEE

A good number of renowned universities and institutions are providing CEE programme at an exorbitant cost. However, the problem is of affordability. Not many will be able to upgrade/ enhance their knowledge if the cost is very high. Not only in India but such demand is from many countries of Latin America, Africa, Middle East countries. Or in this phase of global melt down, low-cost is the buzz word throughout the world and the challenge is to provide good quality courses at a reasonable prices.

5. How to Turn Them as Opportunities

During the LPG period, nature and structure of employment among engineers has changed which has posed challenge before CEE to enhance their skills in the emerging economic environment. At the same time, India has certain advantage in the area of CEE, as large pool of English speaking Engineers who are also very good in mathematics and computing. Now, the task before CEE is to transform these challenges into opportunities.

5.1 Revamping of CEE

The engineering institution need to come out from the mindset for linear career growth for CEE students. They need to be given all the opportunities which may have been given to EE (regular) students which must include sufficient opportunity regarding green technology, innovation and R&D. Again, engineering institutions are giving emphasis on cross-cultural fabric to its campus. In fact number of foreign nationals in the campus is one of the indicators on which engineering institutions are ranked.

ICT should not be seen as substitute but of ‘face 2 face’ mode but, it should compliment it. All possible use of ICT should be introduced. The faculties and students entrepreneur should be encouraged

to develop cost effective training modules. A group of alumina of DTU has developed a web site, 'agla sem.com' which has all past question papers, notes, most relevant book etc.

5.2 Involving Corporate Sector

To sustain in the competitive environment, corporate sector is involving more in the activities of engineering education than ever before. Their association with engineering institutions has taken a new dimension. moved ahead from being part of Board of Directors, Board of Management or Board of studies of engineering institutions is very common practice. They are playing very effective role in the are signing agreement with the engineering institution/ university to train their employees. Samsung has signed an agreement with the computer engineering department of Delhi Technological University to train its employees in Post-Graduate Programme in Computer engineering. ICICI Bank has signed MoU with ten good engineering colleges (Delhi Technological University is one of them) for development of technology which will benefit the banking processes. Many CEO of Corporate bodies are member of Board of Studies and Board of Management of various engineering institution/ universities throughout the country.

Some of the engineering colleges and engineering universities are signing Memorandum of understanding (MoU) with foreign universities where students stay in India and in other country to complete their degree. However, this is done for engineering education (EE)(regular) courses rather than CEE course. Now, CEE through academic institution and through societies needs to proceed in this direction. As the CEE students are presumably employed, so corporate sector already come in the picture. These days, many of the corporate bodies are in education sector, they introduce this arrangement in CEE by involving their international partners. Corporate houses, as L'Oreal is funding projects for development of eco-friendly technology (Singh, 2011)

5.3 Involving Professional Societies

The Institution of Engineers (IoE) is already involved in CEE programme. Study shows that students are getting benefit of these opportunities spread all over India and some centres are abroad also. For environmental management, International Federation of consulting Engineers (FIDIC acronym), Institute of Electrical and Electronics Engineer (IEEE) are other intgernational bodies for engineers which has developed standards and conduct workshop for making practicing engineers environmental sensitive (Singh, 2011).

5.4 Sensitizing CEE Students regarding Green technology

This is only possible when environmental issues are adequately identified, scientifically understood, appropriate technological solution are applied for their mitigation and sustainable resource utilization methods, the green methods into the ways workers perform their trade, profession or occupation. So, green method is a process of doing an activity which does not harm the environment. A re-orientation of CEE is, hence, required to impart green education which will lead to a highten sense of responsibility towards ecological sensitivity and development of eco-friendly technology (Singh, 2011).

5.5 Sensitizing Students regarding Technological Need of Poor and Deprived Group

All the corporate sector have certain amount of money year marked for social responsibility. The CEE institutions should pull in corporate sector and their funds for sensitizing, developing and distributing relevant technology to the poor and deprived groups. At EE (regular) in DTU, there is mandatory visit to slum by all the students and coming out with some technological suggestion to improve their life, is part of course work in the subject- Engineering Economics. At IIT Delhi, there is Centre for Rural Development & Technology which takes care of the rural technology (IIT, Delhi, 2012). These initiatives should be introduced in the CEE programme also.

6. Conclusion and Recommendation

Two broad trends have emerged in CEE system during the era of LPG. They are as i. The students enrolled in CEE (academic institution) do not look for linear career progression rather they want to get optimal career benefit from the opportunity and ii. All those who pursue CEE for career enhancement prefer to take route of engineering institute, but to acquire knowledge, professional engineers follow route through ICT. It has posed challenges of preparing engineers for global work place. Train them regarding green technology and enhance R&D and innovations in the Curriculum. They need to be sensitized towards technological need of poor and deprived group. Given the socio-economic background of a common CEE students in India, there is need of developing cost-effective CEE. Not only in India, there is such demand in many parts of Latin America, Africa, Gulf countries. For that matter, in the era of

global melt down, cost-effectiveness is one of the determining factor all over the world. Engineering institution should allow to develop entrepreneurial skill of its faculty and students in developing CEE module which can be delivered through ICT. It can done by engineering institutions if revamping of the CEE. Corporate sector and professional bodies may be involved in the management of CEE. They are already present in the campus for engineering education (regular course). There is need to expand their involvement.

Notes:

1. Only degree and diploma holders have been considered. Regular degree level education is of 4-years after higher secondary education (10+2 years of schooling). Regular diploma level engineering education programme is of 3-years duration after secondary education (10 years of schooling).
2. Normal class room teaching is done beyond normal working eight hours so that employed engineering manpower can enhance their educational qualification.
3. It combines the use of self study printed materials with other kinds of teaching techniques and types of media like television, radio, satellite broad caste.
4. Demographic dividend- Young population of India is increasing at a time when young segment in the total population is decreasing in developed countries. So, Indian youth, if trained properly, will be demanded all over the globe.
5. The second study is an All India Council for Technical Education sponsored on-going project with me as P.I. A sample of 100 students each from Delhi Technological University, Jamila Millia Islamia Central University, Delhi Centre & Patna Centre of the Institution of Engineers which together makes them as total sample size of 400 students. The Institution of Engineer (IoE) is a national body of professional engineers. They provide Associate Members of Institution of Engineers (AMIE) degree equivalent to engineering degree. Patna Centre and Delhi Centre of same organisation were surveyed to understand locational difference in centres of same organisation. One is at national capital and another one is in capital of backward state, Bihar.
6. Corporate representatives visit engineering institution to recruit students for their company .

Reference

1. Deshpande, Lalit K., Alakh N. Sharma, Anup K. Karan and Sandip Sarkar (2004), "Liberalisation and Labour: Labour Flexibility in Indian Manufacturing" Institute for Human development, New Delhi, pp. 22.
2. GoI (1998), "Annual Report 1997-98" Government of India, ministry of Industry, New Delhi
3. ILO (2001), "Life at Work in the Information Economy", World Employment Report, International Labour Organisation, Switzerland, pp. 112-113.
4. IIT Delhi (2012), "Centre for Rural Development & Technology", http://crdt.iitd.ac.in/ down loaded on 28/3/2012
5. Kumar Anil (2004), "Continuing Engineering Education in India: an Overview", In the Proceeding of the 9th World Conference on Continuing Engineering Education, Tokayo, May 15-20, 560-565.
6. Mamkoottam, Kuriakose (2000), "Industrial relation in Globalizing India", in Saini, Debi S., Sami A. Khan, (eds), Human resource Management- Perspective for the New era, New Delhi, Response Books, pp. 232.
7. Mukherjee Writankar (2012), "Union Budget 2012-13: Funds for Skill Development ubder National Skill Development under National Skill Development Fund doubled" http://economictimes.indiatimes.com/news/news-by-industry/services/education/union-budget-2012-13-funds-for-skills-development-under-national-skill-development-fund-doubled/articleshow/12292000.cms down loaded on 18/3/2012
8. Singh Seema (2005), "MNCs Effect on Employment of Engineers" The Indian Journal of Technical Education, 28(2), pp. 38-44.
9. Jalal R.S. and Nandan Singh Bisht (2008), "Challenges of Protecting Labour against Technological Unemployment", in (eds.), Emerging Dimensions of global trade: Discussion on Trade related Policies, pp. 208-216.

10. "Is Indian Education System is Ready to Groom for Green Job" (2011), Paper presented in the 53rd annual conference of the Indian society of labour economics at Mohanlal Sukhadia University, Udaipur, India.
11. ---------- (2012.a), "A Study on Emerging Trends in Indian Continuing Engineering Education System", paper to be presented at WCCEE, 2012 at Valencia, Spain between May 17-19, 2012.
12. ----------(2012.b), "Indian Continuing Engineering Education System in Context of Globalisation", AICTE sponsored on-going project, New Delhi.
13. Singh Seema and Anil Kumar, (2003), Continuing Engineering Education: Response of students to system of education and evaluation, Indian Journal of Technical Education, 26, 48-56.
14. Singh Seema and T. Thankachan (2005), "Impact of Globalisation on Engineering Manpower" in M.Sudhir Reddy, K. Ramakrishna Reddy, P. Murali Krishna and K. Lal Kishore eds. Globalisation and Manpower Planning, Discovery Publishing House, New Delhi- 110 002 pp. .278-286

International Scholarly Research Network
ISRN Electronics
Volume 2012, Article ID 529194, 7 pages
doi:10.5402/2012/529194

Research Article

Multithreshold MOS Current Mode Logic Based Asynchronous Pipeline Circuits

Kirti Gupta,[1] Neeta Pandey,[1] and Maneesha Gupta[2]

[1] *Department of Electronics and Communication Engineering, Delhi Technological University, Delhi 110042, India*
[2] *Department of Electronics and Communication Engineering, Netaji Subhash Institute of Technology, New Delhi 110078, India*

Correspondence should be addressed to Kirti Gupta, kirtigupta22@gmail.com

Received 21 September 2012; Accepted 31 October 2012

Academic Editors: A. Mercha and I. Shubin

Multithreshold MOS Current Mode Logic (MCML) implementation of asynchronous pipeline circuits, namely, a C-element and a double-edge triggered flip-flop is proposed. These circuits use multiple-threshold MOS transistors for reducing power consumption. The proposed circuits are implemented and simulated in PSPICE using TSMC 0.18 μm CMOS technology parameters. The performance of the proposed circuits is compared with the conventional MCML circuits. The results indicate that the proposed circuits reduce the power consumption by 21 percent in comparison to the conventional ones. To demonstrate the functionality of the proposed circuits, an asynchronous FIFO has also been implemented.

1. Introduction

Digital VLSI circuits can be broadly classified into synchronous and asynchronous circuits. A synchronous circuit employs a common clock signal to provide synchronization between all the circuit components. The synchronous circuits suffer from the problems of clock distribution and clock skew which becomes a challenge to overcome as the technology scales down. Asynchronous circuits, on the other hand, are attractive replacements to synchronous designs as they perform synchronization through handshaking between their components. Some other advantages of asynchronous circuits include high speed, low power consumption, modular design, immunity to metastable behavior, and low susceptibility to electromagnetic interference [1].

Traditionally, the asynchronous circuits were implemented by using CMOS logic style but due to the substantial dynamic power consumption at high frequencies, CMOS logic style is usually not preferred. MOS Current Mode Logic (MCML) is found to be an alternative to the CMOS asynchronous circuits in the literature [2–5]. A conventional MCML circuit consists of a differential pull-down network (PDN), a current source, and a load. The PDN implements the logic function, the current source generates the bias current I_{SS}, while the load performs the current to voltage conversion [6]. The circuit has static power consumption given as the product of the supply voltage and the bias current. The power consumption can be lowered by either reducing the bias current or the supply voltage. The reduction in bias current is generally not favored as it degrades the speed [7]. Therefore, lowering the supply voltage of the circuit is preferred. One of the techniques suggested in [8, 9] is multithreshold MOS Current Mode Logic (MT-MCML) which uses multithreshold transistors in conventional MCML circuits. In this paper, MT-MCML technique has been applied to implement low-power multithreshold MCML asynchronous pipeline circuits.

The paper first describes the architecture and the operation of MT-MCML circuits in Section 2. In the next section, a brief introduction to asynchronous pipelines is presented. Thereafter, multithreshold MCML asynchronous pipeline circuits, namely, a double-edge triggered flip-flop and a C-element are proposed in Section 4. In the subsequent Section 5, the proposed circuits are simulated in PSPICE using TSMC 0.18 μm CMOS technology parameters and their performance is compared with existing MCML circuits.

An FIFO is also implemented using the proposed circuit. Finally, the conclusions are drawn in the last section.

2. MT-MCML Circuits

MT-MCML circuits are the modified form of the conventional MCML circuits. They use multithreshold CMOS technology for the realization of the logic functions [8, 9]. The circuit of an MT-MCML AND/NAND gate is shown in Figure 1. It consists of two levels of source-coupled transistor pairs (M2-M5) to implement the logic function and a constant current source M1 to generate bias current I_{SS}. The transistors in the upper level (M4, M5) have lower threshold voltage than the transistors in the lower level (M2, M3). The minimum supply voltage for the circuit is defined as the lowest voltage at which all the transistors in the two levels and the current source operate in the saturation region [8] and is computed as

$$V_{MIN} = 3\ V_{BIAS} - \ 3V_{T1} \ + \ V_{TU}, \tag{1}$$

where V_{T1} and V_{TU} are the threshold voltages of the transistor M1 and the transistors in the upper level (M4, M5), respectively.

As an example, an MT-MCML AND/NAND gate with $V_{BIAS} = 800\,\text{mV}$, $V_{T1} = 500\,\text{mV}$, and $V_{TU} = 200\,\text{mV}$ results in a value of $V_{MIN} = 1.1\,\text{V}$ in comparison to the conventional gate which results in $V_{MIN} = 1.4\,\text{V}$ for $V_{T1} = V_{TU} = 500\,\text{mV}$. Thus, MT-MCML circuits can be used in low-power applications as they can operate at low supply voltage than the conventional one.

3. Asynchronous Pipeline

In asynchronous pipelines, data is communicated between the sender and the receiver modules through a handshaking protocol. A very common protocol is the two-phase bundled-data handshaking protocol [10, 11]. Bundled-data channels connect the sender and the receiver through a data bus consisting of separate requests (Req) and acknowledge signals (Ack) and data signals (Data). The sender initiates the data transfer by placing Data on the bus and raises the Req signal, and the receiver then absorbs the data and acknowledges it by raising the Ack signal. Then, the two signals are reset to zero in the same order.

The block diagram of a typical two-phase bundled-data asynchronous pipeline is shown in Figure 2. It comprise of four-stages wherein each stage consists of a functional unit and a control unit. The functional unit has a combinational stage for computing the result of each stage and a matched delay element inserted in the request line. The control unit employs a double-edge triggered flip-flop (DETFF) and a C-element to control the communication between the successive stages.

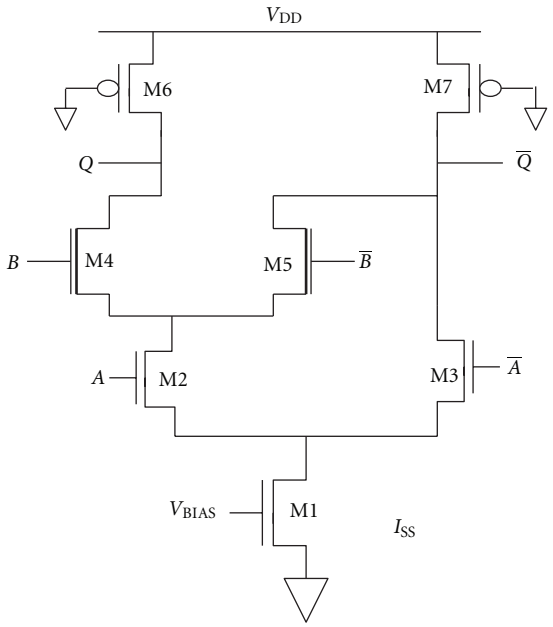

Figure 1: MT-MCML AND/NAND gate.

4. MT-MCML Control Unit

The control unit in asynchronous pipelines consists of two elements, namely, a double-edge triggered flip-flop and a C-element. This section proposes the low-power MT-MCML circuits for both the elements.

4.1. MT-MCML DETFF. A DETFF is an essential element to store the new data produced by the functional unit till the time the successor stage is ready to receive it. It samples the data at the falling and the rising edges of the local clock pulses generated by the C-element.

A block diagram of a DETFF consisting of two opposite level sensitive latches and a multiplexer is shown in Figure 3. When CLK is high, latch L1 becomes transparent and the data stored in the latch L2 is obtained as the output. Similarly, when CLK is low, latch L2 becomes transparent and the data stored in the latch L1 is obtained as the output of the flip-flop. The circuit of the proposed MT-MCML DETFF is shown in Figure 4. It consists of two MT-MCML latches L1, L2 and MCML multiplexer (MUX) with a common source-coupled transistor pair for differential clock input (CLK). The advantage of using common clock source-coupled transistor is the reduction in the routing complexity and the overall area. The transistors in the upper level of latches and the multiplexer (M4-M15) have low threshold voltages values and have been highlighted in the figure.

4.2. MT-MCML C-Element. A C-element is a fundamental component of asynchronous pipelines. It is a state holding element wherein if both inputs are same, that is, low (high), the circuit produces the output which is equal to the input value, that is, low (high), respectively, otherwise the output

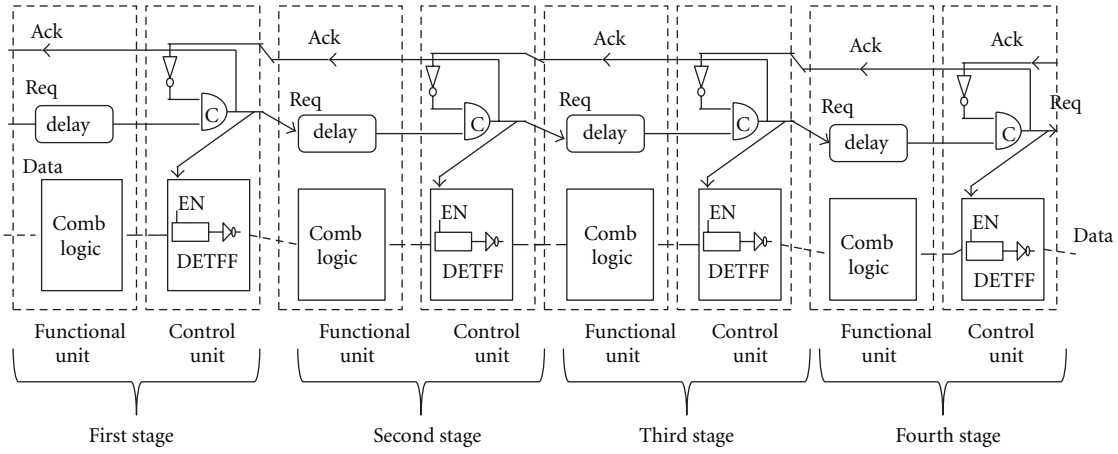

Figure 2: Block diagram of two-phase asynchronous pipeline.

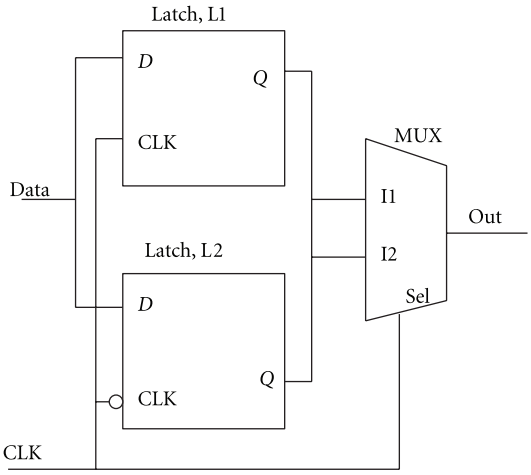

Figure 3: Block diagram of a DETFF.

remains at the previous state value. A state diagram is given in Figure 5 which can be expressed by a Boolean function:

$$C = \left[\hat{C} \cdot (A + B)\right] + (A \cdot B), \tag{2}$$

where A, B are the inputs and $\hat{C}$ is the previous state of the output.

The circuit of the proposed MT-MCML C-element is shown in Figure 6. In circuit, the two stacked transistors (M2, M8) form an AND structure whereas the parallel connection of transistors (M3, M4) performs the OR operation. The cross-coupled transistor pair (M9, M10) forms the latch structure. The transistors in the upper level of the C-element (M8-M11) have low threshold voltages values and have been highlighted in the figure. When both the inputs (A, B) have the same value then the bias current either flows through the two right most branches or the left most branches. This, however, makes the output (C) of the circuit same as the input value. Conversely, when both the inputs (A, B) have different values, the output stores the previous value by making the bias current flow in the latch structure branches only.

5. Simulation Results

This section first presents the simulation results for the proposed control unit elements, namely, DETFF and C-element. Thereafter, the performance of the proposed circuits is compared with the conventional MCML control unit elements. Lastly, the simulation results for an asynchronous FIFO are presented. All the simulations are performed by using TSMC 0.18 μm CMOS technology parameters and load capacitance of 10 fF. The channel length of the transistors is taken as 0.18 μm uniformly. The value of the supply voltage for the MT-MCML and conventional MCML circuits is 1.1 V and 1.4 V, respectively.

5.1. Proposed Control Unit Elements. The proposed MT-MCML control unit elements are implemented with an output voltage swing of 400 mV and a bias current (I_{SS}) of 30 μA and 90 μA for C-element and DETFF, respectively. The bias current of DETFF is taken to be three times the value of bias current in C-element as in DETFF there is a common source-coupled transistor pair that drives the two D-latches and a multiplexer. The aspect ratio of the transistors in the PDN of both the elements is 3 μm/0.18 μm, whereas the aspect ratio for load transistors is 0.46 μm/0.18 μm. The simulation waveforms are shown in Figure 7. In Figure 7(a), it can be observed that in DETFF whenever CLK is low, the previous value stored in L1 is obtained as the output of the DETFF. Similarly, when CLK is high, the previous value stored in L2 is obtained as the output. The simulation waveforms for C-element shown in Figure 7(b) depict that whenever both the inputs (A and B) have the same value an output which is equal to the current vales of the inputs is obtained. Further for different values of the inputs (A and B), the output remains in the previous state value.

The impact of parameter variation on power consumption of the proposed MT-MCML control unit elements is studied at different design corners. It is found that the power consumption of the proposed DETFF varies by a factor of 1.87 between the best and the worst cases. For the proposed

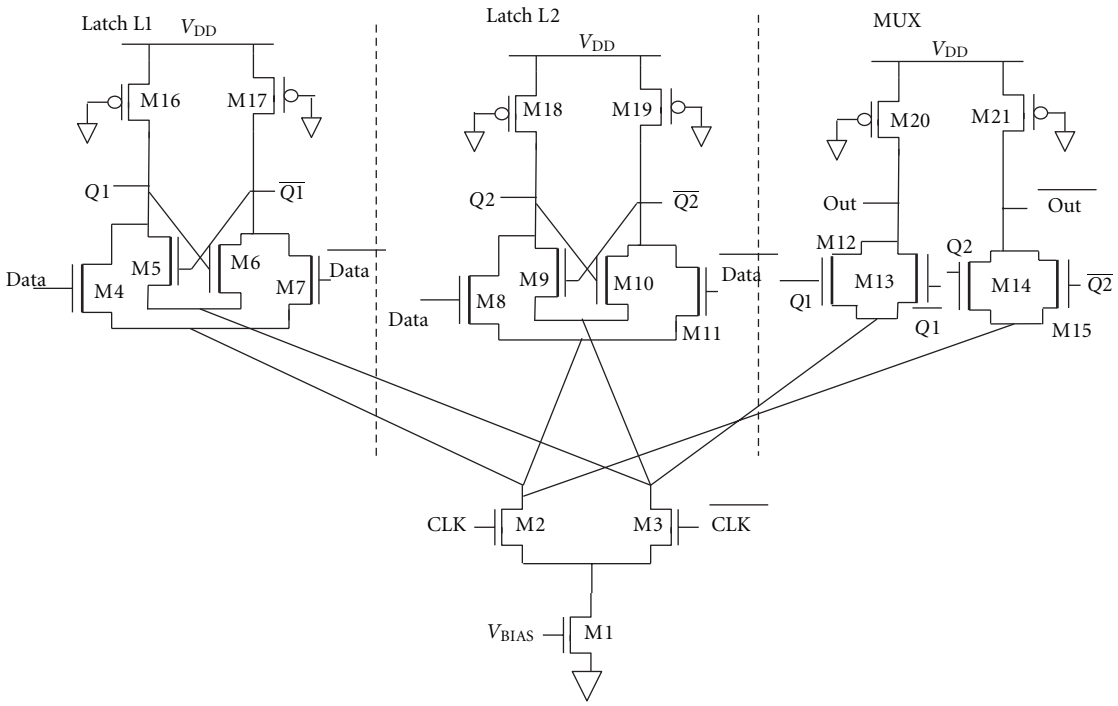

Figure 4: Proposed MT-MCML DETFF.

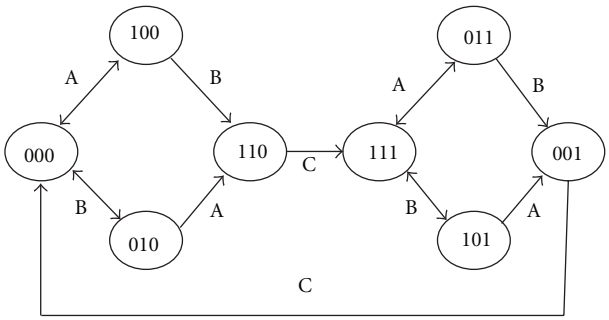

Figure 5: State diagram of the C-element.

C-elements, the power consumption varies by a factor of 1.4 between the best and the worst cases.

5.2. Performance Comparison. The performance of the proposed MT-MCML and the conventional MCML control unit elements has been compared using simulation test benches [3] which are redrawn in Figure 8. The simulation results are listed in Tables 1 and 2. The power result for MCML circuits includes static power due to the presence of the constant current source. The result shows that the proposed MT-MCML circuits reduce power consumption by 21 percent due to the operation at low supply voltage through the use of multiple-threshold voltage transistors. Further, the propagation delay of the proposed MT-MCML control unit elements is slightly higher than the conventional MCML elements due to the increase in transistor sizes in the proposed elements [8]. Thus, the power-delay product (PDP) values for the proposed are reduced accordingly.

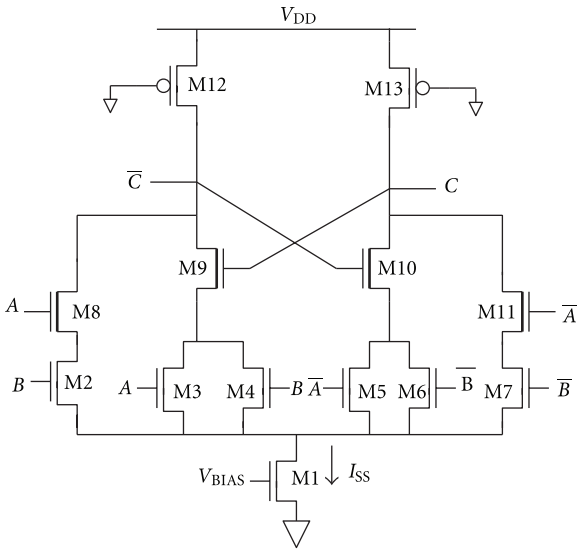

Figure 6: Proposed MT-MCML C-Element.

Therefore, the use of MT-MCML circuits can lead to the design of power-efficient asynchronous pipelines.

5.3. An Application. An asynchronous MT-MCML FIFO is implemented as an application of the proposed control unit elements. The block diagram of a 4-stage FIFO is shown in Figure 9. The handshaking signals shown as Req(in) and Ack(out) communicate the data, Data(in) between sender and the first stage. At the receiver side, the signals Req(out) and Ack(in) are used to synchronize the output

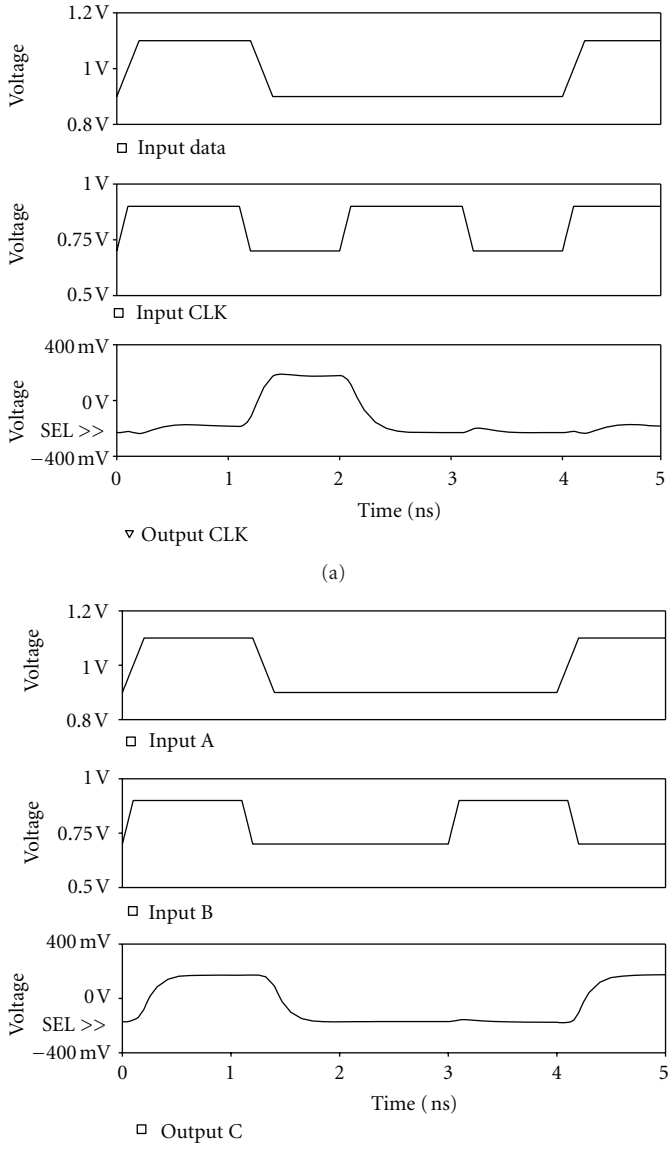

Figure 7: Simulation waveforms of the proposed MT-MCML (a) DETFF and (b) C-Element.

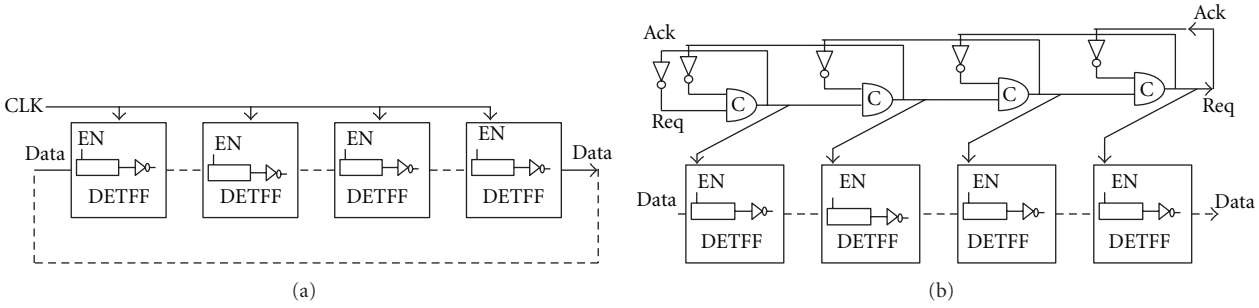

Figure 8: Simulation test bench [3] (a) DETFF and (b) C-element.

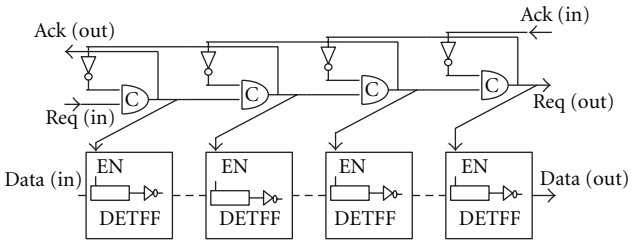

Figure 9: Block diagram of 4-stage asynchronous FIFO.

Table 1: Summary of simulated performance for DETFF.

Parameter	Type of DETFF	
	Conventional MCML	Proposed MCML
Power (μW)	141	111
Propagation delay (ps)	1230	1240
PDP (fJ)	173	138

Table 2: Summary of simulated performance for C-element.

Parameter	Type of C-element	
	Conventional MCML	Proposed MCML
Power (μW)	44	35
Propagation delay (ps)	239	241
PDP (fJ)	11	8

data, Data(out) with the receiver and the last stage. Initially, the input data Data(in) is loaded in the first stage of the FIFO, and the Req(in) is asserted to low to start the data transfer. This results in a transition at the output of a C-element such that the data is stored in the DETFF of the first stage. At the same time an acknowledge signal Ack(out) is given to the sender. The stored data then flows through the different stages in the FIFO. Then, a request signal Req(out) is generated by the last stage to the receiver to enable the receiver to accept the data. This is followed by an acknowledge signal, Ack(in), from the destination to the last stage. The waveforms obtained through the simulation of a four-stage asynchronous FIFO are shown in Figure 10. The first three waveforms correspond to the input data Data(in), request signal (Req(in)), and acknowledge signal (Ack(out)) at the sender section. The last three graphs are the acknowledge signal Ack(in), data Data(out), and request signal Req(out). It can be found that the asynchronous MT-MCML FIFO outputs the sampled data correctly.

6. Conclusions

This paper proposes low-power Multithreshold MOS Current Mode Logic (MT-MCML) asynchronous pipeline circuits. The proposed circuits involve the use of multiple-threshold CMOS technology which helps in reducing the power consumption. The proposed circuits have been simulated using 0.18 μm CMOS technology parameters, and their performance has been compared with the conventional MCML circuits. A performance comparison indicates that

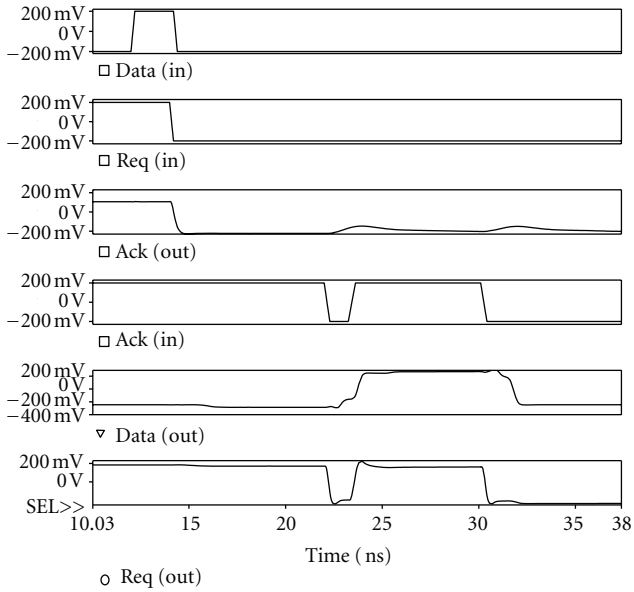

Figure 10: Transient response of the 4-stage multithreshold MCML asynchronous FIFO circuit.

the proposed circuits are power efficient than the conventional ones. An asynchronous FIFO implemented as an application confirms to the functionality of the proposed circuits.

References

[1] C. H. Van Kees Berkel, M. B. Josephs, and S. M. Nowick, "Scanning the technology applications of asynchronous circuits," *Proceedings of the IEEE*, vol. 87, no. 2, pp. 223–233, 1999.

[2] T. W. Kwan and M. Shams, "Design of multi-ghz asynchronous pipelined circuits in MOS current-mode logic," in *Proceedings of the 4th International Conference on Embedded Systems*, pp. 1–6, 2005.

[3] T. W. Kwan and M. Shams, "Design of asynchronous circuit primitives using mos current-mode logic (MCML)," in *Proceedings of the 16th International Conference on Microelectronics (ICM '04)*, pp. 170–173, December 2004.

[4] T. W. Kwan and M. Shams, "Design of high-performance power-aware asynchronous pipelined circuits in MOS Current-Mode Logic," in *Proceedings of the 11th IEEE International Symposium on Asynchronous Circuits and Systems (ASYNC '05)*, pp. 23–32, March 2005.

[5] T. W. Kwan and M. Shams, "Multi-GHz energy-efficient asynchronous pipelined circuits in MOS current mode logic," in *Proceedings of the IEEE International Symposium on Cirquits and Systems*, pp. II645–II648, May 2004.

[6] H. Hassan, M. Anis, and M. Elmasry, "MOS current mode circuits: analysis, design, and variability," *IEEE Transactions on Very Large Scale Integration (VLSI) Systems*, vol. 13, no. 8, pp. 885–898, 2005.

[7] M. Alioto and G. Palumbo, *Model and Design of Bipolar and MOS Current-Mode Logic (CML, ECL and SCL Digital Circuits)*, Springer, Amsterdam, The Netherlands, 2005.

[8] M. Anis and M. Elmasry, "Power reduction via an MTCMOS implementation of MOS current mode logic," in *Proceedings of the IEEE International Conference on ASIC/SOC*, pp. 193–197, 2002.

[9] H. Hassan, M. Anis, and M. Elmasry, "Analysis and design of low-power multi-threshold MCML," in *Proceedings of the IEEE International SOC Conference*, pp. 25–29, September 2004.

[10] M. Shams, J. C. Ebergen, and M. I. Elmasry, *Asynchronous Circuits*, John Wiley's Encyclopedia of Electrical Engineering, 1999.

[11] I. E. Sutherland, "Micropipelines," *Communications of the ACM*, vol. 32, no. 6, pp. 720–738, 1989.

2012 Fourth International Conference on Computational Intelligence and Communication Networks

Object Segmentation by an Automatic Edge Constrained Region Growing technique

Seba Susan, Om Prakash Verma and Jyoti Swarup
Department of Information Technology,
Delhi Technological University,
New Delhi, India

Abstract— **Region growing is a well known technique for image segmentation. However it suffers from certain limitations such as ambiguity regarding initial seed selection and threshold determination for region growing. In this paper we explore the possibility of using region growing technique for segmenting out the foreground object and propose to solve the imperfect results by incorporating the nearest edge information. The whole procedure is rendered automatic by defining a center window containing some part of the object. From this window the seed selection and threshold value for region growing is determined by simple computations. The results on the 'Car' category of the challenging PASCAL VOC 2005 dataset indicate a superior performance to Xavier Bresson's method for object segmentation.**

Keywords- Object segmentation, Region Growing, Canny Edge detector

I. INTRODUCTION

Efficient segmentation of the foreground object in a scene is of ever growing importance in video surveillance applications and computer vision problems. The problem is complicated by the fact that high accuracy segmentation has to be achieved in real time in a real world environment of high background clutter. Several image segmentation techniques have been adapted for object segmentation such as filtering [1], blob analysis [2] and clustering [3]. Some of the works focus on salient objects in the scene. Saliency computation for foreground visual information is explored in the works of [4,5]. Feature based techniques also exist such as [6] which tracks the object by fuzzy clustering of position, velocity and color features of the pixels. The Snake based method has been used for tracking objects by extracting their contours or boundaries [7]. Xavier Bresson's method for object segmentation [18] improves on the active contour model by making use of fast global minimization of the snake energy.

In this paper we extend the conventional region growing method for image segmentation [8-15] for object segmentation purpose by incorporating the nearest edge information. The paper is divided into the following sections: Section II discusses the region growing technique and its inherent disadvantages. Section III introduces the proposed object segmentation methodology incorporating both region growing and edge information. Section IV discusses the experimental results and Section V draws the overall conclusions.

II. LIMITATIONS OF THE REGION GROWING METHOD FOR IMAGE SEGMENTATION

The region growing algorithm [8] for image segmentation is briefly described below:

Select the initial seed pixels and determine threshold T
For each seed pixel do
{
For each of the unlabelled eight neighbors of the seed pixel do
{
If $\left|intensity(seed) - intensity(neighbor)\right| \le T$
then label neighbor with label of seed pixel
and set the neighbor as a new seed pixel
}
}

The similarly labeled pixels in the image correspond to a region. The primary fault in the region growing method is the ambiguity over the initial selection of seeds and determining the proper threshold T for the growing process. Several works have tried to address the issue in the past. In [9] the authors have assigned the center point of the image as the initial seed and Otsu's threshold was used as the similarity criterion. Huang *et al* in [10] use edge and smoothness factors to determine initial seed pixels and in [11] the centroid of watershed regions is used as the initial seed. In [12] two discontinuity measures, average contrast and peripheral contrast control the region growing process. The segmentations directly obtained by region growing are often imperfect leading to over-segmentation [9], hence corrective procedures are often applied once the regions are grown by the conventional method. For instance, in [13] region growing is followed by a region merging step to reduce the over-segmentation followed by use of edges to

978-0-7695-4850-0/12 $26.00 © 2012 IEEE
DOI 10.1109/CICN.2012.154

correct the region boundaries. This concept of using edge information to improvise on segmentation results is also used in our work for object segmentation. Another work integrating edge and region information is [15] in which edge detection was done prior to region growing for selection of initial seeds and automatic threshold determination. Some other examples where region growing is followed by the region merging corrective step include [10] and [14].

III. PROPOSED OBJECT SEGMENTATION BY EDGE CONSTRAINED REGION GROWING

The steps for segmenting the foreground object as proposed in our work are detailed below on a step by step basis using an example image for demonstration where the object to be segmented is a car.

Step 1: Read the input image and convert it to gray.

Fig. 1: Original Image

Step 2: Consider a center window *w* of size 20x20 which contains some parts of the object, in this case, the car.

Fig. 2: 20x20 center window

Step 3: The difference between the median of the pixel values in the window and the mean pixel value is selected as the threshold.

$$T = |median_w - mean_w| \quad (1)$$

Assuming that majority of the pixels in the window *w* belong to the car, the median of the pixel values denotes the most frequent occurring pixel in the car body. The mean value within the window on the other hand is influenced by the overall contrast within the car body, and if the mean approaches the median this implies that the car is more or less uniformly of the same color indicating a threshold of approximately zero.

For the above window in Fig. 2,

$mean_w = 198.1074$

$median_w = 194$

$Threshold\ T = 4.1074$

Step 4: The pixel value within the window having a minimum deviation from the mean is selected as the single initial seed for growing the car.

$$Initialseed = (x_i, y_i) = \arg\min_{(x,y)}(|w(x,y) - mean_w|) \quad (2)$$

Step 5: The region is grown using the conventional region growing algorithm outlined in Section II with the initial seed (x_i, y_i) computed from Step 4 and threshold T determined from Step 3.

Fig.3: Result of region growing from a single initial seed

Step 6: Find the nearest edge to each pixel in the grown region with the Canny edge detector [16] being the popular choice for a robust, strong edge detector giving strong connected edges. The Euclidean distance norm is used to compute the nearest edge pixel for every pixel in the grown region in Fig. 3. The set of nearest edge pixels for the region grown in Fig. 3 is shown in Fig. 4.

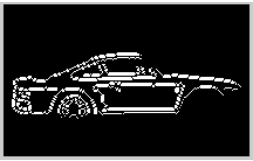

Fig.4: Nearest edge pixels for grown region in Fig. 3

Step 7: Morphological closing is done with a structural element of size equal to 5 pixels to fill in the gaps between edge pixels. The holes in the resulting image are filled with a structuring element of size of 2 pixels. The single largest connected component obtained is the foreground object. The size of the morphological tools is determined through a lot of experimentation for the best results.

Fig.5: Morphological closing

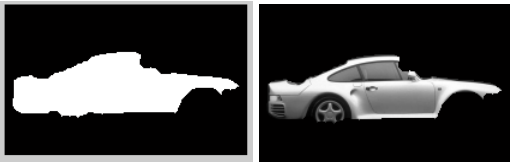

Fig.6: Filling of holes and the corresponding object

IV. EXPERIMENTAL RESULTS AND DISCUSSION

The experiments are performed on 100 images from the 'CAR' category of the challenging PASCAL VOC 2005 dataset [17]. The MATLAB 7.9 software is used for implementing the codes. The Precision-Recall graphs for the 100 images are shown in Fig. 7 and indicate a very high level of Precision as seen from the Precision graph skewed to the right.

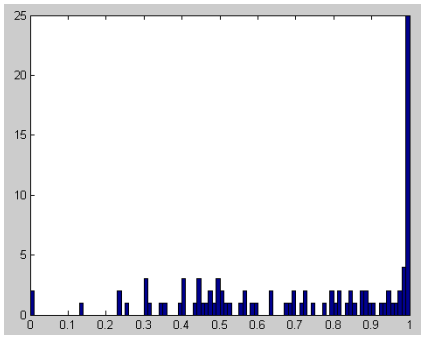

(a)

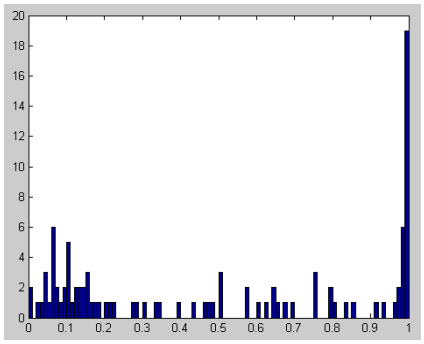

(b)

Fig.7: (a) Precision (b) Recall Graphs for proposed Object Segmentation technique

The graphical results in Fig. 7 imply that in most of the cases the car is segmented out with high accuracy by the proposed method as shown in the examples in Fig. 8.

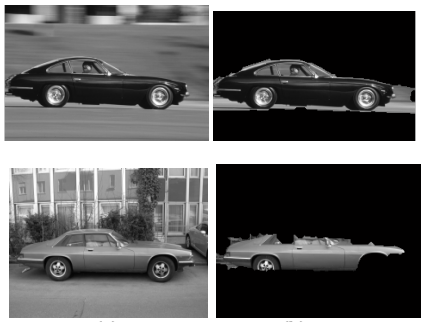

(a) (b)

Fig. 8: Object Segmentation using proposed method- Easy images

The Recall graphs in Fig. 7 are not as good as the Precision graphs since for some difficult images some parts of the background is also segmented as shown in Fig. 9.

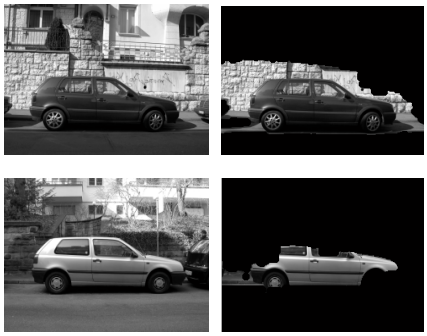

(a) (b)

Fig.9: Object Segmentation using proposed method- Difficult images

We compare our method with that of Xavier Bresson's object segmentation [18] technique that makes use of the active contour model. The results of the Precision-Recall graphs shown in Fig. 10 and the segmentation results corresponding to examples in Figs. 8,9 are shown in Fig. 11,12 respectively. The Precision graph in this case is skewed to the left indicating poor segmentation.

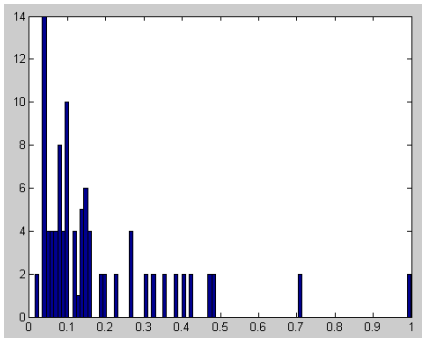

(a)

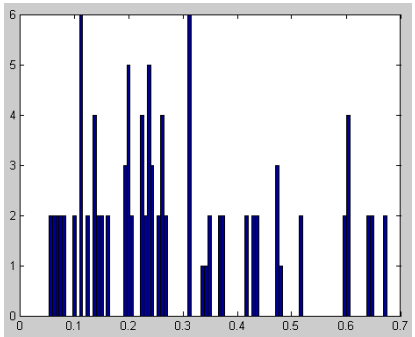

(b)

Fig.10: (a) Precision (b) Recall Graphs for Xavier Bressons active contour model

Fig.11: Object Segmentation result for the (easy) examples in Fig. 8 using Xavier Bresson's active contour model

Fig.12: Object Segmentation for the (difficult) examples in Fig. 9 using Xavier Bresson's active contour model

The results indicate that our algorithm performs better in cluttered and indistinct backgrounds where the contour of the car is not so distinct. The primary advantage of our algorithm is that the car is segmented out from the seed pixel which is a part of the car body. Therefore the accuracy of the object being segmented is higher than other algorithms.

V. CONCLUSION

A new object segmentation technique is proposed in this paper that uses the conventional region growing technique for segmenting out the foreground object. The defects in segmentation are rectified by incorporating edge information for filling of missing areas or removing extra parts. The region growing process uses automatic seed selection and threshold determination both computed from a center window wherein the whole of or parts of the object is expected to lie. The Precision-Recall graphs indicate good segmentation results on a challenging dataset which outperforms Xavier Bresson's method for object segmentation.

REFERENCES

[1] Ehquierdo and M.Ghanbari, "Nonlinear Gaussian filtering approach for object Segmentation," *IEE Pmc.-yls. Image Signal Process, Vol. 146, No.* 3, *June 1999.*

[2] C. Carson, S. Belongie, H. Greenspan, and J. Malik, "Blobword: Image Segmentation Using E-M and Its Application to Image Querying*," IEEE Trans. Pattern Anal. Mach. Intell.,* Vol. 24, pp. 1026-1038, 2002.

[3] B.Heiselle, U.Kressel, W.Ritter, "Tracking non-rigid moving objects based on color cluster flow", *CVPR,* 1997.

[4] L.Itti, C.Koch, E.Neibur, " A model of saliency based visual attention for rapid scene analysis", *IEEE Trans. Pattern Anal. Mach. Intell.,*20(11), pp. 1254-1259, 1998.

[5] J.Harel, C.Koch, P.Perona, "A Graph based visual saliency" *NIPS,* 2006.

[6] D.Xie, W.Hu, T.Tan, J.Peng, "A Multi-Object tracking system for surveillance video analysis", *ICPR,* 2004.

[7] N. Peterfeund, " Robust tracking of position and velocity with Kalman snakes", *IEEE Trans. Pattern Anal. Mach. Intell.,*vol. 21, pp.564-569, 1999.

[8] R. Adams and L. Bischof, "Seeded region growing," *IEEE Trans. Pattern Anal. Machine Intell.*, vol. 16, pp. 641–647, 1994.

[9] O.P.Verma, M.Hanmandlu, Seba Susan, M.Kulkarni, Puneet Kumar, "A Simple Single seeded region growing algorithm for color image segmentation using adaptive thresholding", *IEEE Conf. Procc. CSNT 2011*, pp. 500-503.

[10] C.Huang, Q.Liu, L. Xiaopeng, " Color Image Segmentation by seeded region growing and region merging", *Intl conf. on fuzzy systems and knowledge discovery,* vol. 2 , pp. 533-536.

[11] J.Tang," Color Image Segmentation algorithm based on region growing", *Intl conf on Computer engg. And technology*, vol. 6, pp. 634-637, 2010.

[12] S.A.Hojjatolesami, J.Kittler," Region growing : A new approach", *IEEE Trans. On image processing* , 7(7), 1998.

[13] J.Xuan, T.Adal, Y.Wang, "Segmentation of magnetic resonance brain image : integration of region growing and edge detection", *Proc. IEEE Intl. Conf. on Image Processing,*vol. Ill, pp. 544-547, Washington DC, Oct. 23-26, 1995..

[14] J.Camapum, A.O.Silva, A.N.FreitasH. de F. Bassani, F.M.O. Freitas," Segmentation of clinical structures from images from the human pelvic area", *SIBGRAPI'* 04.

[15] H.L Anderson, R. Bajcsy and M. Mintz, "A modular feedback system for image segmentation", *University of Pennsylvania GRASP Lab., Tech, Report 1O*, 1997

[16] Canny, J., "A Computational Approach To Edge Detection," *IEEE Trans. Pattern Analysis and Machine Intelligence*, 8(6):679–698, 1986.

[17] A fully annotated PASCAL database provides appropriate images for object segmentation [online]
http://pascallin.ecs.Soton.ac.uk/challenges/VOC/databases.html#UIUC

[18] Xavier Bresson, Pierre Vandergheynst and Jean-Philippe Thiran, "A Variational Model for Object Segmentation Using Boundary Information and Shape Prior Driven by the Mumford-Shah Functional," *International Journal of Computer Vision 68(2),* 145–162, 2006.

Particle Creation in Higher Dimensional Space-time with Variable G and Λ

http://adsabs.harvard.edu/abs/2012IJTP...51.3951S

Singh, C. P.; Beesham, A.

International Journal of Theoretical Physics, Volume 51, Issue 12, pp.3951-3962

In this paper we consider higher dimensional FRW type cosmological models with time-varying gravitational constant G= G(t) and decaying vacuum energy Λ= Λ(t) in context of the open thermodynamical system of particle creation. The particle creation rate is determined by variable G and Λ. An Exact solution of the gravitational field equations is obtained by assuming the exact power-law solution of the scale factor of the universe. We evaluate the various cosmological parameters and discuss their physical significance in detail for radiation and matter-dominated phases of the universe. The solutions are also relevant for quintessence (accelerating) universe. We also discuss the relevance of the solutions for 5-dimensional Kaluza-Klein FRW type model with and without particle creation in radiation and matter-dominated phases as special case. We obtain the solution where the gravitational constant increases with time during no particle creation. The cosmological constant Λ, however, decreases with time in all the cases.

Keywords: Cosmology, Exact solutions, Particle creation, Vacuum energy density
DOI: 10.1007/s10773-012-1287-3

Physica E 48 (2013) 75–79

Contents lists available at SciVerse ScienceDirect

Physica E

journal homepage: www.elsevier.com/locate/physe

Propagation characteristics of silver nanorods based compact waveguides for plasmonic circuitry

Venus Dillu, Shruti, Triranjita Srivastava, Ravindra Kumar Sinha *

TIFAC—Center of Relevance and Excellence in Fiber Optics and Optical Communication, Department of Applied Physics, Delhi Technological University (Formerly Delhi College of Engineering), Bawana Road, Delhi 110042, India

HIGHLIGHTS

- Silver nanorods based plasmonic waveguide is proposed.
- 3D FDTD and PWE methods are used for examining the basis waveguide.
- Proposed waveguide works for visible regime.
- Straight waveguide, bend and Y-splitter have been devised.
- Quality factor, confinement factor and losses are calculated.

GRAPHICAL ABSTRACT

We propose ultra-compact waveguides for plasmonic circuitry based on silver nanorods array embedded vertically into silicon on insulator substrate for nanoscale guidance of optical frequencies.

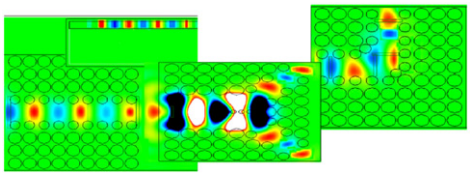

ARTICLE INFO

Article history:
Received 9 July 2012
Received in revised form
8 November 2012
Accepted 26 November 2012
Available online 7 December 2012

ABSTRACT

We propose ultra-compact waveguides for plasmonic circuitry based on silver nanorods array embedded vertically into silicon on insulator (SOI) substrate for nanoscale guidance of optical frequencies. Silver nanorods array palisade silicon to form core of SOI waveguide and is theoretically modeled for the first time. Propagation characteristics of the structure are obtained using finite difference time domain (FDTD) computations, exposing bandgap in the visible regime for transverse magnetic modes and are verified by the plane wave expansion (PWE) method. Narrow transmission bandwidth of ~10 nm with quality factor and confinement factor of 97.5% and 92% is achieved respectively, confirming strong confinement of the propagating mode at 633 nm and the losses calculated in decible per micrometer (dB/μm) for the waveguide is found to be .75 dB/μm for straight waveguide. Further, Y-splitter designed from the basis equally bifurcate power and the outputs received at the two ends are in phase yielding a viable 50–50 power splitter. Bend design routing light in nano-dimensions is also implemented successfully, offering components for high density plasmonic circuitry.

1. Introduction

Plasmonics as a subject deals with constricting electromagnetic (EM) radiation into subwavelength devices and offers extraordinary applications outdoing preceding technologies. Superfast computer chips [1], ultra-sensitive chemical–biomedical sensors [2], surface enhanced Raman spectroscopy (SERS) [3,4], cancer treatment [5], high performance solar cells [6], and ultra-efficient waveguide devices and nano-cicuitry [7,8] are few of the accomplishments achieved through plasmonics. Besides, the recent advancement in nanotechnology and nanophotonics has revolutionized the field of plasmonics promising miniaturization of circuitry to nanoscale dimensions and provides huge data transmission at the bandwidth of photonics [9–12]. But exhaustive research is needed to be able to make compact high density circuits which can be easily integrated with planar circuits requiring all its components on the same chip [13–14].

Among all the metallic elements, silver has the smallest damping constant Γ and is the best-performing choice at optical frequencies i.e. 400–700 nm [15]. Gold can be used as well but it has a larger Γ than silver and is often the metal of choice at lower near infrared (NIR) frequencies. Also, gold has high interband

* Corresponding author.
E-mail address: dr_rk_sinha@yahoo.com (R.K. Sinha).

1386-9477/$ - see front matter © 2012 Elsevier B.V. All rights reserved.
http://dx.doi.org/10.1016/j.physe.2012.11.025

losses in the visible spectrum. Similarly, copper, platinum, and palladium are avoided due to large interband losses over most of the visible spectrum. Thus, silver has predominately been the material of choice for plasmonic applications around the optical frequencies. Ag particles in air have plasmon resonances at 350–480 nm but they can be red-shifted in a controlled way over the entire 500–1500 nm spectral range by partially embedding them in SiO_2, Si_3N_4 or Si [16]. Kwata et al. reported subwavelength optical imaging through metallic nanorod array [17] presenting the performance of plasmonics. Silver wires behave as surface plasmon resonators and electromagnetic energy transport through metallic nanowires deposited on the dielectric substrate [18]. Hence the properties of nanostructured silver make it most suitable for the next generation plasmonics [19].

Metal nanowires/nanorods are adept choice for designing compact plasmonic waveguides since it is an attractive option mainly due to nanoscale—confinement, guiding, imaging and show comparatively low propagation losses [20,21] because of their unique optical properties. But integrating the horizontally lying nanorod structures with main circuitry is a challenge and hinders the efficient excitation of the surface plasmon polaritons (SPPs) which are excited using the end fire excitation technique [22] or the prism coupling [23], which is often cumbersome to be used in chip design.

To get over this, laying silver (Ag) nanorods perpendicularly into semiconductor material, opens up the option of making planar components for plasmonic circuitry as well as allow efficient coupling with parallel devices. So, we propose a new design for compact plasmonic waveguide in which square lattice array of silver nanorods are embedded in silicon on insulator (SOI) substrate, Fig. 1(a) with main purpose to show stronger confinement with appreciable propagation length of 633 nm wavelength, exhibiting substantial quality factor and thus can be efficiently implemented in high density on-chip circuits due to its planar geometry. Nanorods having negative dielectric constant are embedded into SOI with palisade high refractive index Si core and have SiO_2 base as substrate resulting in the proposed core for light propagation. Ag nanorods provide lateral confinement within the nano sized low loss Si core in contrast to lossy planar metal structure, arrayed structure provides bandgap and texturing due to base of metal rods, yields the momentum to the propagating plasmon through the waveguide. Insulator as substrate offers vertical confinement also making it rugged and compatible for integrated circuitry. The high refractive index core of silicon retains the propagating mode and the bandgap forbids the mode from leaking. Arrayed basis waveguide exhibits a bandgap in the visible region; however, the introduced defect provides a strong field confinement to the propagating 633 nm wavelength with a bandwidth of 10 nm, and can be used as a narrow band-pass filter as well. Pyayt et al. [24] employed tapered silver nanowire with polymers but it can be bothersome at high temperature.

Usefulness of this approach is that, such designs are compatible with the commercially examined available technology [25] and provides us the synergistic results of plasmonics via photonics and electronics [26] along with easy integration with planar circuitry. We have obtained strong confinement and low loss in the proposed waveguides. More importantly it is easy to introduce defects by removing nanorods to make various devices (straight waveguide, bend, S-bend, Y and T-splitters, couplers etc.) in the reported arrayed geometry without inducing an unwanted stress at bends and corners which is noticeable in case of metal sheets or films when they are cut at sharp bends or when holes and grooves are incised into metal. Hence the basis geometry can be easily employed to devise various optical components such as couplers, splitters, multiplexers, demultiplexers etc., thereby, opening new possibilities in the ultra compact plasmonic circuitry design.

2. Structure design and simulation method

The basis structure comprises of arrangement of silver nanorods in a square lattice lying perpendicularly on the silicon-on-insulator as substrate. The waveguide is designed by introducing defects in the periodicity. Proposed straight waveguide is composed of a line defect in the basis waveguide comprising of periodically arranged silver nanorods (with dielectric constant, $\varepsilon = -13.6089 + i0.995$ at 633 nm) embedded to an optimized depth of 50 nm into the SOI substrate. The schematic representation of the basis waveguide cross section (x–y plane) and top view (x–z plane) are shown in Fig. 1(a) and its inset respectively.

Values of various parameters of the components used in designing the devices are as mentioned here, the silver nanorods of radius (r_{Ag}) 45 nm, height (h_{Ag}) 150 nm and lattice constant $a_{Ag} = 110$ nm are arranged in a square lattice arrangement into silicon layer of refractive index $n_{Si} = 3.5$ with thickness (h_{Si}) 100 nm to a depth of 50 nm into it. SiO_2 layer of refractive index

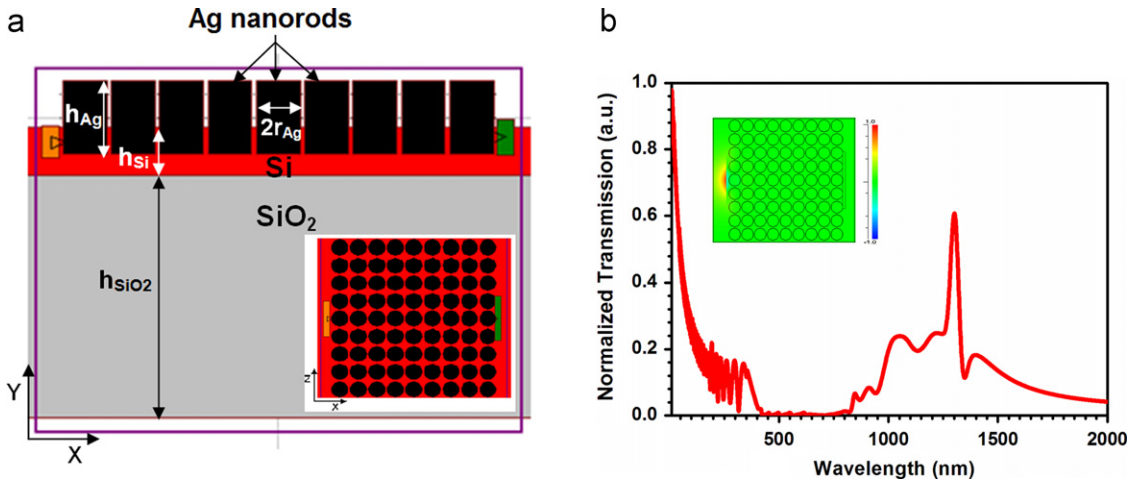

Fig. 1. (a) Schematic of the basis waveguide cross-section (x–y plane) and top view in inset (x–z plane) of proposed basis waveguide comprising of silver nanorods on silicon on insulator (SOI) substrate. (b) Normalized transmission for the basis structure showing bandgap within 400–800 nm and inset show E_y field profile depicting the light is forbidden from propagation.

$n_{SiO_2} = 1.45$ with thickness (h_{SiO_2}) 500 nm is chosen as a substrate. Such a basis waveguide has been found to exhibit a bandgap in the visible regime, this is shown in Fig. 1(b) as the normalized transmission depict gap within the visible regime and the simulated E_y field profile is represented in the inset of Fig. 1(b) indicating the gap offered by the periodic structure. The length of the waveguide is 1 μm. The defect in the straight waveguide is designed by removing silver nanorod linear array with diameter 90 nm and optimizing the adjacent rod radii to 35 nm resulting in nanometer sized defect. The bend design also has similar defect as in straight waveguide till 400 nm of length and then light bends at the corner with the aid of an additional nanorod introduced at the bend, traversing the remaining length of the waveguide. In Y-splitter the light is launched in a wider defect by removing three rows of nanorods and then the presence of four additional nanorods of radii 25 nm each bifurcate the propagating mode into the arms of the splitter each with a defect width of 90 nm.

Bandgap for the structure is verified by using plane wave expansion (PWE) simulations and the results yield accurate measurement of gap (Fig. 2(a)) and also confirm the results of transmissions characteristics (Fig. 1(b)). We have optimized various controlling parameters by running the scan over a range of parameter giving the option for choosing the appropriate values. The gap map calculated using the PWE method shows prominent transverse magnetic (TM) gap offered by the structure, as portrayed in Fig. 2(a) and largest gap is marked as Band-1. The gap-map is scanned for a range of radii giving the optimized radius value of 45 nm obtained from the central value of the maximum gap region i.e. Band-1 yielding the frequency value of 1.57 in units of $\omega a/2\pi c$. The structure is also scanned over a range of wavelengths; the graphical representation of the measured gap-map for the structure is indicated in Fig. 2(b) which shows that the bandgaps are larger around 600 nm wavelength and we can tailor our device near this wavelength. However by introducing a line defect we have proposed a straight, bend waveguides and Y-splitter which is discussed later in Section 3.

3. Results and discussion

In order to obtain the propagation characteristics of such waveguides, the 3D Finite Difference Time Domain (FDTD) method is employed. The simulation has been performed using perfectly matched layer (PML) boundary conditions with PML width = 500 nm along the *x*, *y* and *z* directions and average grid size of 6.25 nm was taken along the *x*- and *z*-axis whereas, 10 nm along the *y*-axis. The light wave of wavelength 1550 nm is launched into the device perpendicular to the longitudinal axis of the Ag nanorods. We first examined the normalized transmission spectrum for the complete structure with no defect as a function of wavelength and this can be observed from Fig. 1(b) that the structure offers a transverse magnetic (TM) bandgap for wavelength range of 400 nm to 800 nm. This is also realised by observing the contour plot of Electric field (E_y) along the propagation direction for the launched wavelength in the inset of Fig. 1(b) which shows that the light is prohibited from propagating through the structure resulting in the bandgap. The gap is also verified by the PWE method and is pictorially presented in Fig. 2(a) and (b).

It is to be mentioned that since, the bandgap in the basis waveguide covers the visible region and silver support plasmons in visible spectrum, hence, the device was optimized for 633 nm anticipating its vast grounded applications. Thus, in the following we discuss the properties of the various waveguides and devices based on the defect in the basis waveguide at 633 nm.

Maier and his group have reported that electromagnetic energy can be carried along the array of Cu rods in air [27] which supports that it is possible to design plasmonic circuits with silver nanorods embedded into SOI which can carry the EM energy in the defect region of silicon fenced by metal rods and having SiO_2 beneath Si. The narrow defect forms the core of the waveguide where the energy propagates.

3.1. Straight waveguide

The basis waveguide is engineered for linear defect, which is introduced by removing the central row of nanorods, resulting in a straight waveguide, as shown in the inset (i_1) of Fig. 3(a). Also the radii of the nanorods lying in the adjacent rows (radius = 35 nm) were tuned to insist the propagation of the launched light at 633 nm. The depth to which the rods are inserted is optimized to be 50 nm; by doing so we found that the maximum intensity of the mode stays in Si defect region as compared to that when kept superficially above silicon slab or when inserted completely. Electromagnetic energy traverses through the defect and the presence of metal nanorods leads to the confinement of this energy within the subwavelength defect. The textured interface at the base of the nanorods and Si slab leads to the generation of the localized plasmons and hence, provides strong confinement of light within the waveguide. Further, the inset (i_2) in Fig. 3(a) illustrates the top view and lateral view of the contour mode profile of transverse electric field (E_y) respectively which depicts that the mode stays within the desired subwavelength linear defect waveguide.

On introducing the linear defect, the structure acts like a waveguide and the defect parameters (radius, height etc.) are optimized for 633 nm wavelength because by preparing silver

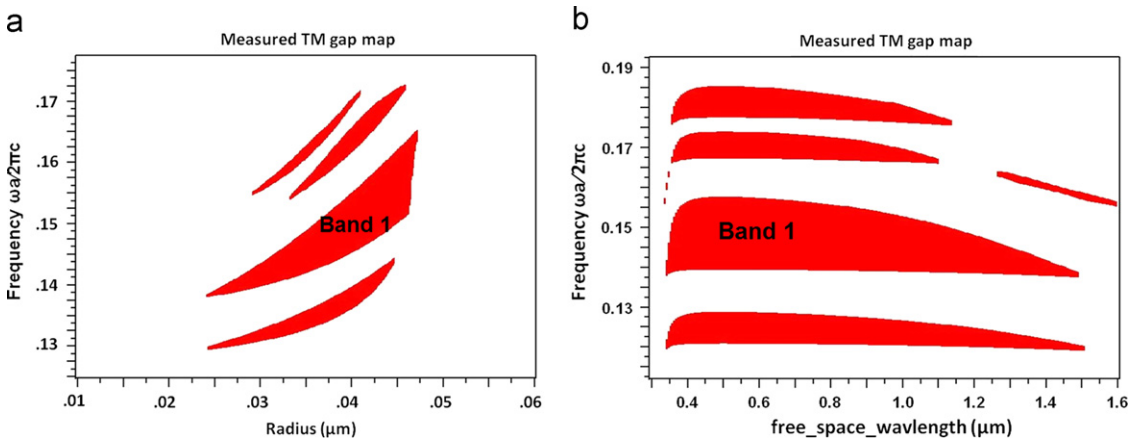

Fig. 2. (a) and (b) Measured TM gap map representing the gap region offered by the structure scanned over a range of radii and wavelengths respectively.

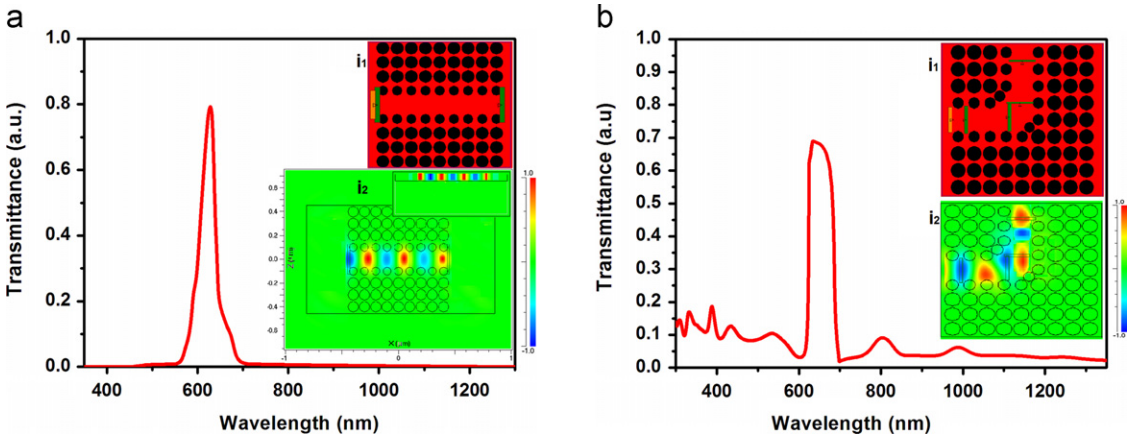

Fig. 3. (a) Normalized transmission for the proposed straight waveguide showing peak at $\lambda=633$ nm, schematic of the structure and the E_y field profile in the x–z and x–y planes are given in the inset. (b) Bend waveguide is shown with the resonating peak at 633 nm and the inset shows the structure and the E_y field profile depicting how the energy is bending in the waveguide.

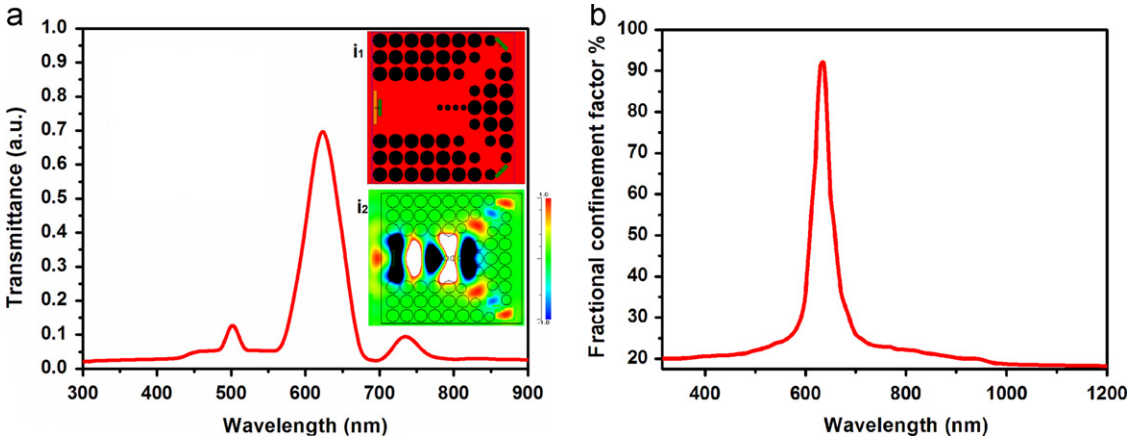

Fig. 4. (a) Normalized transmission for the proposed Y-splitter with resonating peak at $\lambda=633$ nm. Schematic and the E_y field profile showing energy splitting into the two arms is given in the inset. (b) Variation of fractional confinement factor with wavelength indicating maximum confinement for 633 nm wavelength.

nanostructures of different sizes and shapes the SPR wavelengths can be tuned for different wavelengths [28,29]. Also, it is observed that the plasmons in silver resonate over visible frequency range [16] therefore it is suitable to design devices having applications and requirement of the visible regime.

The normalized power transmittance for the nano-sized straight waveguide indicates the resonating peak at 633 nm as shown in Fig. 3(a) and is calculated by measuring the fraction of power at output with respect to the input. The straight waveguide exhibits a quality factor of 97.5% for $\lambda=633$ nm. Also, the fractional confinement factor i.e. ratio of power at the output of the core to the output of the whole waveguide is described later in this section. We see that 92% confinement for the propagating wavelength is for 633 nm and is calculated to be less for the rest of the wavelengths validating that the device is tuned for 633 nm wavelength, as shown in Fig. 4(b).

3.2. Bend waveguide

Apart from straight waveguide, the basis waveguide can also be utilized for making bend through it. An efficient bend design is devised by centrally removing the silver nanorods approximately at right angles. For the light to bend at the corner, an additional silver nanopillar with an optimized radius is introduced at the corner of the bend which acts as a reflector, as shown in the inset (i_1) of Fig. 3(b) and the curve plotted in the figure represents the normalized power transmission, which shows a major peak transmission at wavelength 633 nm along with a few smaller peaks. The propagating mode is able to take sharp bends with ease. The computed field (E_y) profile obtained on investigation of the bend design appears in the inset (i_2) of Fig. 3(b), exhibiting confinement of the modal power within the bend waveguide.

3.3. Y-splitter

The Y-splitter devised from the basis waveguide consists of y-shaped defect in the basis waveguide (top view as shown in the inset (i_1) of Fig. 4(a)). The pillars adjacent to the defect are optimized to a radius of 35 nm and additional nanorods of radius 25 nm introduced at the junction of the two bifurcating arms assist splitting. It is found that the introduced defect and its optimization provide easy propagation for 633 nm wavelength. The output power obtained at the end of the individual arms is found to be equal and incident light reaches the monitor at the end of the two arms in same phase. The normalized power transmission obtained from the proposed Y-splitter shows a peak at the optical wavelength of 633 nm and it is observed that the result overlaps for the two arms of the splitter, as shown in Fig. 4(a) hence it can work as 50–50 power splitter. Y-splitter shows confinement of modal power within the defect region of the waveguide. The contour map of the field E_y depicts and

indicates how the incident energy divides at the origin of the splitting arms of the splitter see the inset (i_2) of Fig. 4(a).

Further, the fractional modal power i.e. confinement factor for different wavelengths is investigated for the line defect as shown in Fig. 4(b). Fractional confinement factor is defined as ratio of power at the output of the core to the output of the whole waveguide. It is observed that the optimized straight waveguide shows the peak confinement factor of 92% for the propagating wavelength of 633 nm and is calculated to be less for the rest of the wavelengths validating that the device is tuned for 633 nm wavelength. The propagation length for the defect is calculated to be 1 μm which is more than sufficient when we have to make nano-sized circuit components. Subwavelength confinement of the 633 nm wavelength within the narrow defect opens the way for dense circuitry. Tolerance limit for various rod parameters was calculated, which comes out to be 5 nm in case of rod radii whereas 10 nm with respect to height of the rod which makes it to be a very sensitive device as well. We calculated the loss in dB/μm for all the considered structures and found it to be .75 dB/μm, .89 dB/μm and .77 dB/μm for the straight waveguide, bend waveguide and Y-splitter respectively, thereby exhibiting more loss in the bend waveguide as compared to the straight waveguide and Y-splitter. When the waveguide is bent to form bend design or Y-splitter, the propagating modes in these waveguides experience perturbation from the initial condition (i.e. w.r.t. the straight waveguide) at the bends and corners, which leads to losses thereby resulting in little broadening of the transmittance curve for bend design and Y-splitter shown in Figs. 3(b) and 4(a) respectively as compared to the transmittance curve for straight waveguide in Fig. 3(a). This can be seen by the calculated losses mentioned above, which depicts that in the straight waveguide we get low losses as compared to the bend waveguide and Y-splitter. In literature the transmission losses of about 6 dB/μm for gold and silver array structure particles are reported by Atwater [7] and the losses of 1.2 dB/μm for 1.5 μm wavelength in gold nanodots on SOI [30] which can be improved by incorporating the proposed geometry for making various devices. Hence, the proposed waveguides with high confinement ~92% with ~.75 dB/μm loss may lead to high density nanophotonic device. With these waveguides one can positively realize nanoscale circuitry i.e. "lab on a chip" [7] and make light route through nanoscale dimensions. Also, with the proposed bend design and Y-splitter, propagating modes can be bent with low losses. Since the device dimensions itself is in nano range, these designs can be used for high density integrated circuits. Apart from light transmission, nanoscale routing, waveguiding, and chip circuitry can also be used for making nano plasmonic sensors, Mach–Zehnder interferometer for calculating minute phase changes, EM field enhancement etc. It also provides a convenient planar geometry that can be easily integrated with other components forming the plasmonic circuitry.

4. Conclusion

In conclusion, we have proposed and analyzed compact Ag nanorods based plasmonic waveguides and devices for the visible regime of electromagnetic spectrum to be used for integrated plasmonic circuitry. Embedded design on SOI offers strongly confining geometry which can be utilized well as the waveguides and also make it robust. Induced defects in the basis waveguide restricts the mode in nano-sized defect and efficiently guide the propagating mode at 633 nm with low losses, which can also be tuned for other wavelengths by altering the various waveguide parameters such as, periodicity or radii of rods or the width of the defect. The quality factor achieved is 97.5%, which is good in case of plasmonics, appreciable propagation length of 1 μm is reached which is far more than sufficient in case of compact dense circuits and high fractional confinement of 92% with comparable losses exposes motivation for its implication to make other parallel devices. Successful implementation of bend design and Y-splitter affirms that such waveguide assist the possibility of making lab on a chip. The proposed planar geometry with strong lateral and vertical confinement of the modes renders easy integration with chip circuitry. The investigations provided here validate the use of nano-structures for the SPP propagation and hence, miniaturize the optical devices for specific applications.

Acknowledgment

The authors gratefully acknowledge (i) the initiatives and support toward establishment of "TIFAC—Center of Relevance and Excellence in Fiber Optics and Optical communication at Delhi College of Engineering, Delhi" through Mission Reach Program of Technology Vision 2020, Government of India and (ii) UGC sponsored major research project in the area of Photonic Crystal Fibers for sensing and telecom. applications.

References

[1] S.J.B. Yoo, Electronics Letters 45 (2009) 584.
[2] J. Homola, Chemical Reviews 108 (2008) 462.
[3] S. Nie, S.R. Emory, Science 275 (1997) 1102.
[4] X. Zhang, Q. Zhou, J. Ni, Z. Li, Z. Zhang, Physica E 44 (2011) 460.
[5] C. Loo, A. Lowery, N.J. Halas, J. West, R. Drezek, Nano Letters 5 (2005) 709.
[6] V.E. Ferry, L.A. Sweatlock, D. Pacifici, H.A. Atwater, Nano Letters 8 (2008) 4391.
[7] H. Atwater, Scientific AmericanApril Issue (2007) 56.
[8] S.A. Maier, M.L. Brongersma, P.G. Kik, S. Meltzer, A.A.G. Requicha, H. Atwater, Advanced Materials 13 (2001) 1501.
[9] W.L. Barnes, A. Dereux, T.W. Ebbesen, Nature 424 (2003) 824.
[10] X. Guo, M. Qiu, J. Bao, B.J. Wiley, Q. Yang, X. Zhang, Y. Ma, H. Yu, L. Tong, Nano Letters 9 (2009) 4515.
[11] T.W. Ebbesen, C. Genet, S.I. Bozhevolnyi, Physics Today (2008) 43.
[12] E. Ozbay, Science 311 (2006) 189.
[13] M. Hochberg, T.B. Jones, C. Walker, A. Scherer, Optics Express 12 (2004) 5481.
[14] G. Veronis, S. Fan, Applied Physics Letters 87 (2005) 131102.
[15] P.B. Johnson, R.W. Christy, Physical Review B 6 (1972) 4370.
[16] H.A. Atwater, A. Polman, Nature Materials 9 (2010) 205.
[17] A. Ono, J. Kato, S. Kwata, Physical Review Letters 95 (2005) 267407.
[18] T. Laroche, C. Girard, Applied Physics Letters 89 (2006) 233119.
[19] M. Rycenga, C.M. Cobley, J. Zeng, W. Li, C.H. Moran, Q. Zhang, D. Qin, Y. Xia, Chemical Reviews 111 (2011) 3669.
[20] C.J. Barrelet, A.B. Greytak, C.M. Leiber, Nano Letters 4 (2004) 1981.
[21] A. Ono, J. Kato, S. Kwata, Physical Review Letters 95 (2005) 267407.
[22] A.W. Sanders, D.A. Routenberg, B.J. Wiley, Y. Xia, E.R. Dufresne, M.A. Reed, Nano Letters 6 (2006) 1822.
[23] D.F. Pile, T. Ogawa, D.K. Gramotnev, T. Okamoto, M. Haraguchi, M. Fukui, S. Matsuo, Applied Physics Letters 87 (2005) 061106.
[24] A.L. Pyayt, B. Wiley, Y. Xia, A. Chen, L. Dalton, Nature Nanotechnology 3 (2008) 660.
[25] P. Dainesi, A. Kung, M. Chabloz, A. Lagos, P. Fluckiger, A. Ionescu, P. Fazan, M. Declerq, P. Renaud, P. Robert, Photonics Technology Letters 12 (2000) 660.
[26] R. Zia, J.A. Schuller, A. Chandran, M.L. Brongersma, Materials Today 9 (2006) 20.
[27] S.A. Maier, M.L. Brongersma, H.A. Atwater, Applied Physics Letters 78 (2001) 16.
[28] Y. Xia, N.J. Halas, MRS Bulletin 30 (2005) 338.
[29] M.E. Stewart, C.R. Anderton, L.B. Thompson, J. Maria, S.K. Gray, J.A. Rogers, R.G. Nuzzo, Chemical Reviews 108 (2008) 494.
[30] S. Maier, M.D. Friedman, P.E. Barclay, O.J. Painter, Applied Physics Letters 86 (2005) 071103.

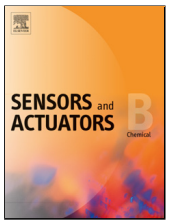

Title: Quantum dots based platform for application to fish freshness biosensor

Authors: K. Kamil Reza, Manish Kumar Singh, Surendra K. Yadav, Jay Singh, Ved Varun Agrawal, B.D. Malhotra<ce:footnote id="fn0005"><ce:note-para>All these authors have equally contributed</ce:note-para></ce:footnote>

PII: S0925-4005(12)01255-5
DOI: doi:10.1016/j.snb.2012.11.059
Reference: SNB 14835

To appear in: *Sensors and Actuators B*

Received date: 21-9-2012
Revised date: 15-11-2012
Accepted date: 17-11-2012

Please cite this article as: K.K. Reza, M.K. Singh, S.K. Yadav, J. Singh, V.V. Agrawal, B.D. Malhotra, Quantum dots based platform for application to fish freshness biosensor, *Sensors and Actuators B: Chemical* (2010), doi:10.1016/j.snb.2012.11.059

Quantum dots based platform for application to fish freshness biosensor

K. Kamil Reza[a*], Manish Kumar Singh[a,b*], Surendra K. Yadav[a,b*], Jay Singh[c], Ved Varun Agrawal[a], B. D. Malhotra[d^]

[a]*Department of Science and Technology Centre on Biomolecular Electronics, Biomedical Instrumentation Section, National Physical Laboratory, Dr. K.S. Krishnan Marg, New Delhi 110012, India*
[b]*Department of Physics, Motilal Nehru National Institute of Technology, Allahabad 211004, India*
[c]*Department of BIN Fusion Technology and Department of Polymer-Nano Science and Technology, Chonbuk National University, Jeonju, Jeonbuk 561-756, Korea*

[d]*Department of Biotechnology, Delhi Technological University, Shahbad Daulatpur, Delhi 110042, India*

ABSTRACT

Laser ablated tin oxide quantum dots (SnO_2 QDs ~1-5 nm) uniformly dispersed in a colloidal solution have been electrophoretically deposited onto indium-tin-oxide (ITO) glass for immobilization of xanthine oxidase (XO_x) for fabrication of fish freshness biosensor. The results of electrochemical response studies conducted on XO_x/SnO_2 QDs/ITO bio-electrode reveal higher sensitivity (0.5148 μA/μMcm^{-2}), lower K_m value (0.022 μM), faster response time (10s), and wide linear range of 1- 400μM with regression co-efficient as 0.999, higher charge transfer rate constant 1.63 s^{-1}.

Keywords: SnO_2 QDs, electrophoretic deposition, xanthine oxidase, electrochemical sensing, fish freshness.

---

^Corresponding author:Email:bansi.malhotra@gmail.com, Tel.: +91-11-27294668; Fax: 91-11-27871023

** All these authors have equally contributed.*

1. Introduction

The fish production in the present-day world is estimated to have risen from 147 million tons in 2010 to 152 million tons in 2011 due to increased consumption. As a part of food safety and food security, there is an urgent need for availability of sensitive and cost-effective methods that can be utilized for estimation of fish freshness. In this context, xanthine liberation arising as a result of metabolic function [1] is considered to be an important marker that can be used to indicate the freshness of fish at an early stage. Besides this, abnormal presence of xanthine in a human may lead to a variety of diseases like gout, xanthineuria and kidney failure, due to its accumulation in blood vessels [2].

Quantum dots (QDs) also known as the artificial atoms have recently attracted much interest because of their unique electrical and optical properties arising due to quantum confinement of the energy levels resulting in enhanced charge transport phenomenon [3,4]. The majority of analytes like enzymes, nucleic acids, antigens are known to have specific binding sites that may perhaps be coupled with the nano-sized compatible quantum dots [5]. It has been reported that electrochemical properties of these tiny nanocrystals arise because of their large surface-to-volume ratio, high surface reaction activity and better charge transfer capability [6-11]. The high-performance liquid chromatography (HPLC) and high performance capillary electrophoresis (HPCE) are commonly used analytical methods for detection and quantification of xanthine These methods are time-consuming, expensive and are not user friendly. Compared to these, electrochemical biosensors are known to be simpler, rapid, sensitive and require no complex sample preparation.

The tin oxide (SnO_2) nanostructures have recently been reported to be biocompatible [12], provide stable physiological environment and are cost-effective. These SnO_2

nanostructures can be utilized for many applications including electrode materials [13], optoelectronic devices [14], sensors [15-17] and as biological labels [18]. The laser ablation in liquid (LAL) has recently been shown to be an interesting technique for fabrication of quantum dots [19]. We report results of studies relating to the fabrication of laser ablated SnO_2 QDs thin film onto indium tin oxide (ITO) via electrophoretic deposition (EPD) technique for application to fish freshness biosensor.

2. Experimental.

2.1 Material and methods

Xanthine oxidase (EC1.1.3.22, from microbial source) has been obtained from Sigma, Germany. Tin oxide quantum dots have been prepared from tin pellets of 99.9% purity, purchased from (Specpure Johnson Mathey, U.K). The xanthine, ascorbic acid, lactic acid, perchloric acids have been purchased from Fine Chemicals New Delhi, India. All other reagents are of analytical grade and have been used as received without any further purification. All aqueous solutions have been prepared in double distilled water. Phosphate buffer solution (PBS) is prepared from Na_2HPO_4 and NaH_2PO_4 reagents.

2.2 Mechanism of SnO_2 quantum dots formation

Tin pellet of 99.9% purity is placed at the bottom of glass vessel containing 20 mL of double deionised water. The pellet is ablated for 60 minutes by focused beam of 1064 nm of pulsed Nd: YAG (Spectra Physics, Quanta Ray, U.S.A.) laser operating at 35 mJ/ pulse energy with 10 Hz repetition rate and 10 ns pulse width [19]. A laser pulse interacts with tin immersed in double distilled water and a plasma plume is generated at the liquid–solid interface due to the absorption of the laser pulse. The confined plasma creates a shock wave that results in higher

pressure and increase in plasma temperature (6000 K). As a consequence, the ejection of ions, atoms, and clusters from the target may react with liquid molecules at the interfacial region between plasma and liquid at a liquid–solid interface [20]. The transient reactions and rapid quenching result in clusters encounter and interact with the solvent, inducing the following chemical reaction:

$$Sn(clusters) + 4H_2O \rightarrow Sn(OH)_4 + 2H_2\uparrow \quad \text{----------(1)}$$

$$Sn(OH)_4 \xrightarrow{\text{high (pressure /temperature)}} SnO_2 + 2H_2O \quad \text{----------(2)}$$

The local high temperature and pressure in the LAL process provide appropriate conditions for the formation of SnO_2. Thus obtained solution of colloidal nanoparticles is collected for characterization and preparation of thin film by electrophoretic deposition technique.

2.3 Bioelectrode fabrication

The proposed mechanism for preparation of XO_x/SnO_2 QDs/ITO bio-electrode and immobilization of XO_x onto this electrode are shown in Scheme 1. ITO (indium tin oxide) coated glass sheets are cut into small pieces (0.5cm×2cm) and immersed in a solution of H_2O_2:NH_3:H_2O in the ratio of 1:1:5 (v/v) and are then kept in an ven for about 1h at 80°C. Further the hydrolyzed ITO plates are washed with de-ionized water (DW) and dried at room temperature. For the deposition of SnO_2 QDs film, it is dispersed in autoclaved DW with ratio 1:1 and sonicated for about 30 min for proper dispersion of SnO_2 QDs solution prior to EPD. For 0.25cm^2 area of the electrode, the optimized EPD potential and time are found to be 25mV and 30s, respectively. Multiple samples are prepared for reliability studies. Fresh solution of XO_x

(0.2unit/ml) is prepared in PBS (50 mM, pH 7.0) and is uniformly spread (10μL) onto the desired SnO_2 QDs/ITO electrode. The XO_x/SnO_2 QDs/ITO bio-electrode is stored in a humid chamber for 12h at room temperature. The bio-electrode XO_x/SnO_2 QDs/ITO thus fabricated was washed thoroughly with PB (50mM, pH 7.0) containing 0.9% NaCl to remove any unbound enzyme and stored at 4°C.

2.4 Instruments

The surface topographies of SnO_2 QDs/ITO electrode and XO_x/SnO_2 QDs/ITO bio-electrode have been investigated using atomic force microscopy (AFM) (VEECO, New York, USA) in the non-contact mode. Morphological observations have been carried out using scanning electron microscope (SEM, LEO-440), (Carl Zeiss, Jena, Germany) and transmission electron microscope (TEM, Tecnai G20–stwin) (FEI, Hillsboro, USA) .The images of the nanoparticles have been recorded at an accelerating potential of 200kV. Fourier transform infrared spectroscopy (Spectrum BX II) (Perkin Elmer, Waltham, USA), has been utilized to attest enzyme immobilization onto the film. The contact angle (Model OCA15EC) (Data physics Corporation, San Jose, USA) measurements have been done via Sessile drop method to delineate the hydrophilic/hydrophobic nature of the surface before and after the immobilization of biomolecules. Electrochemical studies (electrochemical impedance spectroscopy (EIS) and the cyclic voltammetry (CV) studies have been conducted on an Autolab Potentiostat/Galvanostat (Eco Chemie, , Utrecht, Netherlands) using a three-electrode system with ITO as the working electrode, platinum (Pt) as the auxiliary electrode and Ag/AgCl as reference electrode in PBS (50 mM, pH 7.0, 0.9% NaCl) containing 5 mM $[Fe(CN)_6]^{3-/4-}$.

3. Results and discussion

3.1 Surface characterization of electrodes

Surface morphology studies of the SnO_2 QDs prepared by electrophoretically deposited onto the hydrolyzed indium tin oxide film surface have been conducted by SEM. The SEM images (Fig. 1a & 1b) of SnO_2 QDs/ITO film show uniformly deposited tiny particles with relatively fine, mesoporous and crevice free surface. The granular appearance after enzyme immobilization on to the SnO_2 QDs/ITO electrode surface transforms into a well-spread structure of XO_x/SnO_2 QDs/ITO bio-electrode (Fig. 1c & 1d), revealing binding between enzyme and thin film of tin oxide on ITO.

AFM images (Fig. 2a) reveal smooth morphology of SnO_2 QDs/ITO film having uniform distribution of QDs with roughness (Ra) = 2.66 nm. Size homogeneity of the QDs arises due to high surface charge along with regular smaller particle size that may perhaps result in a well structured thin film in agreement with results of the SEM studies. However, after the immobilization of XO_x, the surface morphology of SnO_2 QDs/ITO film changes into an uneven surface with increased value of average roughness (R_a) = 5.35 nm indicating that XO_x is adsorbed onto SnO_2 QDs/ITO film with peak height of 20 nm (Fig. 2b). It can perhaps be concluded that XO_x molecules are attached with the SnO_2 QDs/ITO thin film.

The transmission electron microscopic image (Fig. 3a) of the SnO_2 QDs/ITO film surface shows presence of the self–assembled quantum dots. The agglomeration perhaps arises due to presence of strong inter particle interactions. A closer view of tin oxide quantum dots reveals scattered planes throughout the image and a large portion is covered by dark spots as nanoparticles (Fig. 3b). The particle size distribution confirms presence of the majority of the

quantum dots having particle size of around ~2.5 nm. The range of the SnO_2 nanoparticles size varies from 1 to 5 nm.

Contact angle (CA) measurements have been carried out to investigate the hydrophilic nature of the surface before and after the immobilization of biomolecules by the Sessile drop method using a drop shape analyser (supporting information). The CA for bare ITO (Fig. S a) been found to be as 120°. The CA for SnO_2 QDs/ITO (Fig. S1b) electrode surface is measured to be as 94°. These results reveal that surface of SnO_2 QDs/ITO electrode is less hydrophobic than the bare ITO. The CA for XO_x/SnO_2 QDs/ITO (Fig. S1c) bio-electrode is 65° indicating binding of XO_x with the SnO_2 QDs/ITO electrode surface.

The FTIR spectra of SnO_2 QDs (supporting information Fig. S2) shows peaks at 791 cm^{-1} , 668 cm^{-1} and 500 cm^{-1} peaks pertaining to the vibration mode (antisymmetric) of metal oxide bonds of Sn-O and 1377 cm^{-1} band arises due to bonding in the protein revealing immobilization of XO_x onto SnO_2 QDs/ITO electrode via electrostatic interactions. The FTIR spectrum of the XO_x/SnO_2 QDs/ITO bio-electrode shows characteristic peaks at 1254 cm^{-1} and 1700 cm^{-1} attributed to the C-N group in aromatic amines, carbonyl compounds (C=O stretching , amide I) and NH_2 in aromatic amines (NH stretching) due to plane bending and C-N stretching of peptide group of XO_x on the bio-electrode. The peak observed at 3522 cm^{-1} is due to O-H stretching band and theorganic backbone ($-CH_2-$) of the XO_x.

3.2 *Electrochemical studies*

The results of cyclic voltammetry (CV) studies of SnO_2 QDs/ITO (Fig. 4 a) reveal that the magnitude of current is higher (0.387 mA ,Curve i) as compared to that of bare ITO electrode (0.327mA, Curve ii). This can be assigned to the redox reaction occurring at SnO_2 QDs/ITO interface due to presence of surface charges. However, after immobilization of XO_x onto SnO_2

QDs/ITO electrode, the magnitude of peak current obtained for XO_x/SnO_2 QDs/ITO (Curve iii) electrode is 0.178 mA that is less than that of SnO_2 QDs/ITO electrode due to complex formation between XO_x and SnO_2 QDs indicating binding of XO_x with SnO_2 QDs electrode that perhaps hinders charge transport.

Fig. 4 (c) shows response of the XO_x/SnO_2 QDs/ITO bio-electrode obtained as a function of scan rate varying from (10 - 100 mV/s). Both anodic and cathodic peak currents are proportional to the square root of scan rate (mV/s). The peak currents show linear behaviour with square root of the scan rate (mV/s) (Fig. 4 c, inset (i)), suggesting that the electrode reaction is a diffusion controlled process. The diffusion coefficient (D) of the redox group of XO_x/SnO_2 QDs/ITO bio-electrode has been calculated using the Randel-Sevcik equation (equation 3)

$$I_p = 2.69 \times 10^5 \, n^{3/2} \, A \, D^{1/2} \, C \, v^{1/2} \quad \text{----------} \quad (3)$$

where i_p is peak current (A), n is electron stoichiometry, A is electrode area (0.25 cm^2), D is diffusion coefficient, C is concentration of redox species (5 x 10^{-6} mol/cm^3) and υ is scan rate. The magnitude of diffusion coefficient has been found out to be as 3.46 x10^{-6} cm^2/s.The values of heterogeneous electron transfer rate constant of XO_x immobilized SnO_2 QDs/ITO electrode has been calculated using the Laviron model [21]. The value of electron transfer rate obtained as 1.63s^{-1} indicates fast electron transfer between immobilized XO_x and electrode due to the presence of SnO_2 QDs in the matrix.

In EIS, the impedance is measured by charge transfer resistance (Nyquist diameter, R_{CT}) in presence of electrolyte solution which depends on the dielectric and insulating characteristics at the electrode/electrolyte interface shown in (Fig. 4b). The R_{CT} values of XOx/SnO2 QDs/ITO (curve (ii)), SnO2 QDs/ITO (curve (iii)) have been recorded as 1.83 Ω and 1.24 Ω, respectively.

The increased R_{CT} value of XO_x/ SnO_2 QDs/ITO bio-electrode over SnO_2 QDs/ITO bio-electrode is perhaps due to impediment in the electron transfer.

The effect of pH value on the performance of the biosensor is of great importance since activity of the immobilized enzyme is pH dependent. The oxidation peak current of the XO_x/SnO_2 QDs/ITO bio-electrode at different pH (6.0-8.0) values in the presence of the same concentration of xanthine (100 μM) has been measured in PBS (50mM 0.9% NaCl) containing $[Fe(CN)_6]^{3-/4-}$ 5mM at scan rate of 50mV/s (Fig. 4d**).** The highest magnitude of current is obtained at pH 7, indicating that the XO_x/SnO_2 QDs /ITO bio-electrode is most active at pH 7 at which XO_x molecules retain their natural structures (inset of Fig. 4d).

3.3 *Response measurements*

The electrochemical response studies of the XO_x/SnO_2 QDs/ITO bio-electrode have been performed as a function of xanthine concentration (1-400 μm) in PBS (pH 7.0) (50 mM 0.9% NaCl) containing $[Fe(CN)_6]^{3-/4-}$ 5mM at scan rate of 50mV/s (Fig. 5). The magnified image of the sensing response of selected area is shown in the inset of Fig. 5. This is due to the liberation of H_2O_2 liberation according to biochemical reaction, which eventually releases electrons along with uric acid. The peak value obtained at 0.38V in CV spectra corresponds to oxidation. The magnitude of the oxidation peak increases linearly with increase in the xanthine concentration. Under optimized conditions, the steady-state current of the fabricated biosensor shows the linear range to be as 1-400μm and the response time of 10s. The sensitivity of the XO_x/SnO_2 QDs/ITO bio-electrode has been estimated to be as 0.5148 μA/μM cm^{-2} with the regression coefficient of 0.999.

The Michaelis-Menten constant (K_m) for the XO_x/SnO_2 QDs/ITO bio-electrode, estimated by Hanes plot i.e. graph between [substrate concentration] and [substrate concentration/current]

has been found to be as 0.022μM with regression coefficient of 0.99. The value of K_m depends on various factors such as matrix and the conformational changes in the enzyme structure as the enzyme kinetics is microenvironment sensitive. The lower K_m value indicates increased affinity of XO_x/SnO_2 QDs/ITO bio-electrode that is attributed to favourable orientation of the biomolecules (XO_x) and higher loading onto the surface of SnO_2 QDs/ITO electrode. The response time of the XO_x/SnO_2 QDs/ITO bio-electrode found to be as 10s is attributed to faster electron communication feature of SnO_2 QDs/ITO electrode.

3.4 E*ffect of interferents and stability of bioelectrode*

The stability of the XO_x/SnO_2 QDs/ITO bio-electrode has been investigated by measuring the amperometric response at a xanthine concentration of 100 μM over a period of 10 weeks (supporting information of Fig S3a). The XO_x/SnO_2 QDs/ITO bio-electrode has been used daily and is stored at 4°C when not in use. The response of XO_x/SnO_2 QDs/ITO bio-electrode gradually decreases after about 6 weeks. It decreases to approximately 25% of the initial response after 10 weeks. This suggests that XO_x/SnO_2 QDs/ITO bio-electrode has a good stability of enzyme electrode. The sensitivity, linearity, K_m value, response time, storage time and % age loss of the bio-electrode are summarized in Table I (supporting information) along with those reported in literature.

The selectivity of the XO_x/SnO_2 QDs/ITO bio-electrode has been evaluated in the presence of other biological compounds such as glucose (5 mM), ascorbic acid (0.05 mM) and lactic acid (0.5 mM) (shown in supporting information of Fig S4**).** SnO_2 QDs film prevents the diffusion of glucose, ascorbic acid, glucose ascorbic acid to the electrode. It has been found that

the XO_x/SnO_2 QDs/ITO electrode responds to uric acid indicating that anodic detection of xanthine suffers from the interference of uric acid at high concentration.

3.5 S*tudies with real samples*

Xanthine detection in real samples has been conducted in fresh sol fish samples. The sol fish is cut it into small pieces for chopping (5 gm) and is made it into a fine paste in presence of 5 ml of 0.5 M $HClO_4$. The denatured samples are mechanically stirred for about 10 minutes and are then centrifuged at 4000 rpm for 5 minutes. Then its pH is adjusted to 7.0 with NaOH. The supernatant is further stirred and centrifuged for a few minutes. After adjusting the pH to 7.0, it is diluted 10 times to the initial volume. Xanthine concentration is determined immediately from one part as per the standard procedure and rest of the solution is further analyzed up to 15 days. The increase in xanthine concentration as a function of days can be seen (shown in the supporting information of Fig.S3b)

4. Conclusions

It has been demonstrated that LAL synthesized SnO_2 quantum dots can be used for xanthine detection by the electrochemical method. The uniform size of granular SnO_2 QDs provide a better substrate, improved sensitivity, enzyme activity and faster electrochemical response (10s) towards the xanthine analyte. This biosensor exhibits higher sensitivity ($0.5148\mu A/\mu Mcm^{-2}$), lower K_m value 0.022 μM with linear regression at 0.999 and wide linear range of 1-400 μM. Keeping in view the excellent characteristics of this fish freshness biosensor, efforts should be made to associate international agencies for speedy commercialization of this important device. Besides this, it should be interesting to utilize SnO_2

quantum dots based electrode for fabrication of other biosensors such as tea freshness, food pathogens and food toxins detection etc.

Acknowledgements

We thank Director, National Physical Laboratory, New Delhi, India for providing the facilities. The financial support received under Department of Science and Technology projects (GAP-081132) is gratefully acknowledged. We thank Prof. Ram Gopal, University of Allahabad for the use of Laser facilities.

See Supporting information for FTIR, results of Contact Angle Measurements, Interference study, Stability Curve and Real Sample Analysis.

References:

[1] S. K. Yadav, J. Singh, V. V. Agrawal and B. D. Malhotra Nanostructured nickel oxide film for application to fish freshness biosensor. Appl. Phys. Lett. 101, (2012), 023703-23704.

[2] D.L Nelson, M. M Cocx, Lehninger Principles of Biochemistry; Whfreeman, Newyork, (2008), 874-875

[3] A. P. Alivisatos, Semiconductor Clusters, Nanocrystals, and Quantum Dots. Science 271, (1996), 933-937.

[4] J. M. Klostranec and W. C. W. Chan, Quantum Dots in Biological and Biomedical Research: Recent Progress and Present Challenges, Adv. Mat. 18, (2006),1953-1964.

[5] R. Freeman, B. Willner, and I. Willner,Integrated Biomolecule–Quantum Dot Hybrid Systems for Bioanalytical Applications. T. J. Phys. Chem.Lett. 2, (2011), 2667-2677.

[6] R. Cui, H.-C. Pan, J.-J. Zhu, and H.-Y. Chen, Versatile Immunosensor Using CdTe Quantum Dots as Electrochemical and Fluorescent Labels, Anal. Chem. 79, (2007), 8494-8501.

[7] D.Shan,Y Wang,., H. Xue, & S. Cosnier, Sensitive and selective xanthine amperometric sensors based on calcium carbonate nanoparticles. Sensors and Actuators B: Chemical 136, (2009), 510-515

[8] P. R. Solanki, A. Kaushik, A. A. Ansari, G. Sumana, and B. D. Malhotra, Zinc oxide-chitosan nanobiocomposite for urea sensor, Appl. Phys. Lett. 93, (2008), 163903-163903.

[9] R. Devi, Yadav, S. & Pundir, C. S. Amperometric determination of xanthine in fish meat by zinc oxide nanoparticle/chitosan/multiwalled carbon nanotube/polyaniline composite film bound xanthine oxidase. Analyst 137, (2012) 754-759.

[10] Y. Wang and L.Tong, Electrochemical sensor for simultaneous determination of uric acid, xanthine and hypoxanthine based on poly (bromocresol purple) modified glassy carbon electrode. Sensors and Actuators B: Chemical 150,(2010).43-49

[11] W. d. J. R Santos, M.Santhiago, I. V. P. Yoshida & L. T. Kubota, Electrochemical sensor based on imprinted sol–gel and nanomaterial for determination of caffeine. Sensors and Actuators B: Chemical 166–167,(2012), 739-745

[12] J. Liu, Y. Li, X. Huang, and Z. Zhu, Tin Oxide Nanorod Array-Based Electrochemical Hydrogen Peroxide Biosensor, Nano.Res. Lett. 5, 1177 (2010).

[13] G. Feng, W. Shufen, C. Hongming, and L. Chunzhong, Synthesis and optical properties of SnO_2 nanorods.Nanotechnology 19, (2008), 095708.

[14] S. Han, B. Jang, T. Kim, S. M. Oh, and T. Hyeon, Simple Synthesis of Hollow Tin Dioxide Microspheres and Their Application to Lithium-Ion Battery Anodes Adv. Funct. Mat. 15, (2005), 1845-1850.

[15] X. Xu, J. Zhuang, and X. Wang, SnO2 Quantum Dots and Quantum Wires: Controllable Synthesis, Self-Assembled 2D Architectures, and Gas-Sensing PropertiesJ. Am. Chem. Soc. *130*, (2008), 12527-12535.

[16] A. A. Ansari, A. Kaushik, P. R. Solanki, and B. D. Malhotra, Electrochemical Cholesterol Sensor Based on Tin Oxide-Chitosan Nanobiocomposite Film.Electroanalysis 21, (2009). 965-972.

[17] C.W. Liao, J.C. Chou, T.P. Sun, S.K. Hsiung, and J.H. Hsieh, Preliminary investigations on a glucose biosensor based on the potentiometric principle. Sens. and Actu. B: Chem. 123, (2007), 720-726.

[18] Z. Deng, B. Peng, D.Chen, F. Tang, and A.J. Muscat, A New Route to Self-Assembled Tin Dioxide Nanospheres: Fabrication and Characterization. Langmuir, 24(19), (2008),11089-11095.

[19] M. K. Singh, M. C. Mathpal, and A. Agarwal, Optical properties of SnO_2 quantum dots synthesized by laser ablation in liquid, Chem. Phys. Lett. 536, (2012),87-91.

[20] G. W. Yang, Laser ablation in liquids: Applications in the synthesis of nanocrystals. Prog. in Mat. Sci. 52, (2007), 648-698.

[21] E. Laviron, General expression of the linear potential sweep voltammogram in the case of diffusionless electrochemical systems. Journal of Electroanalytical Chemistry and Interfacial Electrochemistry 101, (1979), 19-28.

Figure captions:

Fig. 1 (a). SEM images of electrophoretically deposited thin film of SnO_2 QDs shows a uniform distribution of the quantum dots on the surface of ITO. (b) Magnified image shows few pores with homogeneous size of quantum dots providing a fine platform for enzyme immobilization as large number of surface atoms can be seen. (c) Surface topography of enzyme immobilized on SnO_2 QDs/ITO electrode and (d) enlarged view of XO_x/SnO_2 QDs/ITO bio-electrode.

Fig. 2. Two dimensional and three dimensional AFM images of (a) SnO_2 QDs/ITO electrode with 30 nm heights of thin film deposition and (b) enzyme immobilization is confirmed as XOx/SnO2 QDs/ITO bio-electrode show a 20 nm increment in height of the film.

Fig. 3 (a). TEM images of SnO_2 QDs, huge number of the quantum dots can be seen in this big chunk of the particles. (b) A closer view of this tiny tin oxide quantum dots where planes are visible as well.

Fig. 4. (a) CV of (ii) ITO (i) SnO_2 QDs/ITO electrode and (iii) XO_x/SnO_2 QDs/ITO bio-electrode. (b) EIS studies of (i) ITO (iii) SnO_2 QDs/ITO electrode and (ii) XO_x/SnO_2 QDs/ITO bio-electrode. (c) CV of bio-electrode as a function of scan rate (10 - 100 mV/s) and inset magnitude of current versus potential difference as function of square root of scan rate.(d) CV studies of XO_x/SnO_2 QDs/ITO bio-electrode as a function of pH from 6-8 in phosphate buffer, inset shows the change of conjugative current response as a function of pH on XO_x/SnO_2 QDs/ITO bio-electrode.

Fig. 5. Electrochemical response of XO_x/SnO_2 QDs/ITO bio-electrode with respect to xanthine concentration (1-400μM) in PBS at the scan rate of 50 mV/s.

Scheme 1. Schematic illustration for the fabrication of SnO_2 quantum dots based Xanthine Biosensor.

Fig. 1

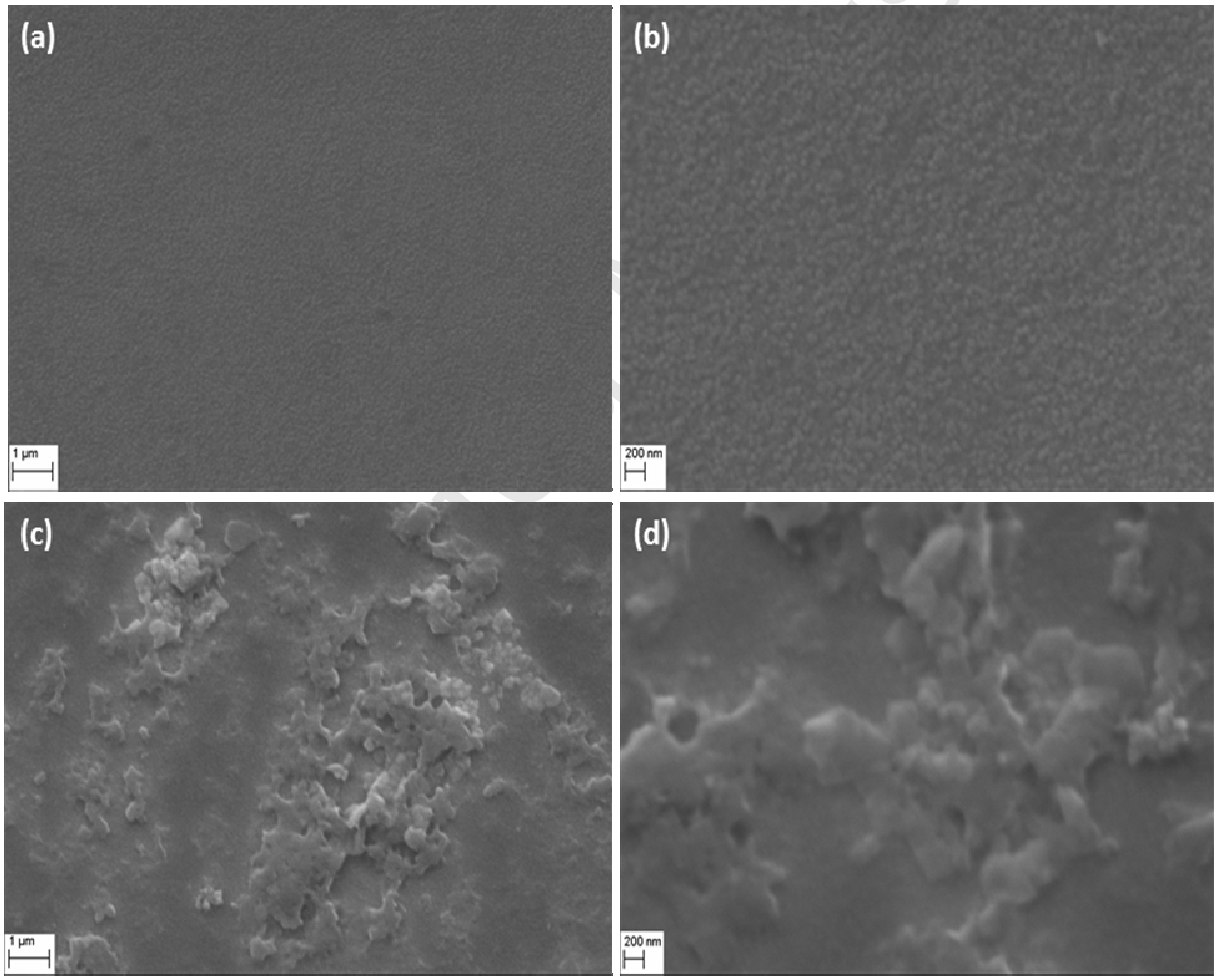

Fig. 2

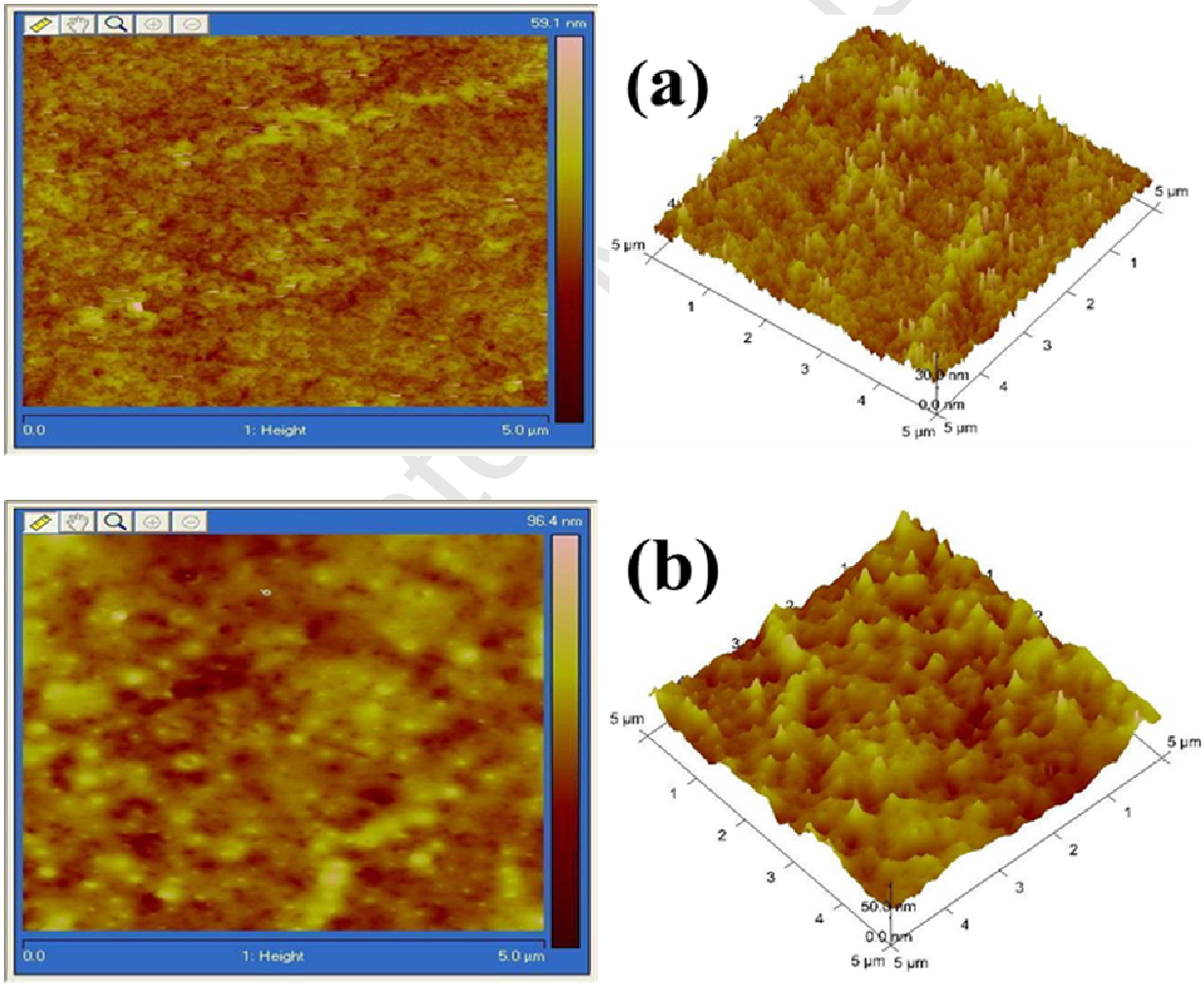

Fig. 3

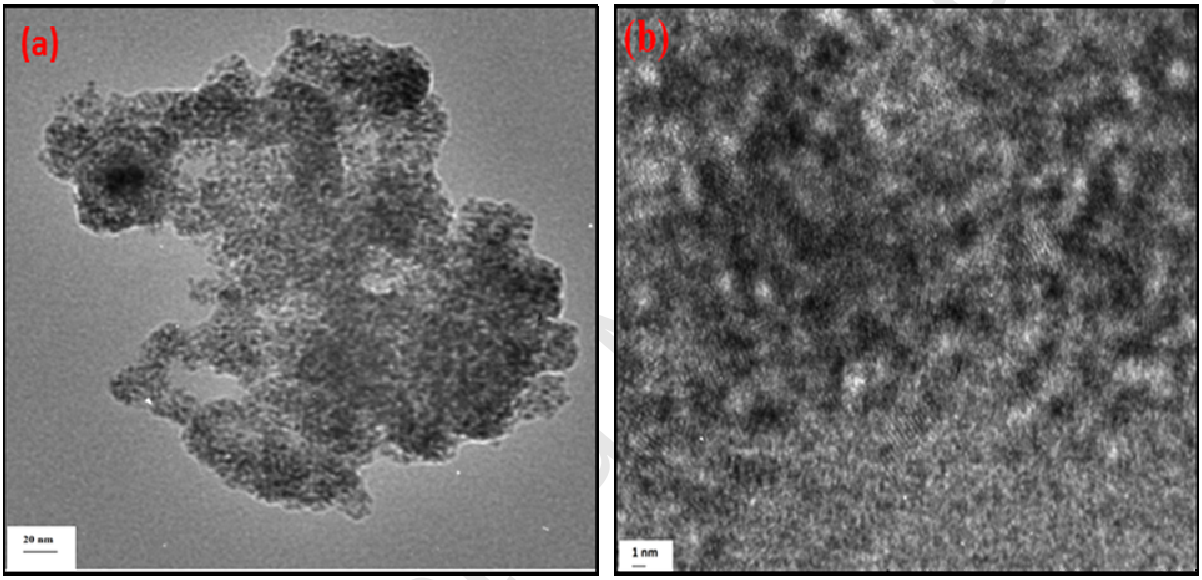

Fig. 4

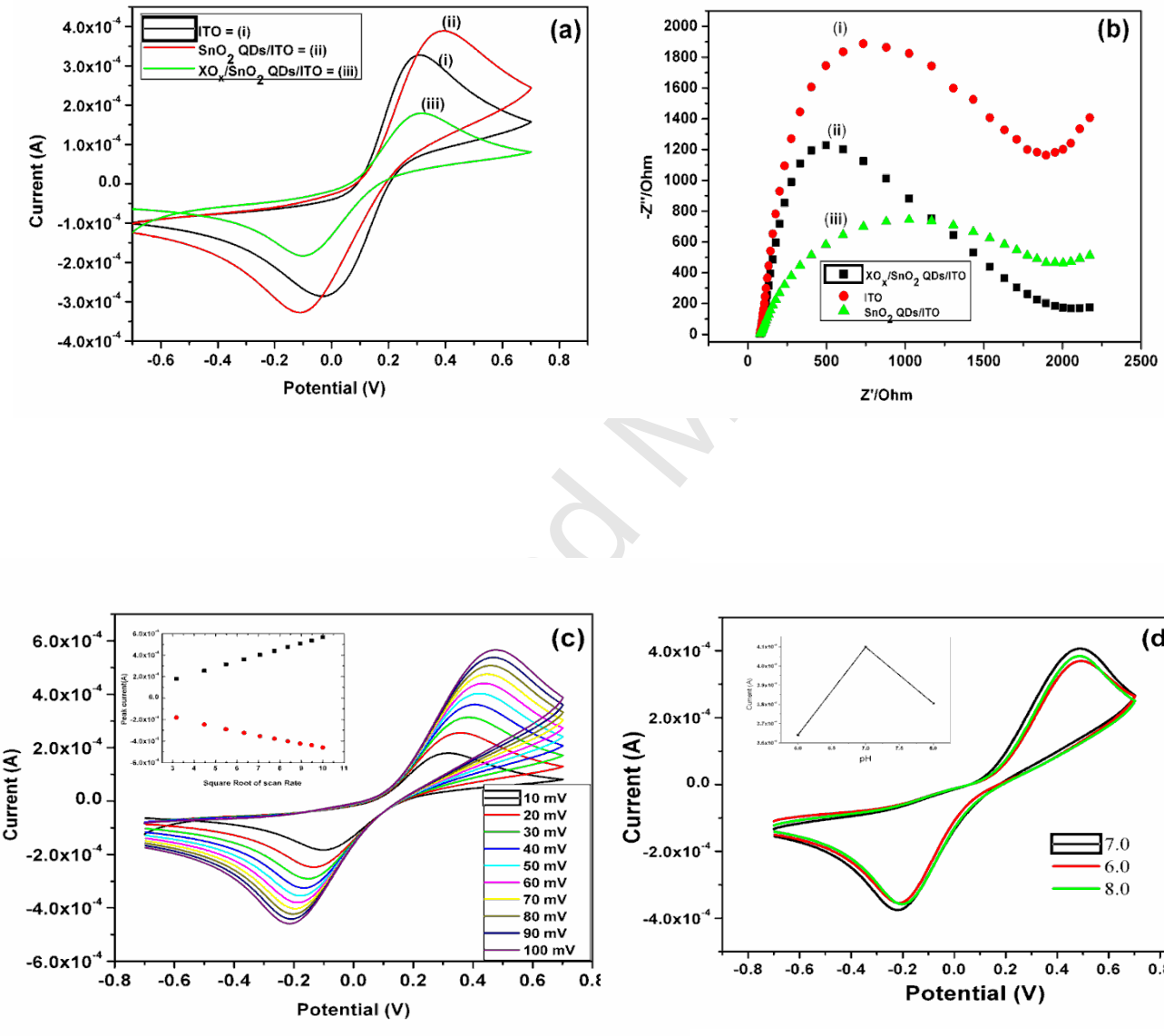

Fig. 5

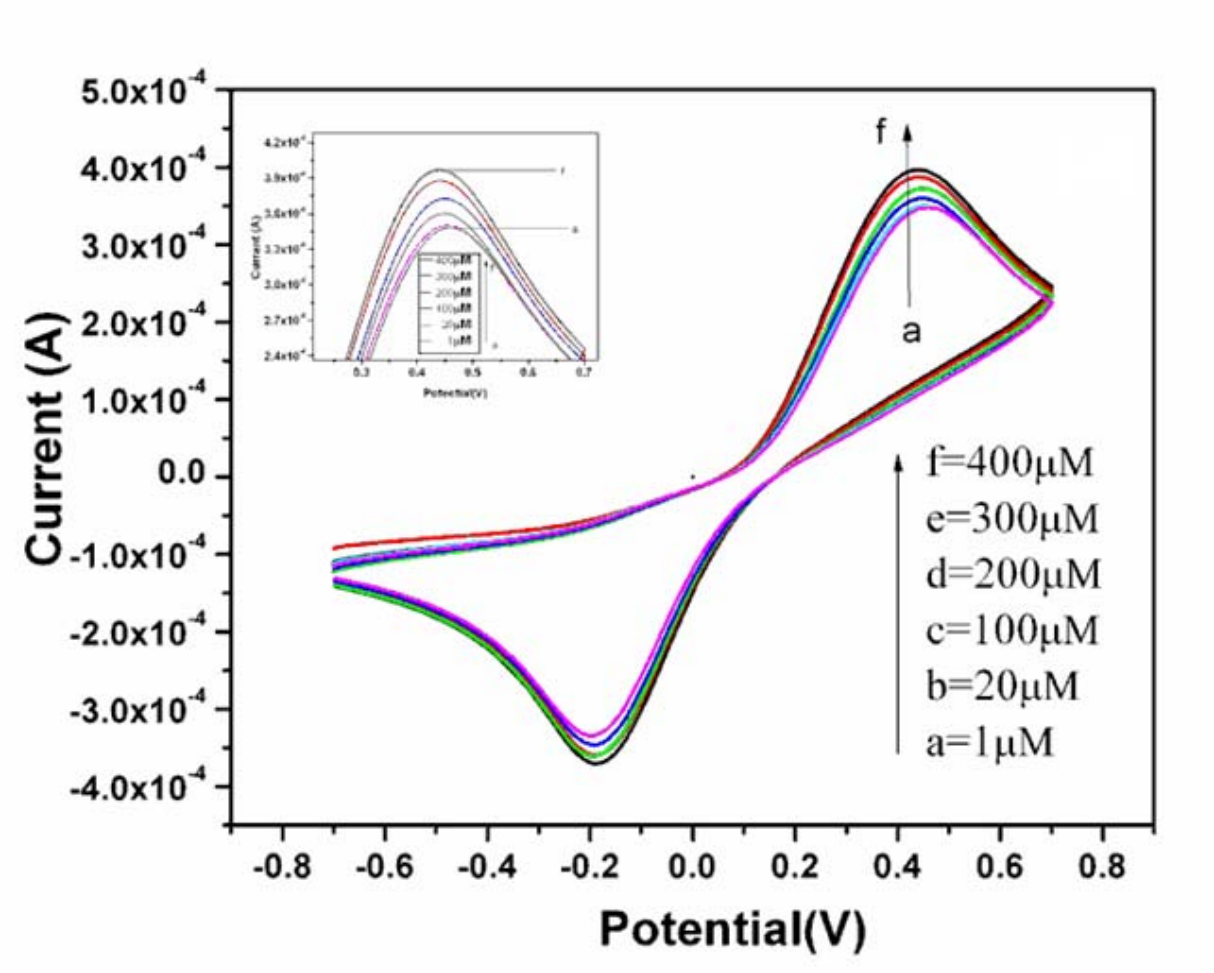

Scheme 1

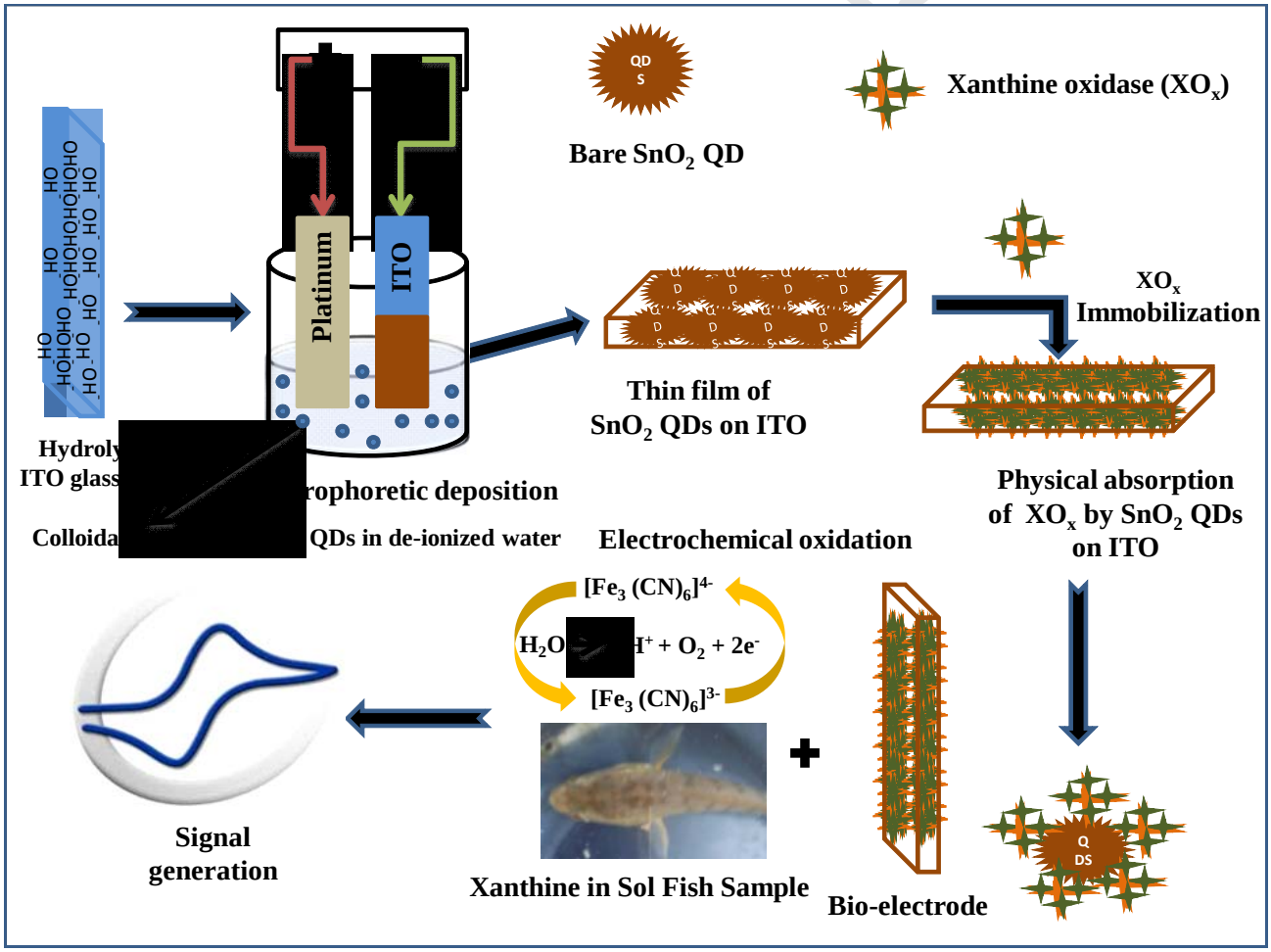

International Scholarly Research Network
ISRN Electronics
Volume 2012, Article ID 890615, 7 pages
doi:10.5402/2012/890615

Research Article

Single OTRA Based Analog Multiplier and Its Applications

Rajeshwari Pandey,[1] Neeta Pandey,[1] B. Sriram,[1] and Sajal K. Paul[2]

[1] *Department of Electronics and Communication Engineering, Delhi Technological University, Delhi 110042, India*
[2] *Department of Electronics Engineering, Indian School of Mines, Dhanbad 826004, India*

Correspondence should be addressed to Neeta Pandey, n66pandey@rediffmail.com

Received 30 August 2012; Accepted 2 October 2012

Academic Editors: H. A. Alzaher and E. Tlelo-Cuautle

This paper presents an analog multiplier using single operational transresistance amplifier (OTRA). The proposed circuit is suitable for integration as it does not use any external passive component. It can be used as a four-quadrant multiplier. Theoretical propositions are verified through PSPICE simulations using 0.5 μm CMOS parameters provided by MOSIS (AGILENT). The simulation results are in close agreement with theoretical predictions. The workability of the proposed multiplier is also tested through two applications, namely, a squarer and an amplitude modulator.

1. Introduction

Analog multipliers find extensive application in the field of telecommunication, control, instrumentation, measurement, and signal processing [1]. A number of circuits are reported in literature relating to analog multipliers [1–12]. Circuits presented in [2–7] are based on Gilbert multiplier [12] and are suitable for CMOS integrated technology. The other class of the circuits is implemented using active analog blocks such as operational transconductance amplifier [1], differential difference current conveyors [8], current feedback amplifiers [9], current-controlled current conveyor [10], and current difference buffered amplifier [11].

Recently the OTRA has emerged as an alternate analog building block [13–26] which inherits all the advantages of current mode techniques. The OTRA is a high gain current input voltage output device. The input terminals of OTRA are internally grounded, thereby eliminating response limitations due to parasitic capacitances and resistances [13] at the input. Several high performance CMOS OTRA topologies have been proposed in the literature [13–16]. In the recent past OTRA has been extensively used as an analog building block for realizing a number of analog signal processing [17–21] and generation circuits [22–24]. This paper presents a single OTRA based low voltage analog multiplier which does not use any external passive components and hence is suitable for integration. The proposed circuit can be used as a four quadrant multiplier without any change of topology. The workability of the proposed multiplier is demonstrated through two applications, namely, a squarer and an amplitude modulator.

2. The Proposed Multiplier Circuit

2.1. OTRA. OTRA is a three-terminal device, shown symbolically in Figure 1 and its port relations are characterized by the following matrix:

$$\begin{bmatrix} V_p \\ V_n \\ V_O \end{bmatrix} = \begin{bmatrix} 0 & 0 & 0 \\ 0 & 0 & 0 \\ R_m & -R_m & 0 \end{bmatrix} \begin{bmatrix} I_p \\ I_n \\ I_O \end{bmatrix}, \quad (1)$$

where R_m is transresistance gain of OTRA. For ideal operations R_m approaches infinity and forces the input currents to be equal. Thus OTRA must be used in a negative feedback configuration.

Figure 2 Shows the CMOS realization of OTRA [15] which consists of the cascaded connection of the modified differential current conveyor (MDCC) [8] and common source amplifier. MDCC performs the current differencing operation and forces the two input terminals to be virtually

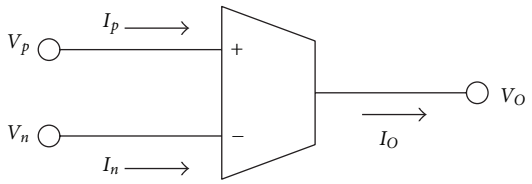

Figure 1: OTRA circuit symbol.

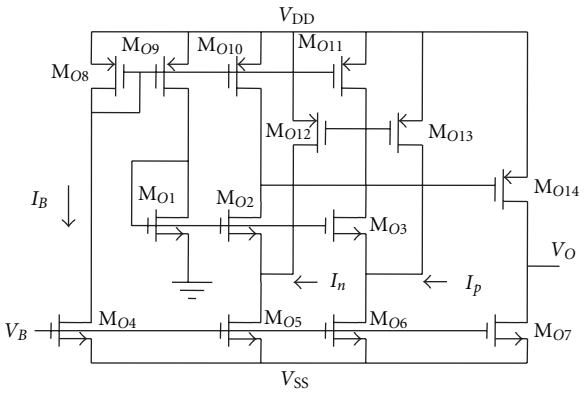

Figure 2: Figure 6 CMOS implementation of OTRA [15].

grounded whereas the common source amplifier provides high gain.

2.2. Basic Multiplier Circuit. Figure 3 Shows OTRA based multiplier structure. The transistors M_1, M_2, M_3, and M_4 are matched transistors and operate in the linear region. In this paper v_1 and v_2 represent small signals, whereas V_{C1}, V_{C2}, and V_{DC} are the bias voltages. OTRA inputs keep the sources of the two transistors M_1 and M_2 virtually grounded. The drain current for the MOS transistor operating in triode region is given by [27]

$$I_D = k\frac{W}{L}\left((V_{GS} - V_T) - \frac{V_{DS}}{2}\right)V_{DS}, \tag{2}$$

where k is transconductance; W and L respectively represent the channel width and length of the of the MOSFET. The other terms have their usual meaning.

Using (2) the currents through p and n terminals of OTRA, that is, i_p and i_n, respectively, can be expressed as

$$\begin{aligned} i_p &= K_n\frac{W}{L}\left(((V_{DC} + v_1) - V_T) - \frac{v_2}{2}\right)v_2 \\ &\quad + K_n\frac{W}{L}\left((V_{C1} - V_T) - \frac{v_o}{2}\right)v_o, \end{aligned} \tag{3}$$

$$\begin{aligned} i_n &= K_n\frac{W}{L}\left((V_{DC} - V_T) - \frac{v_2}{2}\right)v_2 \\ &\quad + K_n\frac{W}{L}\left((V_{C2} - V_T) - \frac{v_o}{2}\right)v_o. \end{aligned} \tag{4}$$

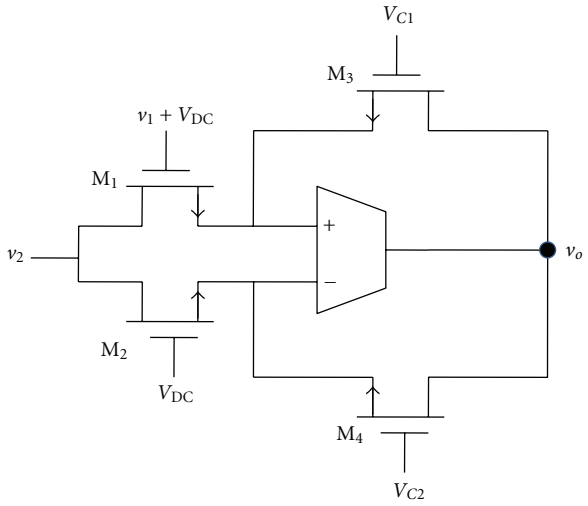

Figure 3: Proposed OTRA based multiplier structure.

As R_m approaches infinity the input currents are forced to be equal resulting in

$$v_o = \frac{v_1 v_2}{(V_{C2} - V_{C1})} = K v_1 v_2, \tag{5}$$

where K is a proportionality constant and is the inverse of difference of gate voltages of M_3 and M_4.

2.3. Implementation Scheme for Superimposition of a Small Signal on DC Bias. As can be seen from Figure 3 the gate voltage of M_1 is $(V_{DC} + v_1)$ which is a small signal superimposed over a dc bias. This voltage addition can be implemented using a scheme proposed in Figure 4 wherein v_x is a small signal voltage and V_C is a bias voltage.

If M_{P1} and M_{P2} are matched transistors and are operating in saturation then their drain currents will be equal resulting in

$$\frac{1}{2}K_p\frac{W}{L}\left((v - V_C) - V_{tp}\right)^2 = \frac{1}{2}K_p\frac{W}{L}\left((v_x - v) - V_{tp}\right)^2, \tag{6}$$

which gives

$$v = \frac{(V_C + v_x)}{2}. \tag{7}$$

The voltage given by (7) can be used as the gate voltage for transistor M_1 of Figure 3. Similarly gate voltage for transistor M_2 can be obtained from (7) by making $v_x = 0$. Substituting these values of gate voltages in (5) the output of the multiplier gets modified to

$$v_o = K' v_1 v_2, \quad \text{where } K' = \frac{K}{2}. \tag{8}$$

2.4. The Proposed MOS Based Multiplier Structure. The complete MOS based multiplier structure is depicted in Figure 5 which incorporates the voltage addition scheme of Figure 4.

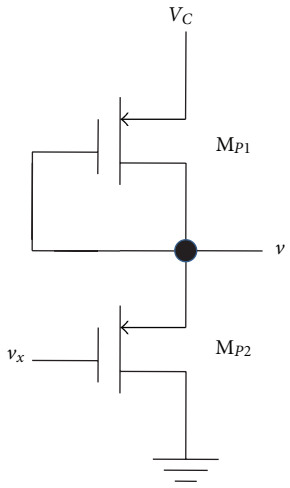

Figure 4: Scheme for implementing an ac superimposed on dc bias.

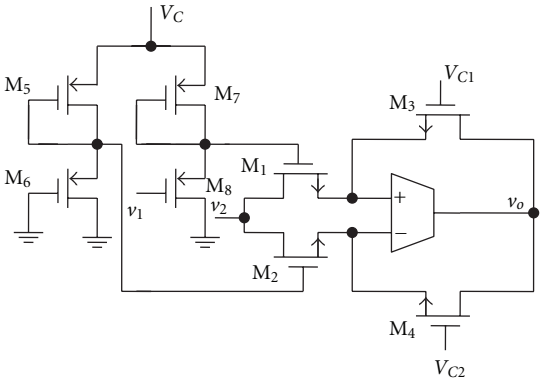

Figure 5: Complete multiplier circuit.

As the transistors M_1, M_2, M_3, and M_4 need to operate in the triode region for proper operation of the multiplier the following conditions should be satisfied:

$$\begin{aligned}\left(\frac{(V_C+v_1)}{2}-V_{tn}\right)&>v_2,\\ \left(\left(\frac{V_C}{2}\right)-V_{tn}\right)&>v_2,\\ (V_{C1}-V_{tn})&>v_o,\\ (V_{C2}-V_{tn})&>v_o.\end{aligned}\tag{9}$$

Now using (7) along with (9) the conditions for input signals v_1 and v_2 can be computed as

$$\begin{aligned}V_{tp}<v_1&<\left(V_C+2V_{tp}\right),\\ v_2&<\frac{(V_C+v_1)}{2}-V_{tn}.\end{aligned}\tag{10}$$

These equations suggest that the dynamic input range of the multiplier is controlled by V_C.

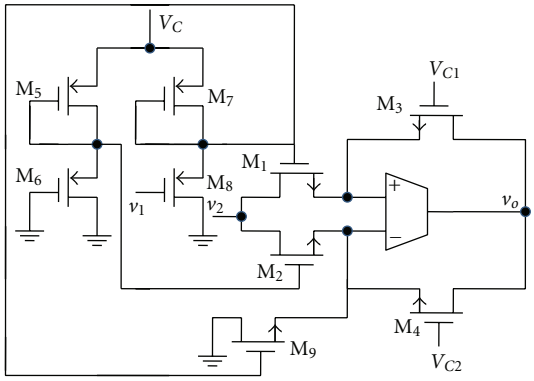

Figure 6: Complete multiplier circuit with C_{gs} compensation of transistor M_1.

3. Nonideal Analysis

In this section the effect of finite transresistance gain of OTRA on multiplier is considered and compensation is employed for high frequency applications. Ideally the transresistance gain R_m is assumed to approach infinity. However, practically R_m is a frequency dependent finite value [13]. Considering a single pole model for the transresistance gain, R_m can be expressed as

$$R_m(s)=\left(\frac{R_0}{1+s/\omega_0}\right).\tag{11}$$

For high frequency applications the transresistance gain $R_m(s)$ reduces to

$$R_m(s)\approx\left(\frac{1}{sC_p}\right),\quad \text{where } C_p=\frac{1}{R_0\omega_0}.\tag{12}$$

For high frequency applications the effect of transistor capacitances needs to be considered. Taking this effect into account the currents i_p given by (3) modifies to

$$\begin{aligned}i_p=K_n\frac{W}{L}\left(((V_{DC}+v_1)-V_T)-\frac{v_2}{2}\right)v_2\\ +K_n\frac{W}{L}\left((V_{C1}-V_T)-\frac{v_o}{2}\right)v_o+v_1sC_{gs1},\end{aligned}\tag{13}$$

where C_{gs1} is the gate to source capacitance of M_1; however, the current i_n remains the same as (4). The effect of C_{gs1} can be compensated by adding a MOSFET M_9, operating in triode region, at the inverting terminal of OTRA as shown in Figure 6. The effective gate to source capacitance of M_9 should be equal to C_{gs1}. This would result in i_n as

$$\begin{aligned}i_n=K_n\frac{W}{L}\left((V_{DC}-V_T)-\frac{v_2}{2}\right)v_2\\ +K_n\frac{W}{L}\left((V_{C2}-V_T)-\frac{v_o}{2}\right)v_o+v_1sC_{gs1}.\end{aligned}\tag{14}$$

The third term in (14) results due to gate to source capacitance of M_9.

Table 1: Aspect ratio of the transistors in OTRA circuit.

Transistor	W (μm)/L (μm)
M_{O1}–M_{O3}	100/2.5
M_{O4}	10/2.5
M_{O5}, M_{O6}	30/2.5
M_{O7}	10/2.5
M_{O8}–M_{O11}	50/2.5
M_{O12}, M_{O13}	100/2.5
M_{O14}	50/0.5

Substituting (12), (13), and (14) in (1), v_o, the output of multiplier can be evaluated as

$$v_o = \frac{v_1 v_2/(V_{C2} - V_{C1})}{1 + sC_p/\{K_n(W/L)(V_{C2} - V_{C1})\}}. \quad (15)$$

And hence the 3 dB bandwidth of the multiplier can be expressed as

$$\frac{K_n(W/L)(V_{C2} - V_{C1})}{C_p}. \quad (16)$$

4. Simulation Results

The performance of the proposed multiplier of Figure 5 is verified through SPICE simulation using 0.5 μm CMOS process parameters provided by MOSIS (AGILENT). CMOS implementation of the OTRA [15] shown in Figure 2 is used and supply voltages are taken as ± 1.5 V. Aspect ratios used for different transistors of OTRA are the same as in [15] and are given in Table 1. All the transistors M_1–M_8 were used with equal aspect ratios having $W/L = 1\,\mu/0.5\,\mu$. Control voltage is taken as $V_C = 2$ V, $V_{C1} = 1$ V, and $V_{C2} = 1.25$ V.

Figure 7 depicts the dc transfer characteristics of the proposed multiplier. The transfer curve v_o versus v_1, with v_2 kept constant at 250 mV, is shown in Figure 7(a). It is observed that v_o varies almost linearly with v_1. The nonlinearity curve representing maximum percent deviation of the ideal transfer characteristic as a function of input voltage v_1 is shown in Figure 7(b). It is observed that the maximum nonlinearity over the entire input range does not exceed 2.05%. In Figure 7(c) v_o is plotted with respect to v_1 for different values of v_2. Voltage v_1 is swept from -300 mV to 300 mV while v_2 is varied from -150 mV to 150 mV in steps of 50 mV. It shows that the proposed circuit is a four-quadrant multiplier.

The frequency response of the proposed multiplier is shown in Figure 8 for which v_1 is kept constant at 200 mV whereas v_2 is taken as an ac source having amplitude 250 mV. The 3 dB bandwidth is found to be 8 MHz.

Figure 9 shows the total harmonic distortion (THD) as a function of input signal amplitude when a constant dc voltage (250 mV) is applied to v_2 while a 1 KHz sinusoidal signal is applied to v_1 with varying amplitude. It can be seen that the maximum THD remains under 0.2% for the entire input range. Total power consumption of the proposed multiplier is 0.83 mw when $v_1 = v_2 = 0$ V, $V_C = 2$ V, $V_{C1} = 1$ V, and $V_{C2} = 1.25$ V.

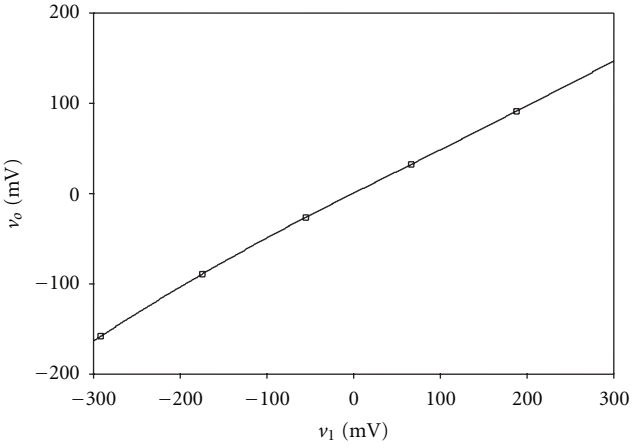

(a) v_o versus v_1 with $v_2 = 250$ mV

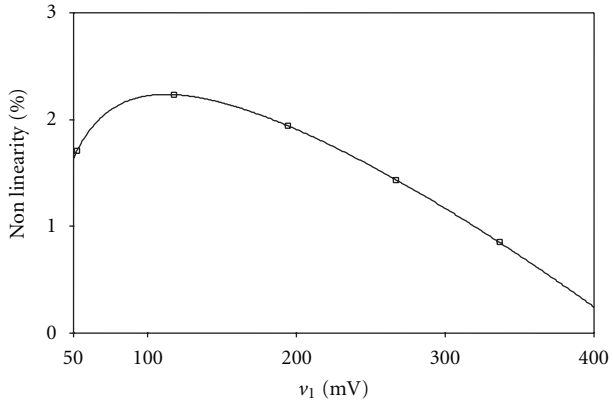

(b) Nonlinearity curve with $v_2 = 250$ mV

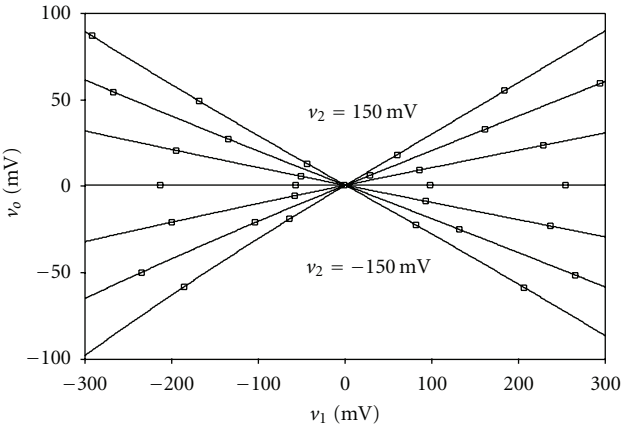

(c) v_o versus v_1 when v_2 is varied from -150 mV to 150 mV

Figure 7: DC transfer characteristic.

5. Applications

5.1. Squarer. The proposed multiplier can be used as a squarer circuit if $v_1 = v_2 = v_{in}$. The output of the multiplier is given by

$$v_o = K' v_{in}^2. \quad (17)$$

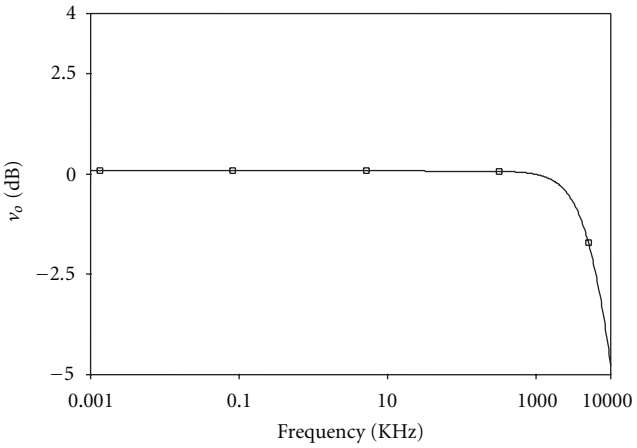

Figure 8: AC characteristic of the proposed multiplier.

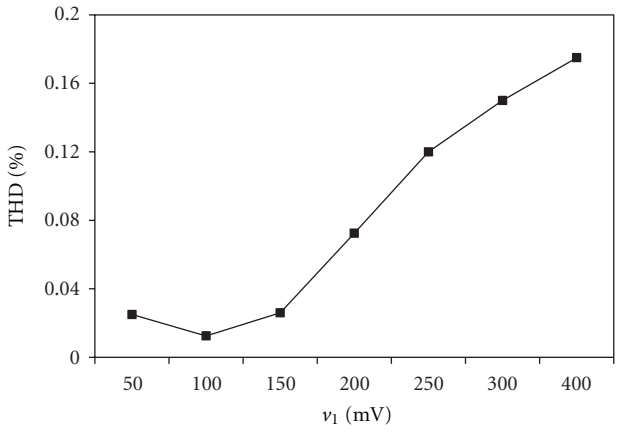

Figure 9: THD versus input signal amplitude.

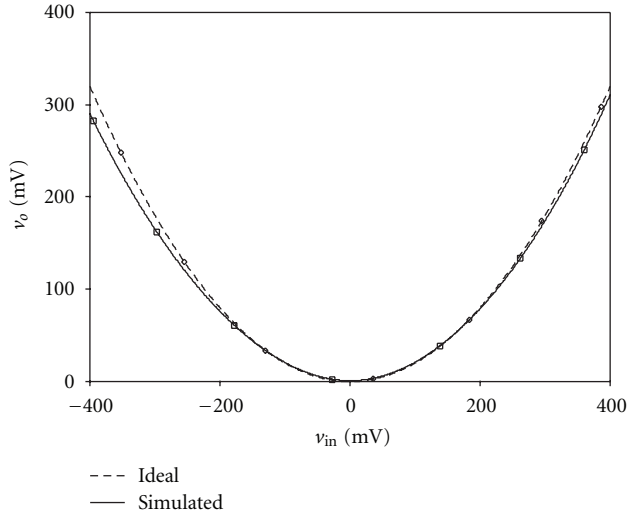

Figure 10: Square transfer characteristics.

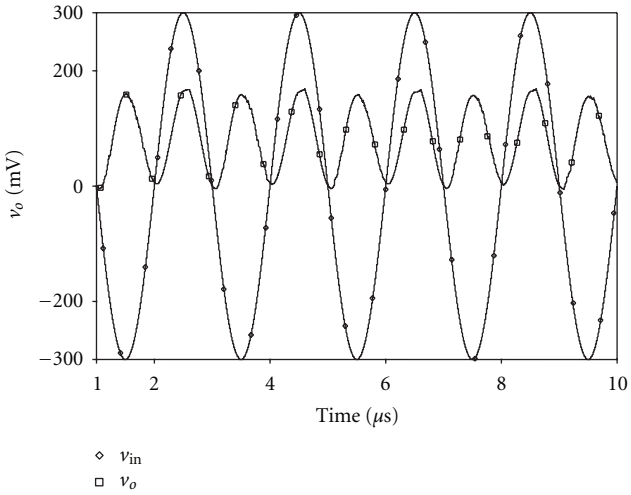

(a) Time domain output of the squarer

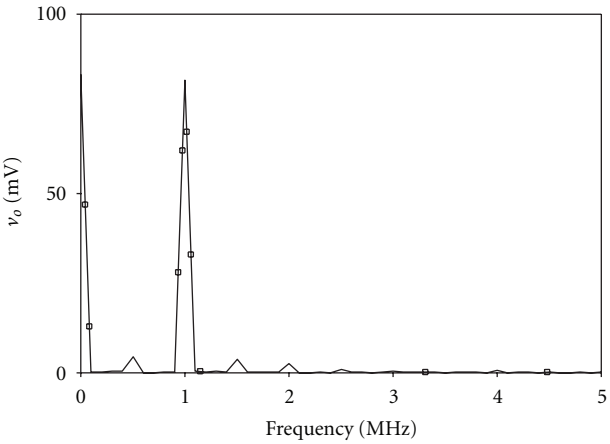

(b) Spectrum of squared sine wave

Figure 11: Output of the squarer.

Figure 10 shows the square transfer characteristics wherein v_{in} is varied from −400 mV to 400 mV.

The observed output of the squarer is shown in Figure 11. The input signal is taken as a 300 mV, 500 KHz sinusoid. The squared output is shown in Figure 11(a) and the spectrum of the squared output is shown in Figure 11(b).

5.2. Amplitude Modulator. The proposed multiplier, being a four-quadrant multiplier, can be used as an amplitude modulator (AM). A 5 KHz signal with 200 mV amplitude is multiplied by 250 mV, 50 KHz signal. Figure 12 shows the output of the proposed multiplier confirming the modulation function. The time domain response of the multiplier is shown in Figures 12(a) and 12(b) displays the frequency spectrum.

6. Conclusion

A single OTRA based analog multiplier is proposed which can be used as a four-quadrant multiplier also. The circuit does not require any passive element thus making it suitable

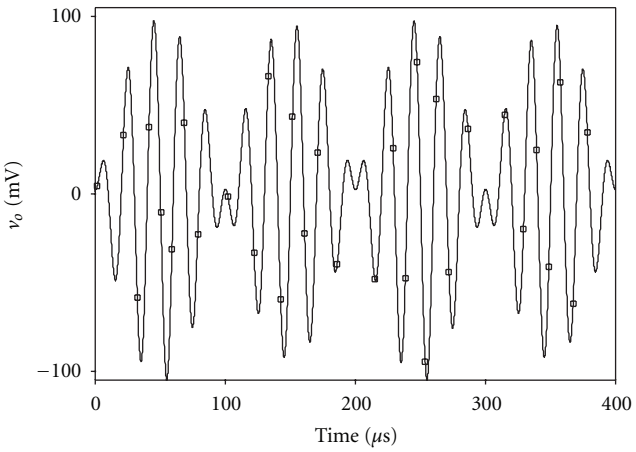

(a) Time domain response

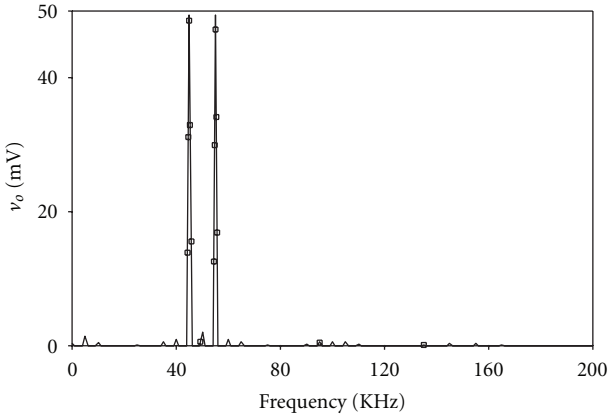

(b) Frequency spectrum

Figure 12: Multiplication of two sinusoids.

for integration. Its application as a squarer and an amplitude modulator is also discussed. Theoretical propositions are verified through PSPICE simulations using 0.5 μm CMOS parameters provided by MOSIS (AGILENT). Various performance parameters are analyzed through simulations and are found in close agreement to theoretical predictions.

References

[1] K. Kaewdang, C. Fongsamut, and W. Surakampontorn, "A wide-band current-mode OTA-based analog multiplier-divider," in *Proceedings of the IEEE International Symposium on Circuits and Systems (ISCAS '03)*, vol. 1, pp. I349–I352, May 2003.

[2] S. I. Liu and D. J. Wei, "Analogue squarer and multiplier based on MOS square-law characteristic," *Electronics Letters*, vol. 32, no. 6, pp. 541–542, 1996.

[3] S. I. Liu and C. C. Chang, "Low-voltage CMOS four-quadrant multiplier based on square-difference identity," *IEE Proceedings Circuits, Devices and Systems*, vol. 143, pp. 174–176, 1996.

[4] G. Weixin, C. Hongyi, and E. Seevinck, "Quadratic-translinear CMOS multiplier-divider circuit," *Electronics Letters*, vol. 33, no. 10, pp. 860–861, 1997.

[5] I. Baturone, S. Sanchez-Solano, and J. L. Huertas, "A CMOS current-mode multiplier/divider circuit," in *Proceedings of the IEEE International Symposium on Circuits and Systems (ISCAS '98)*, pp. 520–523, June 1998.

[6] A. Demosthenous and M. Panovic, "Low-voltage MOS linear transconductor/squarer and four-quadrant multiplier for analog VLSI," *IEEE Transactions on Circuits and Systems I*, vol. 52, no. 9, pp. 1721–1731, 2005.

[7] C. Chen and Z. Li, "A low-power CMOS analog multiplier," *IEEE Transactions on Circuits and Systems II*, vol. 53, no. 2, pp. 100–104, 2006.

[8] H. O. Elwan and A. M. Soliman, "CMOS differential current conveyors and applications for analog VLSI," *Analog Integrated Circuits and Signal Processing*, vol. 11, no. 1, pp. 35–45, 1996.

[9] S. I. Liu and J. J. Chen, "Realisation of analogue divider using current feedback amplifiers," *IEE Proceedings Circuits, Devices and Systems*, vol. 142, no. 1, pp. 45–48, 1995.

[10] M. T. Abuelma'atti and M. A. Al-Qahtani, "A current-mode current-controlled current-conveyor-based analogue multiplier/divider," *International Journal of Electronics*, vol. 85, no. 1, pp. 71–77, 1998.

[11] A. U. Keskin, "A four quadrant analog multiplier employing single CDBA," *Analog Integrated Circuits and Signal Processing*, vol. 40, no. 1, pp. 99–101, 2004.

[12] B. Gibert, "A precision four-quadrant multiplier with subnanosecond response," *The IEEE Journal of Solid-State Circuits*, vol. 3, no. 6, pp. 353–365, 1968.

[13] J. J. Chen, H. W. Tsao, and C. C. Chen, "Operational transresistance amplifier using CMOS technology," *Electronics Letters*, vol. 28, no. 22, pp. 2087–2088, 1992.

[14] K. N. Salama and A. M. Soliman, "CMOS operational transresistance amplifier for analog signal processing," *Microelectronics Journal*, vol. 30, no. 3, pp. 235–245, 1999.

[15] H. Mostafa and A. M. Soliman, "A modified CMOS realization of the operational transresistance amplifier (OTRA)," *Frequenz*, vol. 60, no. 3-4, pp. 70–76, 2006.

[16] A. K. Kafrawy and A. M. Soliman, "A modified CMOS differential operational transresistance amplifier (OTRA)," *International Journal of Electronics and Communications*, vol. 63, no. 12, pp. 1067–1071, 2009.

[17] K. N. S. Ahmed and A. M. Soliman, "Active RC applications of the operational transresistance amplifier," *Frequenz*, vol. 54, no. 7-8, pp. 171–176, 2000.

[18] S. Kılınc and U. Çam, "Cascadable allpass and notch filters employing single operational transresistance amplifier," *Computers and Electrical Engineering*, vol. 31, no. 6, pp. 391–401, 2005.

[19] S. Kılınc, A. U. Keskin, and U. Çam, "Cascadable voltage-mode multifunction biquad employing single OTRA," *Frequenz*, vol. 61, no. 3-4, pp. 84–86, 2007.

[20] S. Kilinc, K. N. Salama, and U. Cam, "Realization of fully controllable negative inductance with single operational transresistance amplifier," *Circuits, Systems, and Signal Processing*, vol. 25, no. 1, pp. 47–57, 2006.

[21] U. Çam, F. Kaçar, O. Cicekoglu, H. Kuntman, and A. Kuntman, "Novel two OTRA-based grounded immitance simulator topologies," *Analog Integrated Circuits and Signal Processing*, vol. 39, no. 2, pp. 169–175, 2004.

[22] K. N. Salama and A. M. Soliman, "Novel oscillators using the operational transresistance amplifier," *Microelectronics Journal*, vol. 31, no. 1, pp. 39–47, 2000.

[23] U. Çam, "A novel single-resistance-controlled sinusoidal oscillator employing single operational transresistance amplifier,"

Analog Integrated Circuits and Signal Processing, vol. 32, no. 2, pp. 183–186, 2002.

[24] R. Pandey, N. Pandey, M. Bothra, and S. K. Paul, "Operational transresistance amplifier-based multiphase sinusoidal oscillators," *Journal of Electrical and Computer Engineering*, vol. 2011, Article ID 586853, 8 pages, 2011.

[25] C. Sanchez-Lopez, E. Tlelo-Cuautle, and E. Martinez-Romero, "Symbolic analysis of OTRAs-based circuits," *Journal of Applied Research and Technology*, vol. 9, no. 1, pp. 69–80, 2011.

[26] C. Sánchez-López, F. V. Fernández, and E. Tlelo-Cuautle, "Generalized admittance matrix models of OTRAs and COAs," *Microelectronics Journal*, vol. 41, no. 8, pp. 502–505, 2010.

[27] A. S. Sedra and K. C. Smith, *Microelectronic Circuits*, Oxford University Press, New York, NY, USA, 2004.

Sol–Gel Derived Nanostructured Zirconia Platform for Vitamin C Detection

P. M. Chavhana,c, Venu Reddya, Pratima R. Solankid, Bansi D. Malhotraa,b and CheolGi Kima,*,z

Author Affiliations

aCenter for Nano-BioEngineering & SpinTronics (nBEST), Department of Materials Science and Engineering, Chungnam National University, Yu-Seong Gu, Daejeon 305764, South Korea
bDepartment of Biotechnology, Delhi Technological University, Delhi 110042, India
cNanocrysatalline Materials Division, Centre for Materials for Electronics Technology (C-MET), Pune 411008, India
dAmity Institute of Nanotechnology, Amity University, Noida, Uttar Pradesh 201303, India

Abstract

The ascorbate oxidase (AsOx) immobilized onto sol gel derived nanostructured ZrO2 film deposited onto indium tin oxide (ITO) glass has been employed for vitamin C detection. The AsOx/NanoZrO2/ITO bioelectrode characterized using spectroscopic and electrochemical techniques reveals response time of 15 s, sensitivity of 0.815 mA/mg dl cm2, detection limit of 20 mg dl−1, an apparent Km value of 19.50 mg dl−1 and can be used to estimate vitamin C concentration up to 500 mg dl−1. This bioelectrode is thermally stable up to 40°C and has a shelf-life of about 6 weeks when stored at 4°C. These results, combined with its structure compatibility with a wide range of biofunctionalization procedures, would make the AsOx/NanoZrO2/ITO biosensor exceptionally useful for a range of detection schemes for clinically important biomarkers.

Manuscript submitted April 20, 2012.
Revised manuscript received November 12, 2012.
Published November 30, 2012.

0013-4651/2013/160(2)/H93/5/

International Journal of Engineering Research & Technology (IJERT)
ISSN: 2278-0181
Vol. 1 Issue 9, November- 2012

Study of Maximum Acceptable Weight of Lift for Indian Male Industrial Workers

Jaswinder Singh
Research Scholar
Department of Production Engineering, PEC University of Technology, Chandigarh, India.

Dr. P Kalra
Professor
Department of Production Engineering, PEC University of Technology, Chandigarh, India.

Dr. R S Walia
Associate Professor
Department of Mechanical and Industrial Engineering, Delhi College of Engineering, Delhi, India

Abstract

Most of studies on Manual Material Handling (MMH) tasks for finding lifting capacity were done on general population; these were not done for underweight, normal weight and overweight workers. MMH task involves the use of the human body to lift, lower or carry loads. The purpose of this study is to evaluate the effect of psychophysical approach on MAWL for underweight, normal weight and overweight male workers with participants lifting weights at different Heights & lifting frequencies. Three male Indian workers with different body mass index (BMI) were participated in this study using general factorial design to find out MAWL of different lifting task combinations by performing free style lifting technique.

1. Introduction

Most manufacturing, industrial or distribution systems require some manual material handling (MMH) tasks. When performed incorrectly or excessively, these tasks may expose workers to physical risk factors, fatigue, and injury. Manual materials handling is among the most frequent and most severe causes of musculoskeletal disorders all over the world [1]. These musculoskeletal disorders not only have a bad effect on worker's health but it also reduces the productivity of workers. Musculoskeletal disorders due to MMH tasks can be prevented by proper designing of MMH tasks by taking maximum load to be lifted less than the manual load lifting capacity under similar circumstance. The psychophysical approach has been widely utilized to determine the MMH task capability. The psychophysical approach proposed by Snook &Irvine [2] has been extensively utilized to investigate human capacity in manual material handling tasks. Maximum acceptable weight of lift (MAWL) is the highest acceptable weight, which can be lifted comfortably. Snook [3] method of calculating MAWL is the most popular way of calculating an individual's handling capability. A subject selects a weight randomly, and adjusts it to the maximum that a person can lift without feeling strain or discomfort, or becoming tired, weakened, overheated, or out-of-breath. Ciriello & Snook studied the effect of size, distance, height and frequency effects on manual materials handling tasks [4]. Wn studied the effect of MAWL for experienced Chinese male workers and found that the MAWL decreased significantly with the box size and lifting frequency, while the mean heart rate increased markedly with the box size and lifting frequency [5]. Wu & Chen showed that the maximum acceptable weights were affected significantly by the adjustment period [6]. The MAWL decreased with an increase in the adjustment time. However, the physiological costs demonstrated no significant difference among the four adjustment Periods. In addition, the effect of the adjustment period on the rating of perceived exertion was significant. In another study by Ciriello it was found that the maximum acceptable weights were affected significantly by the adjustment period [7]. Cheng & Lee studied the maximum acceptable weight of carriage (MAWC) for young Taiwanese males experienced in manual load carriage tasks and found that MAWC decreases with carriage distance, frequency and box width [8]. Maiti & Ray found that the increase in vertical lifting distance caused a significant decrease in load weight for Indian female workers [9]. The purpose of this study is to evaluate the effect of psychophysical approach on MAWL of Indian male workers. So based on the Industrial survey of MMH tasks in North Indian (Punjab) industries various MMH tasks parameters were selected and analyzed in laboratory with different combinations of Box size, Body Mass Index (BMI), Frequency of lift and Vertical distance of lift. MAWL was the psychophysical response factors selected for this study. Analysis of variance (ANOVA) was used for the statistical analysis of the experimental results.

2. WORKERS PARTICULARS

An anthropometric kit was used to measure anthropometrical data. Body weight was measured without shoes using a portable digital scale. The Body Mass Index (BMI) was calculated by dividing body mass of a person (in kilogram) by square of his height (in meter). BMI is used to indicate if an individual is underweight, normal or overweight. WHO categorized persons in three types namely underweight, normal weight and overweight based on their BMI [10]. A normal weight person BMI score is between 18 and 25 kg/m^2. A score below 18 indicates that a person is underweight; a value above 25 indicates that a person is overweight. . Three male industrial workers with different BMI and having 10 years of industrial experience were selected for this laboratory study. Worker with different BMI were selected because same work is done by workers with different BMI in different industries. Their selections were based on criteria of not having any kind of back pain, body discomfort or any sort of disease. The workers were selected from similar age range and engaged in approximately same type of daily Manual load lifting work activities.

Table 1. Anthropometric details of the Workers

Parameter of workers	Under weight	Normal weight	Over weight	Mean
Age (years)	33	28	30	30.3
Weight (kg)	40.2	57.4	61.9	53.2
Height (cm)	158.6	165.3	153.2	159.0
BMI Kg/m^2	16.1	21.08	25.93	21.0
Knee height (cm)	45.2	48.1	43.8	45.7
Crotch height (cm)	64.1	68.4	63.5	65.3
Waist height (cm)	96.7	102.3	92.2	97.1
Chest height (cm)	113.5	122.2	111.9	115.9
Axial height (cm)	125.3	129.4	117.6	124.1
Shoulder height (cm)	129.1	133.8	127.5	130.1
Chest breadth (cm)	29.3	31.4	33.8	31.5
Waist breadth (cm)	27.2	29.2	34.5	30.3
Hip breadth (cm)	28.5	31.2	31.4	30.4
Upper arm length (cm)	26.3	28.5	26.2	27.0
Forearm length (cm)	27.1	27.4	24.9	26.5

2.1. Measuring equipment details

A height adjustable set up was used to vary the lifting heights for lifting the weighted box. Stop watch was used for time measurement and instructing the subjects. Digital weighing equipment was used for measuring and adjusting weights.

3. EXPERIMENTAL DESIGN

The experiments were designed to study the effect of independent factors at different levels on response variables, as shown in table 2. Generalized full factorial design was used. The independent variables were: box size (Large and Small), BMI (Under, normal and overweight worker), frequency of lift (two, four and six lifts per minute) and vertical distance of lift (knee, waist and Shoulder height). Thus, there were fifty four lifting sequences (Two lifting boxes x Three different BMI Worker x Three lifting heights x Three lifting frequencies) for each subject. Each experiment was repeated three times. Free style lifting technique was used for all experiments.

Table 2. MMH task Parameters at Different Levels

S.No	Symbol	Factors	Levels			Units
			Level-1	Level-2	Level-3	
1	A	Box size	Small	Large	-------	cm^3
2	B	BMI	Under weight	Normal weight	Over weight	kg/m^2
3	C	Freq. of lift	2	4	6	lifts/min
4	D	Vertical distance	Knee	Waist	Shoulder	cm
Horizontal distance: 25cm, Environment conditions : 32 ± 2^0C						

The maximum acceptable weight of lift (MAWL) was the primary response variable. Two wooden boxes of sizes 6*4*1.75 and 6*4*2.25 m3 were used for the experiments. These boxes were rectangular in shape which is shown in figure 1.

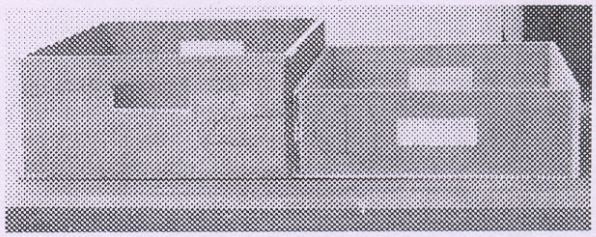

Figure1. Various Boxes used in experiments

3.1. EXPEREMENTAL SETUP

The experiments were conducted in laboratory where room temperature was maintained at32 ± 2^0C. A height adjustable set up was used to vary the lifting heights for

lifting the weighted box. A psychophysical approach was used by the participants to determine the maximum acceptable weight of lift to them for each of the 54 different lifting tasks performed. A free-style lifting method was used and the MAWL was determined psychophysically. The pebbles were used as the load material for the experiments. Lifting of the boxes was done as per the experiment array by the worker on the experimental setup while lowering of the boxes was done by volunteers.

3.2. METHODOLOGY

A psychophysical approach used by Snook [3] to determine the maximum acceptable weight of lift of the workers for each of lifting tasks was used for all experiments. First the anthropometric dimensions of the workers were taken and then they were asked to perform lifting tasks. The instructions given to the participants were the same as those used by Snook & Irvine [2]. A base load of 18 kg was taken for all the experiments. The participants were asked to adjust the weight of the box by adding to maximum the amount that they could lift comfortably at a different lifting frequencies for duration of 8 h. The participants were instructed to lift as much load as they could without straining themselves, or without becoming unusually tired, weakened, overheated or out of breathe. Each participant was encouraged to make weight adjustments. The entire adjustment process took about 15-20min for each task [11]. Once the weight was decided upon, the subject was asked to continue to lift for another 10 min. The final weight was noted down. The above procedure is also shown by flowchart in Figure 2.

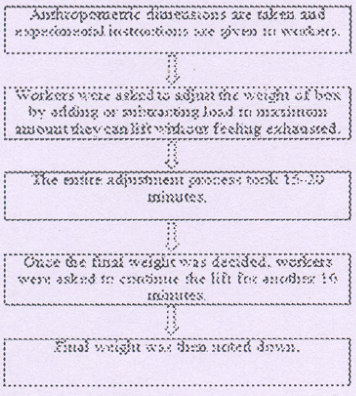

Figure2. Flowchart showing steps for calculating MAWL

4. RESULTS

Results obtained from the experiments were analyzed using the ANOVA, which helps in predicting the significance of independent factor for any desired response function. It indicates which is the most influencing factor or parameter. A confidence interval of 99% has been taken for this analysis. The principle behind significance value is that the p value should be lesser than 0.01 (considering confidence level of 99%) and lesser than 0.05 (considering confidence level of 95%). Significance of all the response variables has been completed using statistical software MINITAB. These response variables studied in this study was MAWL.

Table3. ANOVA results of various parameters for MAWL

Source	Sum of square	DF	Mean square	F value	Prob> F
Model	3234.44	53	61.03	116.74	< 0.0001
A	81.21	1	81.21	155.34	< 0.0001
B	255.98	2	127.99	244.83	< 0.0001
C	639.87	2	319.94	611.99	< 0.0001
D	2065.06	2	1032.53	1975.09	< 0.0001
AB	2.27	2	1.14	2.17	0.1187
AC	1.1	2	0.55	1.05	0.3527
AD	2.07	2	1.04	1.98	0.1424
BC	14.79	4	3.7	7.07	< 0.0001
BD	8.8	4	2.2	4.21	0.0033
CD	148.54	4	37.13	71.03	< 0.0001
ABC	0.31	4	0.076	0.15	0.9643
ABD	0.96	4	0.24	0.46	0.7645
ACD	3.28	4	0.82	1.57	0.1882
BCD	7.77	8	0.97	1.86	0.0742
ABCD	2.43	8	0.3	0.58	0.7909

In above Table 3 Model F-value of 104.77 implies the model is significant. There is only 0.01% chance that a "Model F-Value" this large could occur due to noise. Values of "Prob> F" less than 0.0500 indicate model terms are significant. In this case the main factors box size (A), BMI (B), lifting frequency (C), lifting height (D) were significant. Some of the two-way interaction effects were found to be significant: BMI (B) x lifting frequency (C), BMI (B) x lifting height (D), lifting frequency (C) x lifting height (D) are significant model terms.

5. DISCUSSIONS

Three male workers of different BMI (under, normal and overweight) participated in this study. The purpose of this study was to find out the MAWL for different BMI workers. The main effect of various lifting parameters for MAWL is shown in figures 3. The interactions effects of lifting parameters for MAWL is shown in figure 4.Underweight worker mean MAWL for different box sizes, lifting height and frequencies were less as compared to normal and overweight worker. With the large box size the mean MAWL decreases. With the increase in BMI the MAWL increases.

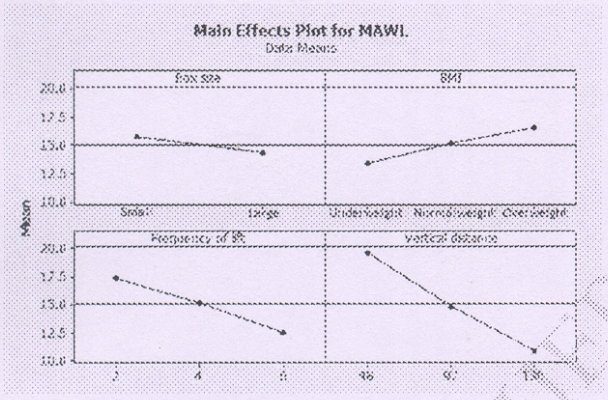

Figure3. Effect of main lifting parameters on MAWL

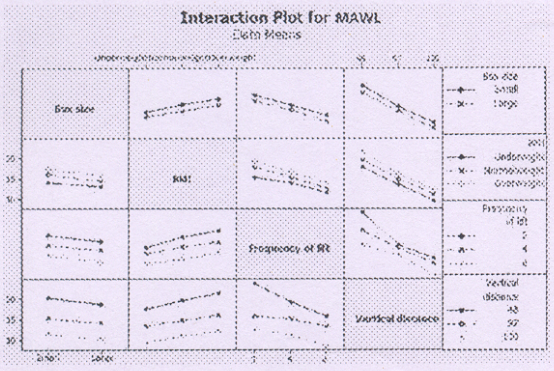

Figure4. Effect of interaction of lifting parameters on MAWL

Analysis of variance in Table 3 showed the maximum acceptable weight of lift was significantly influenced by box size ($p < 0.01$). The effects of box size on MAWL is shown in Figure 3. It was found that the maximum acceptable weight of lift decreased as box size increased. When the box size increased from, Box-1 (small) to Box-2 (large) the mean MAWL decreased, by approximately 8.9% from 15.72 kg to 14.32 kg. The reason behind is that with smaller box subjects preferred lifting more weight as compared to large box.). There was increase in MAWL with increase in BMI as shown in Figure 3. As the BMI increased from underweight to normal weight, the average MAWL increased by nearly 11.10% from approximately 13.45kg approximately 15.13 kg. A further increase of 8.41% from 15.13kg to 16.52 kg was observed when the BMI was increased from normal weight to overweight. Based upon the analysis of variance, the maximum acceptable weight of lift was significantly influenced by frequency ($p < 0.01$).There was decline in MAWL with frequency, shown in Figure 3. As the frequency increased from two lifts/min to four lift/min, mean MAWL declined by nearly 12.70% from approximately 17.39kg to 15.18kg. A further decline of 17.45% from 15.18kg to12.53kg was observed when the lifting frequency increased to six lifts/min. Analysis of variance in Table 3 showed the maximum acceptable weight of lift was significantly influenced by lifting height ($p < 0.01$). There was decline in MAWL with height as shown in Figure 3. As the height increased from Knee to Waist, the average MAWL decreased by nearly 24.51% from approximately 19.54kg approximately 14.75 kg. A further decrease of 26.71% from 14.75kg to 10.81 kg was observed when the lifting height increased to Maximum reach height.

CONCLUSIONS

This study was conducted to evaluate the effect of box size, BMI, frequency of lift and vertical distance on the response variables on lifting capabilities of the Indian male workers, based on the psychophysical approach. The results show that the MAWL decreased significantly with the increase in Box size, lifting frequency and vertical distance and increase with increase in the BMI of the worker. It can be concluded from the study that MAWL is affected by lifting in Box size, BMI of the worker, lifting frequency and vertical distance.

REFERENCES:

[1] NIOSH (1985), "Prevention of musculo-skeletal disorders. Draft Statement", National Symposium on the

Prevention of Work- Related Disease and Injuries. Atlanta, GA: Centers for Disease Control.
[2] Snook, S.H. & Irvine, C.H. 1967, "Maximum acceptable weight of lift", American Industrial Hygiene Association Journal, Vol. 28, 322-329.
[3] Snook, S.H. (1978), "The design of manual handling tasks", Ergonomics, Vol.21, pp.963-985.
[4] Ciriello, V.M. & Snook, S.H. (1983) "A study of size, distance, height and frequency effects on manual materials handling tasks", Human Factors, Vol. 25, pp.473-483.
[5] Wn S.P. (1996), "Maximum acceptable weight of lift by Chinese experienced male manual handlers", Applied Ergonomics, Vol. 28, No. 4, pp. 237-244.
[6] Wu S.P. & Chen J.P. (2002), "Effects of the adjustment period on psychophysically determined maximum acceptable weight of lift and the physiological cost. Industrial Ergonomics", Vol. 31, pp. 287-294.
[7] Ciriello V.M. (2003) "The effects of box size, frequency and extended horizontal reach on maximum acceptable weights of lifting", Industrial Ergonomics, Vol. 32, pp. 115-120.
[8] Cheng Teshiang, Lee Tzu Hsien (2006), "Maximum acceptable weight of manual loadcarriage for young Taiwanese males," Industrial health, Vol. 44, pp. 200-206.
[9] Maiti R. & Ray G.G. (2004), "Determination of maximum acceptable weight of lift by adult Indian female workers", Industrial Ergonomics, Vol. 34, pp. 483–495.
[10] WHO (2003), "Diet, nutrition and the prevention of chronic diseases," WHO technical report series 916, World Health Organization, Geneva.
[11] Wn S.P. (1997), "Maximum acceptable weight of lift by Chinese experienced male manual handlers", Applied Ergonomics, Vol. 28, No. 4, pp 237-244.

International Journal of Engineering Research & Technology (IJERT)
ISSN: 2278-0181
Vol. 1 Issue 9, November- 2012

Study of Maximum Acceptable Weight of Lift for Indian Male Industrial Workers

Jaswinder Singh
Research Scholar
Department of Production Engineering, PEC University of Technology, Chandigarh, India.

Dr. P Kalra
Professor
Department of Production Engineering, PEC University of Technology, Chandigarh, India.

Dr. R S Walia
Associate Professor
Department of Mechanical and Industrial Engineering, Delhi College of Engineering, Delhi, India

Abstract

Most of studies on Manual Material Handling (MMH) tasks for finding lifting capacity were done on general population; these were not done for underweight, normal weight and overweight workers. MMH task involves the use of the human body to lift, lower or carry loads. The purpose of this study is to evaluate the effect of psychophysical approach on MAWL for underweight, normal weight and overweight male workers with participants lifting weights at different Heights & lifting frequencies. Three male Indian workers with different body mass index (BMI) were participated in this study using general factorial design to find out MAWL of different lifting task combinations by performing free style lifting technique.

1. Introduction

Most manufacturing, industrial or distribution systems require some manual material handling (MMH) tasks. When performed incorrectly or excessively, these tasks may expose workers to physical risk factors, fatigue, and injury. Manual materials handling is among the most frequent and most severe causes of musculoskeletal disorders all over the world [1]. These musculoskeletal disorders not only have a bad effect on worker's health but it also reduces the productivity of workers. Musculoskeletal disorders due to MMH tasks can be prevented by proper designing of MMH tasks by taking maximum load to be lifted less than the manual load lifting capacity under similar circumstance. The psychophysical approach has been widely utilized to determine the MMH task capability. The psychophysical approach proposed by Snook &Irvine [2] has been extensively utilized to investigate human capacity in manual material handling tasks. Maximum acceptable weight of lift (MAWL) is the highest acceptable weight, which can be lifted comfortably. Snook [3] method of calculating MAWL is the most popular way of calculating an individual's handling capability. A subject selects a weight randomly, and adjusts it to the maximum that a person can lift without feeling strain or discomfort, or becoming tired, weakened, overheated, or out-of-breath. Ciriello & Snook studied the effect of size, distance, height and frequency effects on manual materials handling tasks [4]. Wn studied the effect of MAWL for experienced Chinese male workers and found that the MAWL decreased significantly with the box size and lifting frequency, while the mean heart rate increased markedly with the box size and lifting frequency [5]. Wu & Chen showed that the maximum acceptable weights were affected significantly by the adjustment period [6]. The MAWL decreased with an increase in the adjustment time. However, the physiological costs demonstrated no significant difference among the four adjustment Periods. In addition, the effect of the adjustment period on the rating of perceived exertion was significant. In another study by Ciriello it was found that the maximum acceptable weights were affected significantly by the adjustment period [7]. Cheng & Lee studied the maximum acceptable weight of carriage (MAWC) for young Taiwanese males experienced in manual load carriage tasks and found that MAWC decreases with carriage distance, frequency and box width [8]. Maiti & Ray found that the increase in vertical lifting distance caused a significant decrease in load weight for Indian female workers [9]. The purpose of this study is to evaluate the effect of psychophysical approach on MAWL of Indian male workers. So based on the Industrial survey of MMH tasks in North Indian (Punjab) industries various MMH tasks parameters were selected and analyzed in laboratory with different combinations of Box size, Body Mass Index (BMI), Frequency of lift and Vertical distance of lift. MAWL was the psychophysical response factors selected for this study. Analysis of variance (ANOVA) was used for the statistical analysis of the experimental results.

2. WORKERS PARTICULARS

An anthropometric kit was used to measure anthropometrical data. Body weight was measured without shoes using a portable digital scale. The Body Mass Index (BMI) was calculated by dividing body mass of a person (in kilogram) by square of his height (in meter). BMI is used to indicate if an individual is underweight, normal or overweight. WHO categorized persons in three types namely underweight, normal weight and overweight based on their BMI [10]. A normal weight person BMI score is between 18 and 25 kg/m^2. A score below 18 indicates that a person is underweight; a value above 25 indicates that a person is overweight. . Three male industrial workers with different BMI and having 10 years of industrial experience were selected for this laboratory study. Worker with different BMI were selected because same work is done by workers with different BMI in different industries. Their selections were based on criteria of not having any kind of back pain, body discomfort or any sort of disease. The workers were selected from similar age range and engaged in approximately same type of daily Manual load lifting work activities.

Table 1. Anthropometric details of the Workers

Parameter of workers	Under weight	Normal weight	Over weight	Mean
Age (years)	33	28	30	30.3
Weight (kg)	40.2	57.4	61.9	53.2
Height (cm)	158.6	165.3	153.2	159.0
BMI Kg/m^2	16.1	21.08	25.93	21.0
Knee height (cm)	45.2	48.1	43.8	45.7
Crotch height (cm)	64.1	68.4	63.5	65.3
Waist height (cm)	96.7	102.3	92.2	97.1
Chest height (cm)	113.5	122.2	111.9	115.9
Axial height (cm)	125.3	129.4	117.6	124.1
Shoulder height (cm)	129.1	133.8	127.5	130.1
Chest breadth (cm)	29.3	31.4	33.8	31.5
Waist breadth (cm)	27.2	29.2	34.5	30.3
Hip breadth (cm)	28.5	31.2	31.4	30.4
Upper arm length (cm)	26.3	28.5	26.2	27.0
Forearm length (cm)	27.1	27.4	24.9	26.5

2.1. Measuring equipment details

A height adjustable set up was used to vary the lifting heights for lifting the weighted box. Stop watch was used for time measurement and instructing the subjects. Digital weighing equipment was used for measuring and adjusting weights.

3. EXPERIMENTAL DESIGN

The experiments were designed to study the effect of independent factors at different levels on response variables, as shown in table 2. Generalized full factorial design was used. The independent variables were: box size (Large and Small), BMI (Under, normal and overweight worker), frequency of lift (two, four and six lifts per minute) and vertical distance of lift (knee, waist and Shoulder height). Thus, there were fifty four lifting sequences (Two lifting boxes x Three different BMI Worker x Three lifting heights x Three lifting frequencies) for each subject. Each experiment was repeated three times. Free style lifting technique was used for all experiments.

Table 2. MMH task Parameters at Different Levels

S.No	Symbol	Factors	Levels			Units
			Level-1	Level-2	Level-3	
1	A	Box size	Small	Large	-------	cm^3
2	B	BMI	Under weight	Normal weight	Over weight	kg/m^2
3	C	Freq. of lift	2	4	6	lifts/min
4	D	Vertical distance	Knee	Waist	Shoulder	cm
Horizontal distance: 25cm, Environment conditions : 32 ± 2^0C						

The maximum acceptable weight of lift (MAWL) was the primary response variable. Two wooden boxes of sizes 6*4*1.75 and 6*4*2.25 m3 were used for the experiments. These boxes were rectangular in shape which is shown in figure 1.

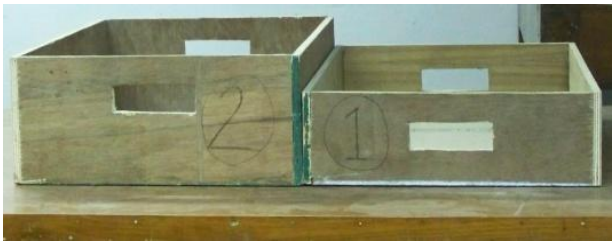

Figure1. Various Boxes used in experiments

3.1. EXPEREMENTAL SETUP

The experiments were conducted in laboratory where room temperature was maintained at32 ± 2^0C. A height adjustable set up was used to vary the lifting heights for

lifting the weighted box. A psychophysical approach was used by the participants to determine the maximum acceptable weight of lift to them for each of the 54 different lifting tasks performed. A free-style lifting method was used and the MAWL was determined psychophysically. The pebbles were used as the load material for the experiments. Lifting of the boxes was done as per the experiment array by the worker on the experimental setup while lowering of the boxes was done by volunteers.

3.2. METHODOLOGY

A psychophysical approach used by Snook [3] to determine the maximum acceptable weight of lift of the workers for each of lifting tasks was used for all experiments. First the anthropometric dimensions of the workers were taken and then they were asked to perform lifting tasks. The instructions given to the participants were the same as those used by Snook & Irvine [2]. A base load of 18 kg was taken for all the experiments. The participants were asked to adjust the weight of the box by adding to maximum the amount that they could lift comfortably at a different lifting frequencies for duration of 8 h. The participants were instructed to lift as much load as they could without straining themselves, or without becoming unusually tired, weakened, overheated or out of breathe. Each participant was encouraged to make weight adjustments. The entire adjustment process took about 15-20min for each task [11]. Once the weight was decided upon, the subject was asked to continue to lift for another 10 min. The final weight was noted down. The above procedure is also shown by flowchart in Figure 2.

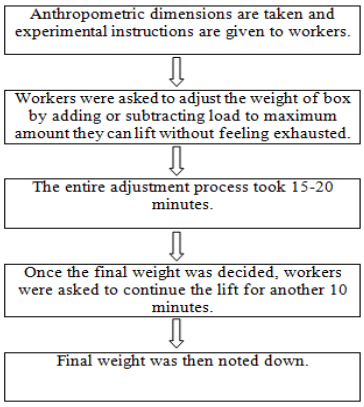

Figure2. Flowchart showing steps for calculating MAWL

4. RESULTS

Results obtained from the experiments were analyzed using the ANOVA, which helps in predicting the significance of independent factor for any desired response function. It indicates which is the most influencing factor or parameter. A confidence interval of 99% has been taken for this analysis. The principle behind significance value is that the p value should be lesser than 0.01 (considering confidence level of 99%) and lesser than 0.05 (considering confidence level of 95%). Significance of all the response variables has been completed using statistical software MINITAB. These response variables studied in this study was MAWL.

Table3. ANOVA results of various parameters for MAWL

Source	Sum of square	DF	Mean square	F value	Prob> F
Model	3234.44	53	61.03	116.74	< 0.0001
A	81.21	1	81.21	155.34	< 0.0001
B	255.98	2	127.99	244.83	< 0.0001
C	639.87	2	319.94	611.99	< 0.0001
D	2065.06	2	1032.53	1975.09	< 0.0001
AB	2.27	2	1.14	2.17	0.1187
AC	1.1	2	0.55	1.05	0.3527
AD	2.07	2	1.04	1.98	0.1424
BC	14.79	4	3.7	7.07	< 0.0001
BD	8.8	4	2.2	4.21	0.0033
CD	148.54	4	37.13	71.03	< 0.0001
ABC	0.31	4	0.076	0.15	0.9643
ABD	0.96	4	0.24	0.46	0.7645
ACD	3.28	4	0.82	1.57	0.1882
BCD	7.77	8	0.97	1.86	0.0742
ABCD	2.43	8	0.3	0.58	0.7909

In above Table 3 Model F-value of 104.77 implies the model is significant. There is only 0.01% chance that a "Model F-Value" this large could occur due to noise. Values of "Prob> F" less than 0.0500 indicate model terms are significant. In this case the main factors box size (A), BMI (B), lifting frequency (C), lifting height (D) were significant. Some of the two-way interaction effects were found to be significant: BMI (B) x lifting frequency (C), BMI (B) x lifting height (D), lifting frequency (C) x lifting height (D) are significant model terms.

5. DISCUSSIONS

Three male workers of different BMI (under, normal and overweight) participated in this study. The purpose of this study was to find out the MAWL for different BMI workers. The main effect of various lifting parameters for MAWL is shown in figures 3. The interactions effects of lifting parameters for MAWL is shown in figure 4.Underweight worker mean MAWL for different box sizes, lifting height and frequencies were less as compared to normal and overweight worker. With the large box size the mean MAWL decreases. With the increase in BMI the MAWL increases.

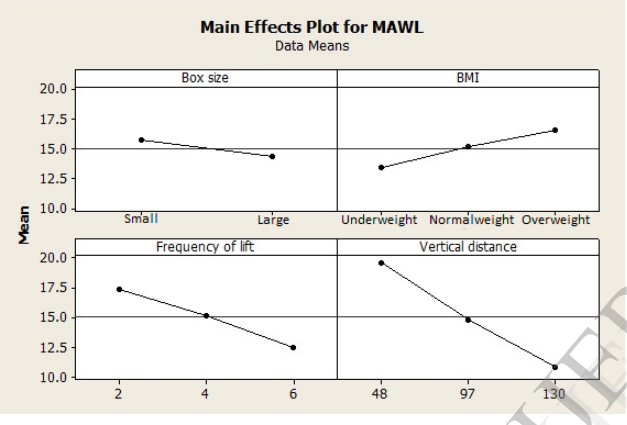

Figure3. Effect of main lifting parameters on MAWL

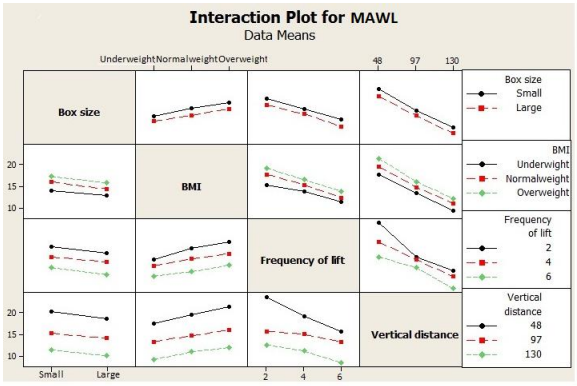

Figure4. Effect of interaction of lifting parameters on MAWL

Analysis of variance in Table 3 showed the maximum acceptable weight of lift was significantly influenced by box size ($p < 0.01$). The effects of box size on MAWL is shown in Figure 3. It was found that the maximum acceptable weight of lift decreased as box size increased. When the box size increased from, Box-1 (small) to Box-2 (large) the mean MAWL decreased, by approximately 8.9% from 15.72 kg to 14.32 kg. The reason behind is that with smaller box subjects preferred lifting more weight as compared to large box.). There was increase in MAWL with increase in BMI as shown in Figure 3. As the BMI increased from underweight to normal weight, the average MAWL increased by nearly 11.10% from approximately 13.45kg approximately 15.13 kg. A further increase of 8.41% from 15.13kg to 16.52 kg was observed when the BMI was increased from normal weight to overweight. Based upon the analysis of variance, the maximum acceptable weight of lift was significantly influenced by frequency ($p < 0.01$).There was decline in MAWL with frequency, shown in Figure 3. As the frequency increased from two lifts/min to four lift/min, mean MAWL declined by nearly 12.70% from approximately 17.39kg to 15.18kg. A further decline of 17.45% from 15.18kg to12.53kg was observed when the lifting frequency increased to six lifts/min. Analysis of variance in Table 3 showed the maximum acceptable weight of lift was significantly influenced by lifting height ($p < 0.01$). There was decline in MAWL with height as shown in Figure 3. As the height increased from Knee to Waist, the average MAWL decreased by nearly 24.51% from approximately 19.54kg approximately 14.75 kg. A further decrease of 26.71% from 14.75kg to 10.81 kg was observed when the lifting height increased to Maximum reach height.

CONCLUSIONS

This study was conducted to evaluate the effect of box size, BMI, frequency of lift and vertical distance on the response variables on lifting capabilities of the Indian male workers, based on the psychophysical approach. The results show that the MAWL decreased significantly with the increase in Box size, lifting frequency and vertical distance and increase with increase in the BMI of the worker. It can be concluded from the study that MAWL is affected by lifting in Box size, BMI of the worker, lifting frequency and vertical distance.

REFERENCES:

[1] NIOSH (1985), "Prevention of musculo-skeletal disorders. Draft Statement", National Symposium on the

Prevention of Work- Related Disease and Injuries. Atlanta, GA: Centers for Disease Control.
[2] Snook, S.H. & Irvine, C.H. 1967, "Maximum acceptable weight of lift", American Industrial Hygiene Association Journal, Vol. 28, 322-329.
[3] Snook, S.H. (1978), "The design of manual handling tasks", Ergonomics, Vol.21, pp.963-985.
[4] Ciriello, V.M. & Snook, S.H. (1983) "A study of size, distance, height and frequency effects on manual materials handling tasks", Human Factors, Vol. 25, pp.473-483.
[5] Wn S.P. (1996), "Maximum acceptable weight of lift by Chinese experienced male manual handlers", Applied Ergonomics, Vol. 28, No. 4, pp. 237-244.
[6] Wu S.P. & Chen J.P. (2002), "Effects of the adjustment period on psychophysically determined maximum acceptable weight of lift and the physiological cost. Industrial Ergonomics", Vol. 31, pp. 287-294.
[7] Ciriello V.M. (2003) "The effects of box size, frequency and extended horizontal reach on maximum acceptable weights of lifting", Industrial Ergonomics, Vol. 32, pp. 115-120.
[8] Cheng Teshiang, Lee Tzu Hsien (2006), "Maximum acceptable weight of manual loadcarriage for young Taiwanese males," Industrial health, Vol. 44, pp. 200-206.
[9] Maiti R. & Ray G.G. (2004), "Determination of maximum acceptable weight of lift by adult Indian female workers", Industrial Ergonomics, Vol. 34, pp. 483–495.
[10] WHO (2003), "Diet, nutrition and the prevention of chronic diseases," WHO technical report series 916, World Health Organization, Geneva.
[11] Wn S.P. (1997), "Maximum acceptable weight of lift by Chinese experienced male manual handlers", Applied Ergonomics, Vol. 28, No. 4, pp 237-244.

Taxonomy of Nature Inspired Computational Intelligence: A Remote Sensing Perspective

Lavika Goel[1], Daya Gupta[2],V.K. Panchal[3] and Ajith Abraham[4]
[1,2]Department of Computer Engineering, Delhi Technological University (DTU), Delhi, India
[1]goel.lavika@gmail.com, [2]dgupta@dce.ac.in
[3] Defense Terrain & Research Lab, Defense & Research Development Organization (DRDO), Delhi, India
[3]vkpans@ieee.org
[4]Machine Intelligence Research Labs (MIR Labs), WA, USA
[4]IT for Innovations, VSB - Technical University of Ostrava, Czech Republic
[4]ajith.abraham@ieee.org

***Abstract* --- The concepts in geospatial sciences are generally vague, ambiguous and imprecise. Also, a combination of spectral, spatial and radiometric resolution of space-borne sensors presents a selective and incomplete look of the geospatial feature/object under its view from the space. Recently, the nature inspired computational intelligence (CI) techniques have emerged as an efficient mechanism to handle diverse uncertainty characteristics. This paper proposes that the human-mind model based computational intelligence techniques, the artificial immune system based computational intelligence techniques; the swarm intelligence based computational intelligence techniques and the emerging geo-sciences based intelligent techniques can be considered as the four pillars of nature inspired CI techniques and hence redefines and extends the taxonomy of nature inspired CI. Researchers have shown keen interest on the applications of natural computing in divergent domains. Scanty references are available on the applications of nature inspired computing in the area of remote sensing. We hence also propose the taxonomy of the most recent nature inspired CI techniques that have been adapted till date for geo-spatial feature extraction and analyze their performances. We also construct a technology timeline of these recent nature inspired CI techniques.**

Keywords--- Natural computation; computational intelligence; geo-spatial feature extraction.

I. INTRODUCTION

Multi-sensor, multi-resolution and multi-spectral geo-spatial information, from satellite remote sensing has become a primary & vital source of information for critical, conclusive and instant decision making in varying real-time critical application across a wide array of domains like *Environmental studies*, *Disaster management* and *Battlefield strategic planning.* The Information referenced to geographic location, characteristics of natural and man-made features and boundaries on earth are termed as geospatial information. The concepts in geospatial sciences are generally vague, ambiguous and imprecise like the landuse / landcover, extent of Great Indian Desert Thar, the paleo-channels and the urban sprawl. Also, a combination of spectral, spatial and radiometric resolution of space-borne sensors presents a selective & incomplete look of the geospatial feature/object under its view from the space. The resolution translates the satellite imageries into granular imprints of the geospatial features [22].

Recently, the nature inspired computational intelligence (CI) techniques which we comprised of techniques based on the *modelization of human mind*, those inspired from the concepts of *artificial immune system, swarm intelligence* based techniques and emerging *geo-sciences based* computing, have emerged as an efficient mechanism to handle diverse uncertainty characteristics. Nature inspired computing has been a crucial means of implementing machine intelligence with human-like behavior and reasoning capabilities. Researchers have shown keen interest on the applications of nature inspired computing in divergent domains. Scanty references are available on the applications of nature inspired computing in remote sensing [15]. The areas which have drawn the attention are landuse / landcover classification, battlefield assessment, obstacle free path planning, object identification, pattern classification, estimation of groundwater availability. From the above, the problem of land cover classification / feature extraction, which hitherto is looked for its solution in classical artificial intelligence platforms like Probabilistic and Bayesian, has been addressed and presented in this paper with new thoughts processing, based on nature inspired techniques of computational intelligence. Figure 1 summarizes and presents an overview of nature inspired computational intelligence and its perspective application areas along with the respective accuracy assessment metrics.

II. NATURE INSPIRED COMPUTATIONAL INTELLIGENCE: TAXONOMY REDEFINED

A new wide range of nature-inspired CI based algorithms has emerged from evolutionary algorithms and geo-sciences based natural phenomenon such as the

978-1-4673-4768-6

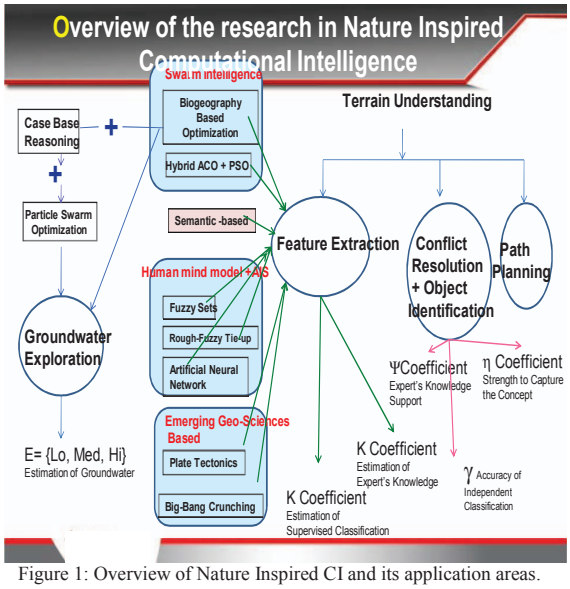

Figure 1: Overview of Nature Inspired CI and its application areas.

theories about the evolution of the earth [1], migration of species in natural habitats [2], behavior of social insects in a group [12], etc. These nature-inspired intelligent techniques can form the basis of building an optimization algorithm, which can adapt itself to suit our purpose of natural terrain feature extraction, and prove to be better by giving more accurate results than the other existing optimization techniques for certain specific applications. Also, the geo-sciences based phenomenon such as the plate tectonics, the big bang theory, etc. can be exploited to develop optimization algorithms that can be blended with the other existing evolutionary algorithms for the purpose of natural terrain feature extraction. Based on the above possibilities, figure 2 below gives the proposed taxonomy of nature inspired computational intelligence techniques that can be used independently or in an integrated way for the development of optimization algorithms that can be targeted for some specific applications. The taxonomy is described next.

A. Based on the modeling of human mind

To provide a solution to the problems posed by classical AI techniques, computational intelligence techniques based on the modelization of human mind were introduced. In effect, the role model for these techniques is the human mind. The above-mentioned computational intelligence techniques differ from the conventional (hard) computing techniques in that, unlike hard computing, they are tolerant of tolerance for imprecision, uncertainty and partial truth to achieve tractability, robustness and low solution cost. Computational models require a mathematically and logically formal representation of a problem. Computer models are used in the simulation and experimental verification of different specific and general properties of intelligence. Computational modeling can help us to understand the functional organization of a particular cognitive phenomenon. All the approaches based on the modelization of human mind tend to be generalized to the form of integrated computational models of

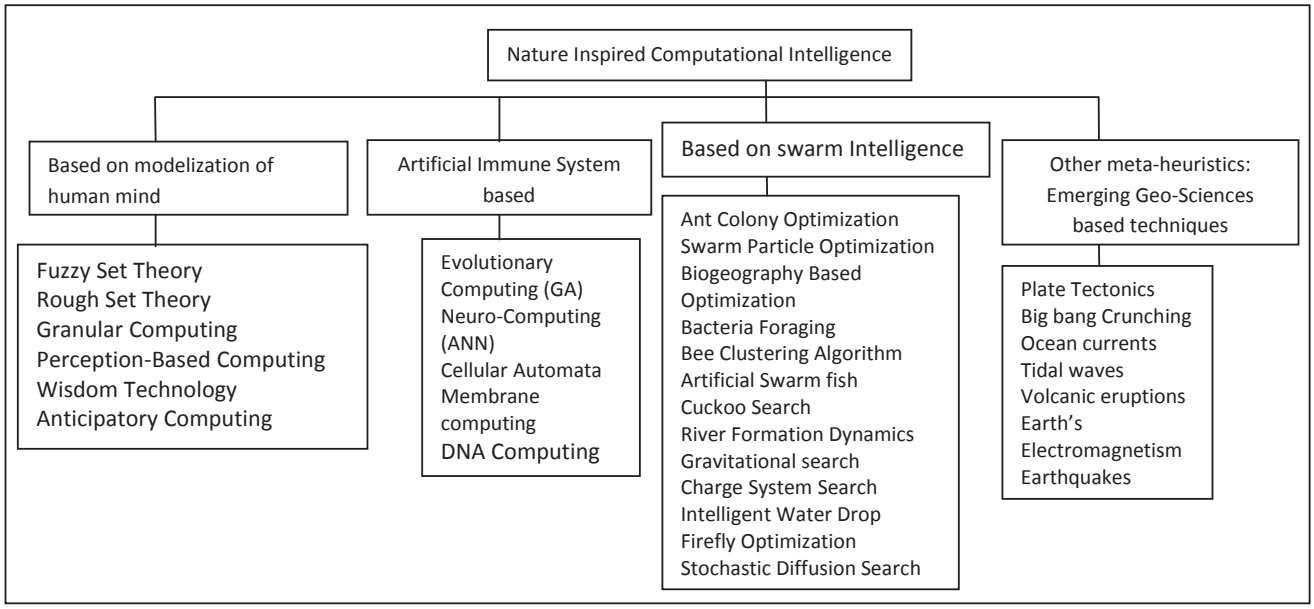

Figure 2: Proposed Taxonomy of Nature Inspired Computational Intelligence Techniques

synthetic / abstract intelligence, in order to be applied to the explanation and improvement of individual and social / organizational decision-making and reasoning. The computational techniques proposed to be under this category are listed below.

- Fuzzy Set Theory
- Rough Set Theory
- Granular Computing
- Perception-Based Computing
- Wisdom Technology
- Anticipatory Computing

B. Based on Artificial Immune System

Artificial Immune System [3] is a framework to design a biologically inspired algorithm. It consists of the following basic elements:

- A representation for the components of the system
- A set of mechanisms to evaluate the interaction of individuals with the environment and each other. The environment is usually simulated by a set of input stimuli, one or more fitness function(s).
- Procedures of adaptation that govern the dynamics of the system i.e. how its behavior varies over time.

The computational intelligence techniques proposed to be under this category are listed below.

- Evolutionary Computing (GA)
- Neuro-computing (ANN)
- Cellular Automata
- Membrane computing
- DNA Computing

C. Swarm Intelligence

Swarm intelligence is any attempt to design algorithm or distributed problem-solving devices inspired by collective behavior of social insect colonies or other animal societies. This field deals with how social insects collectively perform some specific tasks in daily life (that include finding food, building or extending nest, efficiently feeding the brood, responding to external challenges, spreading alarm etc.), modeling their behavior, and using the model as a basis upon which artificial variations can be developed, either by tuning the model parameters beyond the biological relevant range or by adding non-biological features to the model. The social insect colony is a distributed system comprising of direct or indirect interactions among relatively simple (social) agents that can solve the problems in a very flexible and robust way: flexibility allow adaptation to changing environment, while robustness endows the colony with the ability to function even though some individuals may fail to perform their tasks [1, 15]. The nature inspired techniques proposed under this category is listed below.

- Ant Colony Optimization
- Particle Swarm Optimization
- Biogeography Based Optimization
- Bacterial Foraging Optimization
- Bee Clustering Algorithm
- Artificial Swarm fish
- Cuckoo Search
- River Formation Dynamics
- Gravitational Search
- Charged System Search
- Intelligent Water Drop
- Firefly Optimization
- Stochastic Diffusion Search

D. Emerging Geo-Sciences based Techniques

Earth science (also known as geo-science) is an all-embracing term for the sciences related to the planet Earth. It is arguably a special case in planetary science, the Earth being the only known life-bearing planet. The formal discipline of Earth sciences may include the study of the atmosphere, hydrosphere, oceans and biosphere, as well as the solid earth. Typically Earth scientists will use tools from physics, chemistry, biology, chronology and mathematics to build a quantitative understanding of how the Earth system works, and how it evolved to its current state. The following fields of science are generally categorized within the geosciences:

[1] Geology describes the rocky parts of the Earth's crust and its historic development. Major subdisciplines are mineralogy and petrology, geochemistry, geomorphology, paleontology, stratigraphy, structural geology, engineering geology and sedimentology.

[2] Physical geography covers the aspects of geomorphology, oceanography, climatology and biogeography.

[3] Geophysics and geodesy investigate the shape of the Earth, its reaction to forces and its magnetic and gravity fields. Geophysicists explore the Earth's core and mantle as well as the tectonic and seismic activity of the lithosphere.

[4] Soil science covers the outermost layer of the Earth's crust that is subject to soil formation processes. Major subdisciplines include edaphology and pedology.

[5] Oceanography and hydrology describe the marine and freshwater domains of the watery parts of the Earth. Major subdisciplines include hydrogeology

and physical, chemical, and biological oceanography.

[6] Glaciology covers the icy parts of the Earth.

[7] Atmospheric sciences cover the gaseous parts of the Earth between the surface and the exosphere. Major subdisciplines are meteorology, climatology, atmospheric chemistry and atmospheric physics.

Plate tectonics, mountain ranges, volcanoes, and earthquakes are geological phenomena that can be explained in terms of energy transformations in the Earth's crust. Based on the above discussion, we categorize the following nature inspired techniques that can be categorized under geo-sciences as listed below:

- Plate Tectonics
- Big bang Crunching
- Oceanic currents
- Tidal waves
- Volcanic eruptions
- Earth's Electromagnetism
- Earthquakes

As seen above, several nature inspired computational intelligence techniques are available that can be adapted and implemented for real time scenarios such as in robotics, path planning, destination prediction, image classification, object identification etc. We present some of the existing nature inspired intelligent techniques that have been applied for geo-spatial feature extraction application in the next section.

III. Nature Inspired CI Techniques for Geo-spatial Feature Extraction

The Indian Mission Chandrayaan-1 to the Moon in 2008 has definitely written a preface to interplanetary explorations. Also the discovery of hydroxyl water (OH), an essential and vital geospatial feature, by Moon Impact Probe (MIP) credibly put the remote sensing at the fulcrum of geo-spatial land cover feature extraction. With the satellite remote sensing, it has become feasible to observe a vast area of the terrain and knowledge extracted out of these images. Earth Observation Satellite-based (EOS) sensors have emerged into a rapid source of multi-sensor, multi-resolution and multi-spectral *geospatial information* for *decision making* in varying application domains. In this study, it is attempted to explain how the nature inspired methodologies can help in working with fuzzy, granular, and ambiguous objects, under the conditions that:

i. Earth objects are fuzzy in nature
ii. The inter-process collaboration is not crisp/ deterministic and times may not have exact explanation.
iii. The major source of information is the earth observation satellites. They capture different facets of the earth in different wavelength bands. Therefore, combined dataset of the images don't cover the reality in total. This implies incomplete information.

These necessitated newer procedures going and incorporating the structural knowledge into the feature extraction process. In order to encounter with the inherent uncertainty in geo-spatial data, our observation is that *Nature-Inspired Computing* mechanism is aptly fit into the problem-solving framework. A new wide range of nature-inspired computational algorithms is proposed which have emerged from evolutionary algorithms and geo-sciences based natural phenomenon. These nature-inspired intelligent techniques can form the basis of building an optimization algorithm, which can adapt itself to suit our purpose of feature extraction and prove to be better by giving more accurate results than the other existing optimization techniques. Figure 3 provides a timeline of the most recent nature inspired CI techniques that have been adapted till date for land cover feature extraction. Table I below presents the proposed general taxonomy of the existing nature inspired computational intelligence techniques that have been used for geo-spatial feature extraction application till date.

In remote sensing the problem of feature extraction has been solved by using the traditional classical approaches of artificial intelligence like Parallel-o-piped Classification [11, 22], Minimum Distance to Mean Classification [11, 22], Maximum Likelihood Classification [11, 22] etc. A major disadvantage of the above traditional AI techniques of natural terrain feature extraction is that these techniques show limited accuracy in information retrieval and high-resolution satellite image is needed. Also these techniques are insensitive to different degrees of variance in the spectral response data. To provide a solution to the above problems, computational intelligence techniques were introduced in remote sensing for feature extraction. Computational intelligence techniques differ from the above conventional (hard) computing techniques in that, unlike hard computing, they are tolerant of imprecision, uncertainty and partial truth. The principal constituents of computational intelligence techniques categorized under the techniques inspired from modelization of human mind that have been applied for geo-spatial feature extraction are fuzzy logic [24], rough set theory [19] and Rough-Fuzzy Tie-Up [16, 18]. The main goal of the rough set analysis is to synthesize approximation of concepts from the acquired data. Fuzzy logic provides

an inference morphology that enables approximate human reasoning capabilities to be applied to knowledge-based systems. The rough sets handles the imprecision making use of the granular knowledge structure embedded in the training / labeled dataset. The fuzzy handles the ambiguity resident in the image data set whereas, the artificial neural network is good in capturing generalization in the image data set.

Artificial Immune System is a framework to design a biologically inspired algorithm. The computational intelligence techniques proposed under this category are membrane computing [3], cellular automata, artificial neural networks and genetic algorithms**.** Membrane Computing deals with distributed and parallel computing models, processing multisets of symbol objects in a localized manner (evolution rules and evolving objects are encapsulated into compartments delimited by membranes), with an essential role played by the communication between compartments (and with the environment), a hierarchical arrangement of membranes, as in a cell (hence described by a tree), or a net of membranes (placed in the nodes of a graph), as in a tissue or a neural net [3]. Cellular automata concepts are built around a special class of sparse network referred to as Cellular Automata (CA). The versatility of the classification scheme is illustrated through its application in three diverse fields - data mining, image compression, and fault diagnosis. Extensive experimental results demonstrate better performance of the developed scheme over popular classification algorithms in respect of memory overhead and retrieval time with comparable classification accuracy. ANNs can be used for three-dimensional terrain mapping and classification to allow the operation of mobile robots in outdoor environments using laser range finders. We make use of a multi-layer perceptron neural network to classify the terrain into navigable, partially navigable, and non-navigable. The maps generated by this approach can be used for path planning, navigation, and local obstacle avoidance. Genetic algorithms can be used for feature selection wherein feature subsets are evaluated by means of a separability index which uses covariance matrices for evaluating how spread out the probability distributions of data are in a given n-dimensional space.

The computational intelligence techniques like the fuzzy sets based classifier and path planner and the rough set classifier, which have been used recently, are not able to provide good result in case of ambiguity and also result in inaccuracy with low spatial resolution. Also these are not able to handle the continuous and the crisp data separately. Hence we shifted to the fundamentals from Swarm Intelligence, an optimized approach of terrain understanding of satellite multi-spectral images. Swarm Intelligence provides a good number of accuracy even with low spatial resolution image. This technique, with lower cost and higher

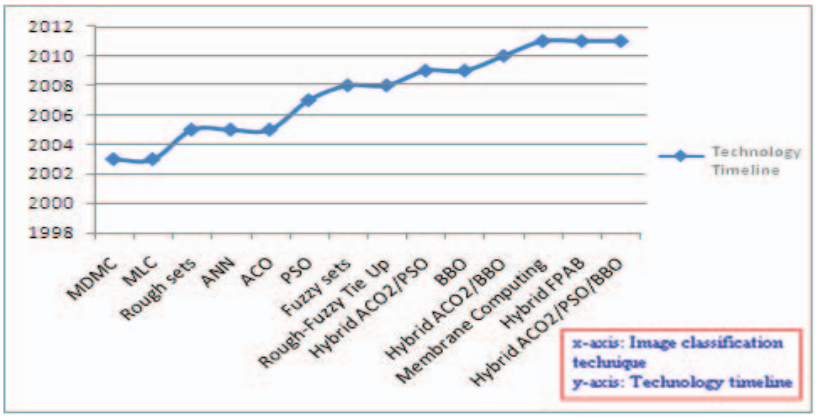

Figure 3: Technology Timeline of Nature Inspired CI Techniques in Remote Sensing

Table I: Taxonomy of nature inspired computational intelligence techniques for feature extraction applications in remote sensing

Nature Inspired Computational Intelligence (for Geo-spatial Feature Extraction)		
Modelization of human mind	Artificial Immune System	Swarm Intelligence Techniques
• Rough Sets Theory • Fuzzy Sets Theory • Rough-Fuzzy Tie-Up	• Membrane Computing • Artificial Neuron Network (ANN)	• Ant Colony Optimization (ACO) • Swarm Particle Optimization (PSO) • Hybrid ACO2/PSO Optimization • Biogeography Based Optimization (BBO) • Extended Biogeography based Optimization • Hybrid ACO2/BBO • Hybrid ACO2/PSO/BBO Optimization • Bacterial Foraging Optimization (BFO)

degree of accuracy, will be able to replace high resolution high cost satellite imageries. The various swarm intelligence techniques that have been adapted for the purpose of geo-spatial feature extraction till date are Ant Colony Optimization (ACO), Particle Swarm Optimization (PSO), Hybrid ACO2/PSO, Bee Colony Optimization (BCO), Bacterial Foraging Optimization (Hybrid FPAB/BBO) and Biogeography Based Optimization (BBO). ACO [12, 20] is used to solve discrete optimization problems. ACO can be applied to a variety of problems such as the travelling salesman problem, feature selection for dimensionality reduction, medical diagnostics, speech, and texture classification problems. However, the main limitation of ACO was the sequential selection of features, which may not lead to an optimal solution. Ant miner requires the discretization method as a pre-processing method and it is suitable only for the nominal attributes [12, 20]. Particle Swarm Optimization (PSO) [8, 23] is a global optimization algorithm for dealing with problems in which a best solution can be represented as a point or surface in an n-dimensional space. Hybrid ACO2/PSO Optimization [14, 21] , unlike a conventional PSO, can directly cope with the nominal attributes, without converting nominal values into numbers in a pre-processing phase. Bee Colony Optimization (BCO) [4, 6, 7] is a recently proposed, nature-inspired meta-heuristic. Bee Colony Optimization is a population-based search algorithm that mimics the food foraging behavior of swarms of honey bees. It has been successfully applied to many combinatorial optimization problems, mostly in transportation, location and scheduling fields. The Algorithm for feature extraction is based on the dancing behavior of honey bees while moving from the nectar source to their hives [4]. Bacterial Foraging Optimization Algorithm [13] for feature extraction is based upon search and optimal foraging decision making capabilities of the E.Coli bacteria. The coordinates of a bacterium represent an individual solution of the optimization problem. Such a set of trial solutions converges towards the optimal solution following the foraging group dynamics of the bacteria population [13]. Biogeography Based Optimization (BBO) is an optimization technique that does not involve reproduction or the generation of "children" [2] and maintains its set of solutions from one iteration to the next, relying on migration to probabilistically adapt those solutions [2]. BBO technique has also been successfully applied for geo-spatial feature extraction [17].

V. CONCLUSIONS

At present, it is not possible to state which technique is best for all situations as the characteristic of each image and the circumstances for each study vary so greatly. Therefore, it is essential that each analyst understand the alternative strategies for feature extraction so that he or she may be prepared to select the most appropriate technique for the feature extraction task in hand. To this end, the concept of nature inspired computational intelligence, which can prove to be an optimized approach of feature extraction from satellite multi-spectral images, has been introduced in this category. These techniques with lower cost and higher degree of classification accuracy will be able to replace high-resolution high cost satellite imageries.

The paper is positioned in the exploration, integration and the adaptation phases of the nature inspired computational intelligence models of problem optimization. We redefine the taxonomy of nature inspired CI techniques and since the problem in hand is the land cover feature extraction (or the satellite image classification in remote sensing terms) problem, our focus here was the development of adaptive optimization models from the terrain perspective. The Land cover feature extraction is taken as a case study. As seen

above, extensive work has been done to develop computational intelligence inspired from nature and natural phenomenon. As far as feature extraction was concerned, a few nature inspired intelligent techniques like those of rough sets, fuzzy sets, membrane computing, ant colony optimization, particle swarm optimization, biogeography based optimization, membrane computing, bacterial foraging optimization etc. could only be adapted and implemented for real time scenarios such as in satellite imaging applications [5]. However, the nature inspired techniques of cuckoo search, firefly optimization, stochastic diffusion search, geo-sciences based techniques of plate tectonics, big bang crunching etc. have never been used to suit the land cover feature extraction applications. Certain nature inspired techniques when integrated with the existing optimization techniques can drastically improve their optimization capability hence leading to better terrain classification. We can explore these techniques further and adapt them for various applications.

REFERENCES

[1] Bonabeau, E., Dorigo, M. and Theraulaz, G., "Swarm Intelligence from Natural to Artificial System", First Edition, Oxford University Press, pp.1-24, 1999.

[2] Dan Simon, "Biogeography Based Optimization", IEEE Transactions on Evolutionary Computation, Vol. 12, No. 6, 2008.

[3] Daya Gupta, Bidisha Das, and V. K. Panchal, "A Methodical Study for the Extraction of Landscape Traits Using Membrane Computing Technique", GEM', WORLDCOMP 2011.

[4] D. Karaboga," An Idea Based On Honey Bee Swarm for Numerical Optimization, Technical Report-TR06, 2005.

[5] Demetrics Stathakis and Anthanassios Vasilakos, "Comparison of computational Intelligence based Classification Techniques for Remotely Sensed optical Image Classification", IEEE Transactions on and Remote Sensing , Vol. 44(8), 2006.

[6] Dervis Karaboga and Bahriye Akay, "A comparative study of Artificial Bee Colony algorithm", Applied Mathematics and Computation, Vol. 214, pp. 108–132, 2009.

[7] Dušan TEODOROVIĆ1,2, Mauro DELL' ORCO, "Bee Colony Optimization – A Cooperative Learning Approach To Complex Transportation Problems", Advanced OR and AI methods in Transportation, 2000.

[8] Kennedy, J.; Eberhart, R., "Particle Swarm Optimization", Proceedings of IEEE International Conference on Neural Networks (IV), pp. 1942–1948, 1995.

[9] Lavika Goel, Daya Gupta, V.K. Panchal, "Hybrid bio-inspired techniques for land cover feature extraction: A remote sensing perspective," Applied soft computing, Elsevier publications, Vol. 12(2), pp. 832-849, 2011. (Impact factor 2.6)

[10] Lavika Goel, "Land cover Feature Extraction using Hybrid Swarm Intelligence Techniques-A Remote sensing perspective", ACEEE International Journal on Signal & Image Processing, Vol. 1(3), 2010.

[11] Long, W., III; Srihann, S, Geoscience and Remote Sensing Symposium, Unsupervised and supervised classifications, "Land cover classification of SSC image: unsupervised and supervised classification using ERDAS Imagine", IGARSS '04 Proceedings, Vol. 4, pp. 20-24, 2004.

[12] M. Dorigo and T. Stuetzle, "Ant Colony Optimization", MIT Press, 2004.

[13] Navdeep Kaur Johal, Samandeep Singh and Harish Kundra, "A hybrid FPAB/BBO Algorithm for Satellite Image Classification", International Journal of Computer Applications (0975 – 8887), Vol. 6(5), 2010.

[14] N. Holden and A.A. Freitas, "A hybrid particle swarm/ant colony algorithm for the classification of hierarchical biological data", In: Proc. 2005 IEEE Swarm Intelligence Symposium (SIS-05), pp. 100-107, 2005.

[15] Omkar, S.N., Manoj, K.M., Mudigere, D. and Muley, D., "Urban Satellite Image Classification using Biologically Inspired Techniques", In Proceedings of IEEE International Symposium on Industrial Electronics, pp. 1767 – 1772, 2007.

[16] Pal, S.K. and Skowron, A., "Rough Fuzzy Hybridization: A new Trend in Decision Making", First Edition, Springer-Verlag publishers, pp.3-23, 1999.

[17] Panchal, V., Singh, P., Kaur, N., Kundra, H., "Biogeography based satellite image classification", International Journal of Computer Science and Information Security, Vol. 6 (2), pp. 269–274, 2009.

[18] Panchal VK, Singhal Naresh, Kumar Shashi, Bhakna Sonam, "Rough-Fuzzy Sets Tie-Up for Geospatial Information", Proceedings of International Conference on Emerging Scenarios in Space Technology and Applications (ESSTA2008), Vol. 1, 2008.

[19] Pawlak, Z. , "Rough set approach to knowledge-based decision support", European Journal of Operational Research, Vol. 99 (1), pp. 48-57, 1997.

[20] R.S. Parpinelli, H.S. Lopes and A.A. Freitas, "Data Mining with an Ant Colony Optimization Algorithm", IEEE Transactions on Evolutionary Computation, special issue on Ant Colony algorithms, pp. 321-332, 2002.

[21] Shelly Bansal, Daya Gupta, V.K. Panchal ,Shashi Kumar, "Remote Sensing Image Classification by Improved Swarm Inspired Techniques" in International Conference on Artificial Intelligence and Pattern Recognition (AIPR-09), 2009 .

[22] Thomas M. Lillesand , Ralph W. Kiefer, "Remote Sensing and Image Interpretation", 6th Edition, Wiley, 2008.

[23] WangDong, Wu Xiang-Bin, "Particle Swarm Intelligence Classification Algorithm for Remote Sensing Images", IEEE Pacific-Asia Workshop on Computational Intelligence and Industrial Application, 2008.

[24] Zadeh,L.A.,"Fuzzy sets", Information and Control, Vol. 8 (3), pp.338- 353, 1965.